Application of Stable Water Isotopes to Quantify the Water Balance of Delta Marsh

By

Marija Glavonjic

A Thesis Submitted to the Faculty of Graduate Studies of

The University of Manitoba

In Partial Fulfilment of the Requirements of the Degree of

Master of Science

Department of Civil Engineering

University of Manitoba

Winnipeg, Manitoba, Canada

Abstract

This thesis as a part of the rehabilitation project Restoring the Tradition at Delta Marsh, details stable water isotope research. Stable water isotopes are applied as a tool to quantify the water balance of the Marsh. A four-year sampling campaign for stable water isotopes was launched. Coupled with the hydraulic and hydrologic modelling, stable water isotopes assist in the understanding of contemporary water balance and the relative contribution of inflows to evaporative losses. Two hydrologically different years (2013 and 2014) are compared to offer insight into the Marsh functioning under differing climatic conditions. A contemporary isotopic framework was developed to determine correlation between end-members influencing Marsh hydrologic change. The framework has shown that the Marsh is not in hydrologic steady-state, which was previously confirmed by 2D hydraulic modelling. An isotope mass balance mixing model was established to evaluate evaporative loss (relative to inflows), and to determine residence time and water yield including marsh-lake dynamic interactions. Time series modelling was performed and confirmed that a time-dependent isotopic model is more suitable than a fraction-dependent model for modelling Marsh isotope composition. Evaporation is the most significant component in the water balance. The isotope mass balance model demonstrated that evaporation to inflow ratio was 22% in 2013 and 24% in 2014. Water residence time was found to be 99 and 140 days in 2013 and 2014, respectively. Water yield for both years was approximately 280 mm/year.

Acknowledgements

This has been a long journey for me and my family which expanded from five to seven members. Finally, I reached the end of this path and would like to thank everyone who contributed to this:

First and foremost, to my advisors Dr. Trish Stadnyk and Dr. Shawn Clark. Trish, thank you for accepting me as your student, for your patience, guidance and support. Without you this journey would have been impossible. Shawn, thank you for asking all those questions about isotopes and helping me to dig deeper to find answers.

Thank you Mr. Parsa Aminian and Mr. Gregory Schellenberg who worked on Delta Marsh project as well, having collected those little bottles of water for isotope analysis for two years prior to my start. Greg, I will never forget my very first trip to Delta Marsh, it was so cold, raining cats and dogs and we were soaked. Thank you for making that trip shorter, otherwise I would have probably ended my journey right then. And thank you both for suggesting names for my twins, which of course I politely refused (Delta and Marsha).

Thank you lovely Dr. Chani Welch for giving me all support throughout the project.

Thank you Mr. Alexander Wall, our lab technician for being so knowledgeable and helpful. Alex, thank you for all those overnight trips you conducted instead of me. Highly appreciated.

I would like to thank to my summer students Mr. Brodie Bright and Mr. Julian Sigurdson for spending so much time in a boat with me collecting samples.

Big thanks to my committee members Dr. Karen Dow and Dr. Gordon Goldsborough for your comments and helping wrap up my writing.

Thank you everyone involved in Delta project. Special thanks to Mr. Bob Emery and Mr. Dale Wrubleski for answering all those questions related to field component of the project. Thank you Ms. Paige Kowal for providing extra information when asked. Your assistance was invaluable.

I would like to thank to my co-office mate and a friend, Kian Abbasneszhadi who gave me all his support from the very beginning (when I was considering graduate school) and helping with all technical aspect throughout the studies. Thank you for all kind words and support. Wish you all the best in your carrier. Thank you, dear Ms. Su Jin Kim for having a coffee break with me and helping with formatting. Thank you for being such a lovely roommate during our conference in Montreal. Dear Ms. Tegan Holmes, thank you for all your help with isotopes, Grapher, and countless support. Wish you all the best in your carriers.

Dear Marguerite and Rene, my lovely neighbors and friends, thank you for always being there for me and my family. I couldn't have done this without you.

I want to give big thanks to my husband and partner in life, who was standing by my side all this time. Thank you, from the bottom of my heart.

Finally, I appreciate all contributions made by Ducks Unlimited Canada and for giving me an opportunity to be a part of such a big project.

End of this journey coincide with this huge world-wide pandemic of Covid-19. I hope we will all face a better, kinder and genuine world after this.

Table of Contents

List of Figures

List of Tables

List of Abbreviations

Abbreviation	Definition
E	Evaporation (mm)
GMWL	Global meteoric water line
E/I	Evaporation to inflow ratio
h	Relative humidity in decimal notation
I	Total inflow volume (m^3)
IMB	Isotopic Mass Balance
J	Upstream inflow volume (m^3)
LEL	Local evaporation line
LMWL	Local meteoric water line
m	Isotope enrichment slope
P	Precipitation (mm)
R	Runoff volume (m^3)
T	Temperature (K)
VSMOW	Vienna Standard Mean Ocean Water
WY	Water yield (mm)
δ	Delta notation in per mille (‰)
δ^*	Theoretical maximum (limiting) isotopic enrichment value
δ_A	Isotopic composition of atmospheric moisture
δ_E	Isotopic composition of evaporation
δ_I	Isotopic composition of inflow

δ_J	Isotopic composition of upstream inflow
δ_L	Isotopic composition of Marsh water
δ_P	Isotopic composition of weighted average precipitation
δ_{GW}	Isotopic composition of groundwater
δ_R	Isotopic composition of river and channel samples
δ_{lmb}	Isotopic composition of Lake Manitoba
δ_Q	Isotopic composition of outflow
δ_o	Initial isotopic composition of the Marsh
δ_{SS}	Steady state isotopic composition of the Marsh
ε^*	Equilibrium separation term
ε_K	Kinetic separation term
α	Isotope fractionation factor

1 Introduction

1.1 Background

Delta Marsh ($50^{o}11'N, 98^{o}19'W$) is a vast coastal wetland located alongside the southern shore of Lake Manitoba, covering approximately 185 km^2, that is host to a dynamic assortment of plant and animal species (fish, water birds, mammals), including a large water fowl population, especially canvasback ducks. It is one of the largest and most well-known freshwater coastal wetlands in North America, of international and regional importance (Ducks Unlimited Canada, 2013). In 1982 the Ramsar Convention nominated the Marsh as internationally important wetland, while in 1988 it was designated as a Manitoba Heritage Marsh, in 1999 as an Important Bird Area, and in 2005 a Provincial Wildlife Management Area (Ducks Unlimited Canada, 2013). It was once a very active hunting destination, attracting hunters from across North America and the world.

Delta Marsh is divided into three sections: west, centre, and east Marsh (Figure A.1 in Appendix A) The Portage Diversion (also known as the Assiniboine River Diversion) is 25 km in length and bisects the Marsh, directing water from Assiniboine River to Lake Manitoba in order to protect Portage La Prairie, Winnipeg, and the farmland along the river from flooding (Bortoluzzi,

2013). There is no direct flow between the centre and east Marsh and Portage Diversion and therefore the diversion is not considered as part of the Marsh. West Marsh is the area west of Portage Diversion, and there is a cut in the diversion allowing overflows from the diversion to enter the marsh in the event of very high flows. West Marsh is connected to Lake Manitoba via two channels (Deep Creek and Cram Creek), but is separated from the rest of the Marsh by the diversion. Center Marsh is the area east of the Portage Diversion and west of highway 240. This area consists mainly of Eaglenest Bays and several surrounding ponds. The area east of highway 240 is the largest area of the Marsh, and is called East Marsh. It consists of many large open water bays and is connected to Lake Manitoba via Delta Channel and Clandeboye Channel (Figure 1.1). In general, the Marsh is shallow (water levels are approximately one meter), but in some channels it can reach 3 m (Hope, 2020).

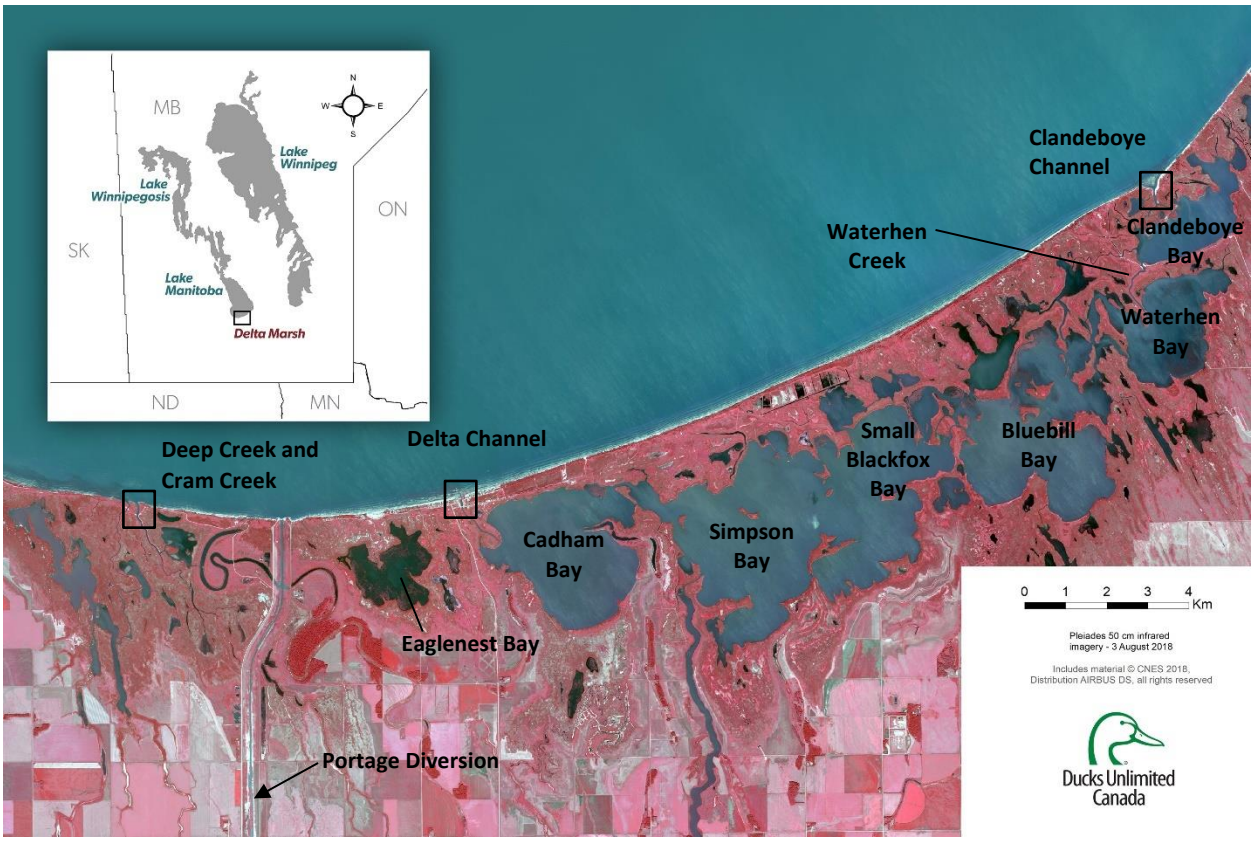

Figure 1.1 - Location plan and imagery of Delta Marsh (Ducks Unlimited Canada, 2020)

More than 10 000 years ago, Lake Manitoba was created during the recession of Lake Agassiz, while initial formation of Delta Marsh started between 3500 and 2500 years ago (Last & Teller, 2002). More details about geomorphology and paleoecological history of Delta Marsh can be found in Aminian (2015). Coastal wetlands have several different roles, but maybe one of the most significant is the protection of a water body from runoff flowing directly from the surrounding watershed, by protecting the adjoining water body from detrimental impacts of high-water quantity and poor water quality (Schellenberg, 2017). The connection between a coastal wetland and its upland watershed is important, especially how anthropogenic (e.g. changes in land cover) and natural changes in the upland watershed impact the coastal wetlands (Schellenberg, 2017).

Over the last fifty years, Delta Marsh has gradually deteriorated in water quality and function, resulting in an increase of cyanobacterial blooms, intrusion of invasive fish and plant species, and consequently a decrease in flora and fauna and a loss of productive recreational use of the Marsh. In 2013, a multi-partner project entitled "Delta Marsh – Restoring the Tradition (RTT)" was initiated by Ducks Unlimited Canada (DUC), the Province of Manitoba, the University of Manitoba, and other partners to identify causal mechanisms of Marsh deterioration and to develop appropriate mitigation measures (Aminian, 2015). It is believed that Delta Marsh function can be improved by exclusion of common carp, evaluation of the new water level of Lake Manitoba and its relationship with the Marsh, decreasing the invasion of hybrid cattails, and reducing the nutrient input to Delta Marsh (Ducks Unlimited Canada, 2009). According to Stanley (2017), meteorological conditions such as wind, temperature, precipitation, and nutrient availability from land, water, and sediments have the biggest impact on algal blooms. Higher water temperature increases production of cyanobacteria during warmer months of July and August, while precipitation increases the volume of nutrient runoff (Stanley, 2017). Phosphorus is considered as an essential nutrient, but with levels beyond necessary for normal plant growth, it can be considered as pollutant (Hope, 2020). Hope (2020) suggested that phosphorus concentrations were greatest in the west part of the Marsh and decrease toward the east.

Common carp is an invasive bottom-feeding (benthivorous) fish species that disturbs the Marsh bed while spawning and searching for food, thereby increasing the turbidity (Badiou & Goldsborough, 2010). Increased turbidity and bed disturbance limit sun penetration causing a drastic decrease in the abundance and variety of submerged vegetation (Hertam, 2010). Hybrid cattails have been taking over large portions of the Marsh causing deterioration in water quality

and more frequent algae blooms. Water level regulation of Lake Manitoba started in 1961 when the Fairford River Water Control Structure (FRWCS) was used to maintain the lake level (Bortoluzzi, 2013). This regulation is believed to have attenuated the natural wet-dry cycle leading to an increase in productive emergent wetland vegetation (Van Der Valk, 2005). Nutrient loading has been significantly changed due to agricultural intensification within the Delta Marsh watershed (Sharpley et al., 2011). The tallgrass prairie, the predominant native land cover of the watershed (Sveinson, 2003), was significantly replaced by agricultural land cover accelerating the production of runoff. Better understanding of hydrology, hydraulics, biology, topography, and physiography and factors that have led to Marsh degradation will help to improve the overall biodiversity of the Marsh, provision of fish and wildlife habitat, water quality improvement, carbon sequestration, and consequently increase waterfowl staging (Schellenberg, 2017).

The current study is part of a three-component Delta Marsh study led by a group within the Civil Engineering Department of the University of Manitoba consisting of hydrologic, hydraulic and stable water isotopes. As part of this study, three-inter related models were developed: a two-dimensional hydrodynamic model of Lake Manitoba (MIKE 21) to capture wind setup effects at ,21); and a hydrologic model of the watershed (MIKE SHE with MIKE 11 routing subroutine) to capture runoff to the Marsh and hydrograph separation.

The focus of the hydraulic study was to better understand the hydrodynamics of Delta Marsh (relationship between water levels of Lake Manitoba and Delta Marsh), how wind from Lake Manitoba influences fluxes to and from the Marsh (Aminian, 2015), assess Portage Diversion

influence, and estimate of wetland inflow and outflow. A 2D hydrodynamic model was setup to assess all these components, and it was discovered that the majority of flow to the Marsh occurs through Clandeboye Channel, which carries 85% of Lake Manitoba inflow. Wind friction across Lake Manitoba also plays a significant role on Marsh water level fluctuations (Aminian, 2015).

The hydrologic study focused on understanding the Marsh water balance, quantifying and defining Marsh inflow contributions from runoff and interactions (inflow/outflow) with Lake Manitoba using a comprehensive hydrological model and assessing the impact of land use changes on relative hydrological response. As found by this study, the majority of the Marsh upland inflow comes from snowmelt during the spring. Portage Creek is the most significant single inflow to Delta Marsh (Schellenberg, 2017). The East Marsh receives relatively little overland runoff, while the West Marsh receives significant runoff. More information about this study and different land use scenarios can be found in Schellenberg (2017).

1.2 Objectives

This study was undertaken in conjunction with a hydraulic and hydrology study of Delta Marsh watershed to assess correlation between stable water isotopes (SWIs) and hydrologic/hydraulic fluxes. This study specifically seeks to better understand the hydrology of Delta Marsh using SWIs as proven tools to help with source water identification. Stable water isotopes can be used as tracers where the signature of precipitation can be followed in the surface runoff and even quantified through the runoff hydrograph. Separation between different sources is useful from nutrient and mineral contribution to the Delta Marsh (e.g. Lake Manitoba can bring higher nutrient content versus groundwater brings higher mineral content), which is important for the

overall Marsh health. SWIs are useful in calculating water balance and quantifying all of the components. Residence time is an important parameter in addressing the water quality and can be obtained using isotopes in conjunction with Marsh volume. Water yield determines the efficiency of a watershed in transforming precipitation into inflow. It is very helpful from a water management perspective (i.e., how much water is produced from a watershed compared to how much is needed by a specific user).

The particular objectives of this study are to:

- Perform a Marsh water balance hydrologic component analysis by combining SWIs with climate, water level and hydrologic flux data;
- Assess the degree of interaction between the Marsh and Lake Manitoba, and relative contributions of 'old' (groundwater) and 'new' (rain, snowmelt) water components;
- Establish a time-series model of SWI signatures of Marsh composition that can be used to predict Marsh water balance; and,
- Estimate evaporative losses (evaporation to inflow ratio), Marsh residence time, and water yield (runoff).

1.3 Gaps in Current Research

Unique aspects of the current research program relative to those found in the literature include:

- Combination of complex modelling and isotope field monitoring;
- Application of isotope hydrograph separation (IHS) to look at up and downstream watershed connectivity and connectivity within the Marsh by combining intensive hydraulic measurements with isotope sampling;

- Extensive monitoring over a vast region at a weekly timescale;

1.4 Study Site Description

Delta Marsh, a wetland along the southern shore of Lake Manitoba, covers approximately 185 km^2 (Figure 1.1), while Delta Marsh Watershed is approximately 575 km^2. The Marsh is separated from Lake Manitoba by a natural sand ridge, but connected by four channels (Cram Creek, Deep Creek, Delta Channel, and Clandeboye Channel) (Bortoluzzi, 2013) (Figure 1.1). Consequently, its hydrology is influenced by the hydrology of the lake. The Marsh consists of several bays and interconnected with channels.

Delta Marsh receives water via overland and channel runoff from the upland watershed, from local precipitation and groundwater recharge, as well as from its direct connection to Lake Manitoba (Bortoluzzi, 2013). The majority of inflow comes through spring freshet, or melt water from accumulated snow (Goldsborough & Suggett, 2015). Water is lost via evapotranspiration and infiltration. The flow through the Marsh is two-directional (to and from the Marsh) so some water is lost as an outflow from the Marsh to the lake, and occasionally to the surrounding watershed (i.e., when the Lake MB and Marsh water levels are higher than the surrounding, flat landscape). Groundwater is always contributing to the Marsh.

2 Literature Review

Isotope hydrology, a relatively young scientific discipline (evolved around 1950), recognized the useful application of isotopes in hydrology. Generally, isotopes are applied in hydrology as tracers of source water, or as water age indicators (IAEA, 2000c).

Atoms of the same element that have a different number of neutrons, and therefore different atomic mass, are called *isotopes.* Many atoms have two or more naturally occurring isotopes (IAEA, 2000a). Atoms that are most abundant in nature have equal numbers of protons and neutrons and are usually called "*light elements*". Atoms whose number of neutrons exceeds the number of protons are called "*rare*" or "*heavy*" since they are less abundant in nature. Isotopes can be classified as stable (non-decaying) and unstable (radioactive). Evolution of isotope science started in early 1913 with Soddy (1913), who was the first to introduce this term. The discovery of oxygen and hydrogen isotopes began around the same time with (Giauque & Johnston, 1929ab) who discovered oxygen-18 and 17 in natural materials, and (Urey et al., 1932) researching deuterium in the residue of a low-hydrogen distillation column.

Isotopes of oxygen and hydrogen are considered ideal tracers of the natural water cycle since they mark the water and move passively with the water or solutes (Aeschbach-Hertig, 2010),

they are naturally occurring, they are stable, and they exhibit systematic variation in precipitation and the hydrologic cycle as a result of phase changes and isotopic fractionation during evaporation (Stadnyk-Falcone, 2008). ^{18}O and ^{2}H have been extensively applied in studies of the origin and dynamics of surface and groundwaters, in studies of atmospheric circulation and paleoclimatic investigations (Vreca et al., 2006). One of the first studies utilizing isotopes in the hydrologic cycle was an application to separate "old" (groundwater) and "new" (meteoric and surface) water components (isotope hydrograph separation, IHS) by (Sklash & Farvolden, 1979). Radioactive tritium (^{3}H) has also been used for tracing groundwater (Clark & Fritz, 1997).

Examples of other naturally occurring isotopes are C, N, S etc. that mark dissolved substances and noble gases (Aeschbach-Hertig, 2010). Stable water isotopes have been used largely to understand changes within the hydrologic cycle. Two stable isotopes of hydrogen: protium, ^{1}H (99.985%) and deuterium, ^{2}H (or D) (0.015%); and three isotopes of oxygen: ^{16}O (99.759%), ^{17}O (0.037%), and ^{18}O (0.204%) exist in nature (relative abundances in nature are shown in brackets). Nine possible isotopologues of the water molecule are: $H_2{}^{16}O$ (99.6%), $H_2{}^{18}O$ (0.2036%), $^{1}H^{2}H^{16}O$ (0.031%), $^{1}H2^{17}O$,$^{1}H^{2}H^{17}O$,$^{1}H^{2}H^{18}O$,$^{2}H_2{}^{16}O$,$^{2}H_2{}^{17}O$, and $^{2}H_2{}^{18}O$ (IAEA, 1981). Only three out of those nine isotopically different molecules occur in nature and are easily detectable: $H_2{}^{16}O$, $H_2{}^{18}O$, and $^{1}H^{2}H^{16}O$ (IAEA, 2000c).

Owing to the small differences in mass, isotopic concentrations of hydrogen and oxygen are represented by delta notation (δ) as deviations in per mil (‰) from Vienna Standard Mean Ocean Water (VSMOW) (Coplen, 1996):

$$\delta_{SAMPLE} = \left(\frac{R_{SAMPLE}}{R_{VSMOW}} - 1\right) \cdot 1000(‰) \quad 2.1$$

where R_{SAMPLE} and R_{VSMOW} stands for isotope ratio ($^{2}R = {}^{2}H/{}^{1}H$ and $^{18}R = {}^{18}O/{}^{16}O$) in the sample and the standard, respectively. The internationally accepted standard for isotopic ratios of $^{2}H/^{1}H$ and $^{18}O/^{16}O$ of VSMOW are:

$$^{2}H/^{1}H = (155.95 \pm 0.08) \text{ x } 10^{-6} \text{ (De Wit, et al., 1980)} \quad 2.2$$

$$^{18}O/^{16}O = (2005.20 \pm 0.45) \text{ x } 10^{-6} \text{ (Baertschi, 1976)} \quad 2.3$$

Positive values of δ indicate enrichment (relative abundance) of the heavy isotope related to the VMSOW standard (i.e., ocean water, or the start of the hydrologic cycle), while negative values indicate depletion (relative absence) (Gat, 1996).

2.1 Isotopic Fractionation

Stable water isotopes occur naturally and therefore the isotopic signature of water utilized or sampled in the environment will be preserved at that specific point in time (within a closed system). Due to slight differences in the molecular behaviour of heavy isotopic species (Stadnyk-Falcone, 2008), systematic isotopic labelling or fractionation results under an open system from a change in the isotopic composition of phase change and diffusive transport in the environment (Gibson, 1996; Gibson & Edward, 2002; Edwards et al., 2004).

Physical properties such as specific gravity and molecular diffusivity (mass–dependent) and chemical properties (e.g. differences in equilibrium exchange rates) among isotopologues govern differences in molecular behaviour; therefore, isotopologues have different rates of transport (Stadnyk-Falcone, 2008). Differences in mass cause lower mobility of the heavier isotopic, and therefore, based on kinetic law, smaller velocity. With that in mind, heavier molecules have lower diffusion velocity and lighter molecules react faster. The heavier molecules generally have higher binding energies (e.g. heat of evaporation) (IAEA, 2000a). The result is that heavier isotopic molecules require more energy to change state or move from one system to the next than the lighter molecules, which can 'escape' or change state more easily (IAEA, 2000a).

Isotopic fractionation is defined as a change in the isotopic composition of a compound by the transition from one state to another (i.e., liquid to vapour, $\varepsilon_{L/V}$), or form (e.g., carbon dioxide into plant organic carbon). During fractionation, heavy and light isotopes partition differently between two phases or compounds. This occurs due to differences in bonding energy, with heavier isotopes having stronger bonds and slower reaction rates (SAHRA, 2005). Therefore, light elements are likely to exhibit isotopic fractionation than heavy counterparts (SAHRA, 2005). Three mass dependent isotopic fractionation processes are distinguished: *thermodynamic* (or *equilibrium)*, *kinetic*, and *transport fractionation*. Mathematically described, isotopic fractionation compares the isotopic ratios of the two compounds in chemical equilibrium ($A \leftrightarrow B$) or the compounds before and after a physical or chemical transition ($A \rightarrow B$) (Orlowski, 2010). *Equilibrium fractionation* occurs when two different phases reach equilibrium (e.g. transformation of water vapour to liquid precipitation). As a result, one of the isotopes becomes enriched due to differences in exchange rates. During *kinetic fractionation* equilibrium is not

attained, and therefore this is unidirectional process (e.g. evaporation of surface waters). The *isotope fractionation factor, α,* is defined as the ratio of two isotopes:

$$\alpha_A\,(B) = \alpha_{B/A} = \frac{R(B)}{R(A)} = \frac{R_B}{R_A} \qquad 2.4$$

which, expresses the isotopic ratio (R) in one phase/compound (B) relative to that in A. By convention, A is always the more common (abundant) species (e.g. ^{16}O, ^{1}H).

In general, the isotopic fractionation factor is close to 1, with very small deviations due to small differences in isotopic ratios. Therefore, the deviation from α (=1) is widely used to define *fractionation* (ε):

$$\varepsilon_{B/A} = \alpha_{B/A} - 1 = \frac{R_B}{R_A} - 1\ (\text{x } 10^3‰) \qquad 2.5$$

When $\varepsilon > 0$, it represents equilibrium enrichment, and $\varepsilon < 0$, represents depletion of the rare isotope in B with respect to A. Since ε is a small number, it is generally given in per mille notation (‰). The equilibrium isotope effect is temperature dependant and is a two-directional process (e.g., change of state from liquid to vapour in a closed system). Unlike equilibrium fractionation, kinetic fractionation is uni-directional chemical reaction. An example is evaporation of water with immediate withdrawal of the vapour from further contact with the water.

2.2 Isotopes in Precipitation

Observations related to isotopic composition in precipitation have been numerous. The biggest endeavor was a joint collaboration between the Global Network for Isotopes in Precipitation (GNIP), International Atomic Energy (IAEA) and the World Meteorological Organization (WMO) (Kendall & Coplen, 2001) to define a flux-weighted average of all meteoric waters around the world for standard comparison (Araguàs-Araguàs et al., 2000).

Atmospheric vapour that condenses forms precipitation. That process is described as Rayleigh distillation or equilibrium fractionation (Dansgaard, 1964):

$$R = R_o f^{\alpha-1} \quad 2.6$$

where R_o is vapour's original isotope ratio ($^{18}O/^{16}O$ or $^{2}H/^{1}H$), R is the ratio after a given proportion of the vapour had reacted (e.g. rained out), f is the fraction of residual vapour in the cloud, α is the equilibrium fractionation factor (vapour to liquid).

Factors and processes that control isotopic composition of precipitation are:

- Meteorological conditions that control evaporation of water from the ocean such as relative humidity, sea surface temperature and wind regime (Gibson et al., 2008);

- Rainout mechanisms affecting the fraction of precipitable water that is removed from air masses (Araguàs-Araguàs et al., 2000);

- Snow formation or evaporation below the cloud base that are considered second-order kinetic effects (Gibson et al., 2008);

- Mixing of different air masses (origin from different oceanic sources) that carry different moisture and different degrees of precipitation rainout (Araguàs- Araguàs et al., 2000) and

- A mixture of recycled water from evapotranspiration over the continents (Gibson et al., 2008);

Several effects control the signature of local precipitation: latitudinal, temperature, continental, altitudinal, and amount effect (Figure 2.1). Tropical oceans are a major source for continental precipitation; oceanic water is evaporated and condensed into clouds. Isotopic ratios become more depleted with increasing latitude: $\delta^{18}O$ depletes by approximately -0.6 ‰ per degree of latitude for coastal and continental stations in Europe and USA, and up to -2‰ per degree of latitude in the colder Antarctic continent (IAEA, 2000b). Temperature effects are not as pronounced as the latitudinal effect, varying from about 0.5 ‰/°C for some higher-latitude and elevation stations to 0‰/°C for the tropical island regions (IAEA, 2000b). The continental effect is also referred as the 'distance from coast' effect. Precipitation undergoes progressive isotopic depletion with increasing distance from the ocean. This varies between areas (continents) and seasons, and is strongly correlated with temperature gradients. As a rule of thumb for altitudinal effects, the isotopic composition of precipitation becomes more depleted in ^{2}H and ^{18}O at higher

altitudes (between -0.15 ‰ and -0.30 ‰/100 m of altitude for ^{18}O) (Schotter et al, 1996). Temperature decreases at higher altitudes cause condensation, and hence this effect is temperature dependent (IAEA, 2000b).

In mid- to high-latitude regions, it was found that isotopes in precipitation are directly correlated with temperature. With progressive storms or rainout, precipitation may become extremely depleted in ^{18}O and ^{2}H (e.g., -15‰ for tropical rainfalls, -7 ‰ within 1 hour in north-western Europe) (IAEA, 2000b). In arid regions especially, enrichment in heavy isotopes of small amounts of rain along evaporation lines are typical.

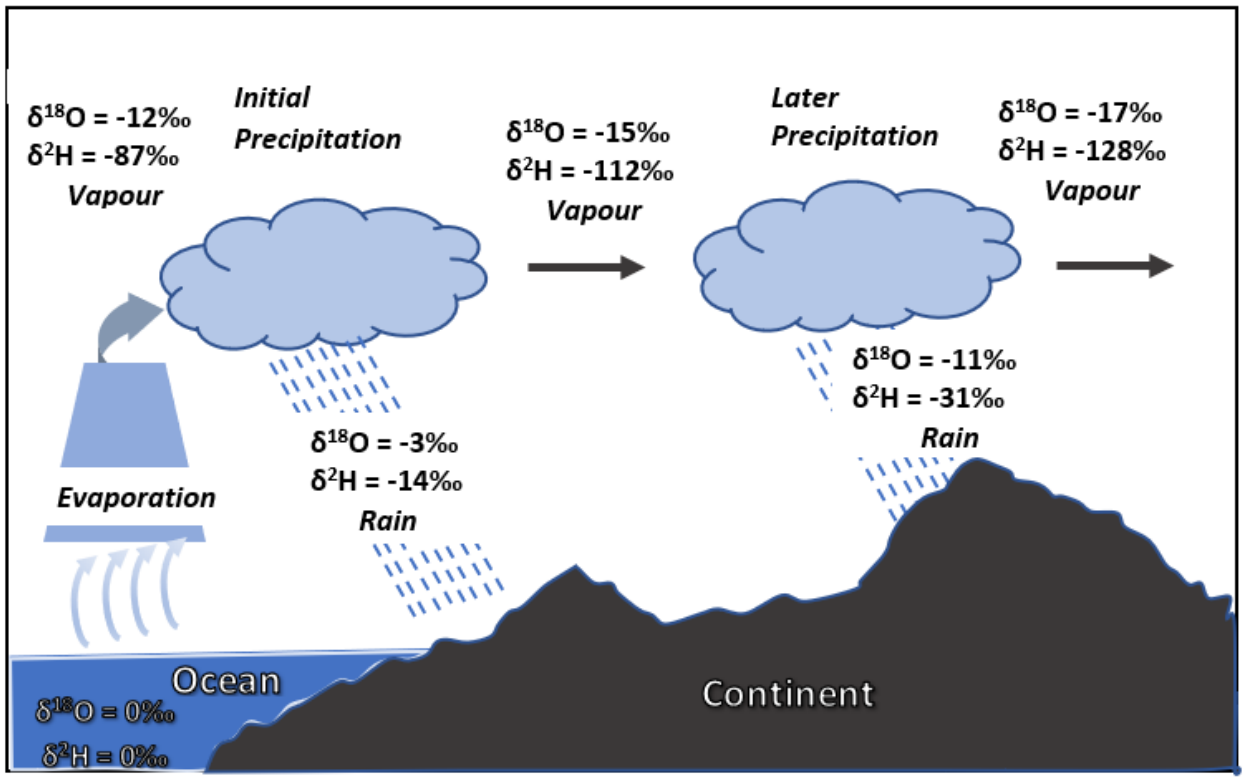

Figure 2.1 - Continental, altitudinal, and fractionation effects on isotopes in precipitation (modified from SAHRA, 2005)

Deuterium and oxygen 18 in meteoric water (precipitation and atmospheric water vapour) are strongly correlated. If plotted on a δ-δ scale (δ^2H vs. δ^{18}O), these data cluster along a straight line, the so-called Global Meteoric Water Line (GMWL) (Craig & Gordon, 1965). The GMWL is given by:

$$\delta^2 H = 8\delta^{18} O + 10\ (‰) \qquad 2.7$$

and has a slope of 8, representing the flux-weighted average of all meteoric water, globally.

Labelling of local scale precipitation derives a Local Meteoric Water Line (LMWL), which reflects temporal variability in isotopic composition of local precipitation (Yi, et al., 2008), and a deviation relative to the global standard. Because of re-evaporation of raindrops and kinetic effects during snow formation (Yi, 2008), the LMWL typically has a lower slope than the GMWL (Rozanski et al., 1993), which is true for all of Canada.

Processes in the global water cycle that drive the variations in δ^{18}O and δ^2H (IAEA, 2000b):

1. Evaporation of surface water
2. Rainout progression of vapour masses

In Canada we typically see a pronounced latitudinal effect producing more depletion further north, and a significant continental effect (more depleted further from the coast). In general, the East coast is more enriched than the West as a result of originated moisture source. The West coast is also higher in elevation, so there are enhanced altitudinal effects resulting in further

isotopic depletion across the Canadian Rockies. Delavau et al. (2015) produced an isoscape for Canada where these effects are visible.

2.3 Evaporation

The biggest source of water in the atmosphere is derived from evaporated ocean and open water (i.e. lake and wetland) bodies. Evapotranspiration from the plants and from the soil also adds to the atmospheric flux, but to a lesser extent (relative to Ocean water). Local surface waters that have undergone evaporation become additionally enriched in heavy isotopes and tend to plot below the LMWL. When evaporated surface data are plotted in $\delta^2H - \delta^{18}O$ space and linearly regressed, this defines the Local Evaporation Line (Figure 2.2), representing the isotopic fractionation in open water that occurs under local atmospheric conditions. If surface water samples are from rivers or flowing waters, this is typically referred to as the Local Mixing Line (LML) (Smith et al., 2015). The typical slope of an LEL in Canada ranges from 4–7 (Gibson et al., 2005), depending on latitude and temperature of the region, as well as amount of open surface water. In a framework, δ^* is the limiting isotopic enrichment, meaning this would be the isotopic composition of a water body approaching desiccation. Isotopic steady state (δ_{SS}) is the concentration of a lake/marsh that is in a hydrologic steady state, δ_A is an isotopic composition of atmospheric moisture, and δ_E Is an isotopic composition of evaporative flux.

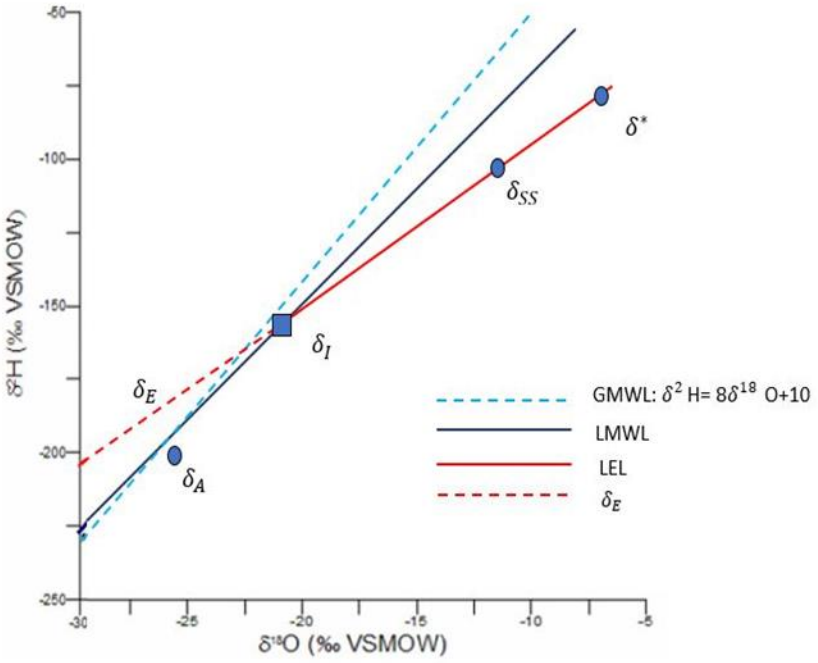

Figure 2.2– Hypothetical δ^2H-$\delta^{18}O$ isotopic framework. GMWL approximated by $\delta^2H=8\delta^{18}O+10$ (Craig, 1961; Dansgaard, 1964); LMWL represents a flux-weighted average of local precipitation; LEL- local evaporation line represents a regression slope of evaporating surface waters. Intersection of LEL and LMWL results in δ_I – flux-weighted composition of input sources; δ_A -isotopic composition of atmospheric moisture, δ^*-limiting isotopic composition, δ_{SS} -steady state isotopic composition, δ_E -isotopic composition of evaporative flux.

Thermodynamic equilibrium between liquid and vapour phases is not typically maintained (e.g. evaporation of an open water body into an unsaturated, turbulent atmosphere) (Stadnyk-Falcone, 2008). As a result, at the air-water interface a viscous boundary layer is formed. Through this layer moisture is transferred at a differential rate. This results in kinetic fractionation. Moisture deficit (1-h) (where h is relative humidity) over the evaporating surface and molecular diffusion of the isotopic species through the air phase control kinetic fractionation (Rozanski et al, 2001). Isotope effects accompanying evaporation into an open (unsaturated) atmosphere or the enrichment in the heavy isotopes in an evaporating, open water body as water is transported via diffusion from liquid to vapour phase across the boundary layer were first described by Craig &

Gordon (1965). A schematic description of the model presented by Craig and Gordon is presented in Figure 2.3. Total fractionation consists of equilibrium and kinetic fractionations ($\varepsilon_{tot} = \varepsilon_{V/L} + \varepsilon_{KIN}$). At the air-vapour interface, isotopic equilibrium between the surface waters (L) and the saturated vapour (V) can be assumed ($\delta_V = \delta_L + \varepsilon_{V/L}$) where the isotopic equilibrium term depends only on temperature and salinity.

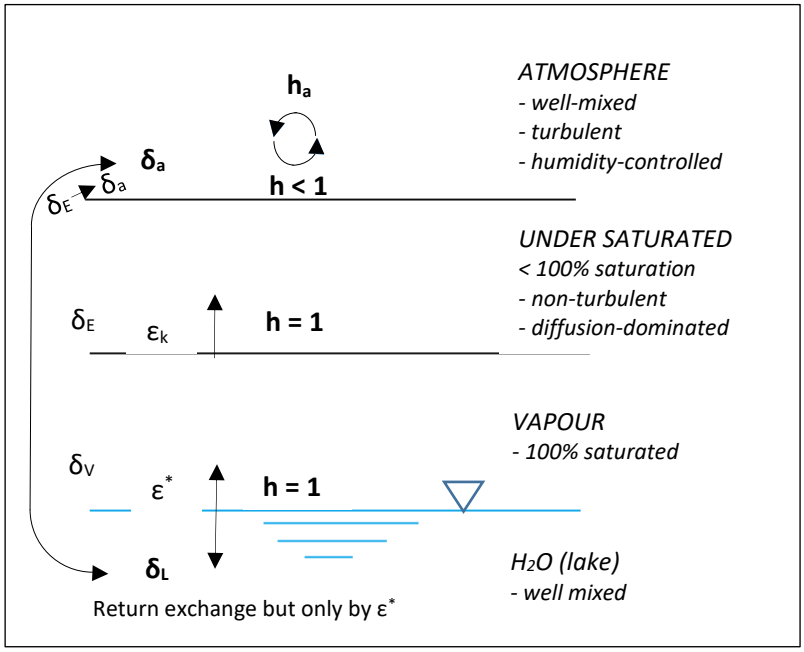

Figure 2.3 - Isotopic fractionation during evaporation (modified from Craig and Gordon, 1965)

Change in isotopic composition of evaporative flux from the boundary layer to the free atmosphere, presented by Craig and Gordon (1965) in Figure 2.3, is the difference between transport fluxes (E_i/E). E is the transport of the common water molecule ($H_2{}^{16}O$) and is defined as the moisture deficit (1-h) divided by the total atmospheric transport resistance, ρ $(mm/day)^{-1}$:

$$E = -\frac{dN}{dt} = \frac{1-h}{\rho} \quad (2.8)$$

E_i is the transport flux (mm/day) of the heavier water molecule ($H_2{}^{18}O$) and is driven by the concentration gradient ($\delta_L - \delta_A$) relative to the specific transport resistance of the heavier isotope (Stadnyk-Falcone, 2008):

$$E = -\frac{dN}{dt} = \frac{(\alpha^* \delta_L - h\delta_A)}{\rho_i} \quad (2.9)$$

where δ_L (‰) is isotopic composition of lake water or reservoir, δ_A (‰) is isotopic composition of atmospheric moisture, α^* is the equilibrium liquid-vapour fractionation.

According to Craig and Gordon (1965), isotopic composition of evaporating moisture, δ_E, represents a proportion of the transport flux of water (E) and "heavy" water (E_i). By defining $\varepsilon = (1-h)\left(\frac{\rho_i}{\rho} - 1\right) = \frac{\varepsilon^*}{\alpha^*} + \varepsilon_k$, the isotopic composition of evaporating moisture (δ_E) is defined (Gonfiantini, 1986):

$$\delta_E = \frac{\frac{(\delta_L - \varepsilon^*)}{\alpha^*} - h\delta_A - \varepsilon_K)}{1 - h + 10^{-3}\varepsilon_K} \text{ (‰)} \quad (2.10)$$

where h is relative humidity and $\varepsilon_k = C \cdot (1-h)$(‰) is kinetic enrichment, using experimentally-derived kinetic constant values (C) of 12.5 ‰ for deuterium and 14.2 ‰ for ^{18}O,

representing fully turbulent, open water condition (Horita et al., 2008), $\varepsilon^*$is equilibrium enrichment, and α^* is equilibrium fractionation factor. Total isotopic fractionation, ε, is comprised of both equilibrium ε^* and kinetic components ε_K $(\varepsilon = \varepsilon^* + \varepsilon_K)$.

The equilibrium fractionation factor, α^*, defined in per mille, is derived by the (Horita & Wesolowski, 1994) formulation:

$$1000ln\,(\alpha^* 18O) = -7.685 + 6.7123\left(\frac{10^3}{T}\right) - 1.6664\left(\frac{10^6}{T^2}\right) + 0.35041\left(\frac{10^9}{T^3}\right) \quad 2.11$$

$$1000ln\,(\alpha^* 2H) = 2.9992\left(\frac{10^9}{T^3}\right) + 1158.8\left(\frac{T^3}{10^9}\right) - 1620.1\left(\frac{T^2}{10^6}\right) + 794.84\left(\frac{T}{10^3}\right) - 161.04 \quad 2.12$$

where $\alpha^{*18}O$ and $\alpha^{*2}H$ are equilibrium fractionation factors for oxygen 18 and deuterium, respectively, T is temperature in degrees Kelvin (K).

Equilibrium between the isotopic composition of precipitation (δ_P) and atmospheric moisture is commonly assumed (Gibson, 2002), in cases where re-evaporated local moisture does not affect the isotopic composition of water vapour above open water bodies (i.e., re-evaporated moisture is transported downwind). In the case of equilibrium conditions, (Gibson et al., 2008) define:

$$\delta_A = \frac{(\delta_p - \varepsilon^*)}{\alpha^*}\ (‰) \quad 2.13$$

Equilibrium between the isotopic composition of atmospheric moisture (δ_A) and precipitation (δ_P) cannot be assumed in seasonal climates and cases where a large water body produces excess water vapour to the atmosphere (e.g. the Great Lakes in Canada) (Gibson et al., 2008; Yi et al., 2008).

The LEL extends from the isotopic composition of the input waters (δ_I) to the limiting isotopic composition (δ^*) (Figure 2.2), or maximum enrichment that the evaporating water body is approaching under local meteorological conditions (Gat, 1981; Gat & Levy, 1978; Gionfiantini, 1986). δ_{SS} is the steady state isotopic composition, which occurs when a system is in hydrologic equilibrium, or when inflow is equal to outflow and a water body is in equilibrium state.

2.4 Groundwater

Much of the isotopic signature of precipitation is preserved by deep groundwater, unless periodic recharge of evaporatively-enriched (or depleted snow melt contributions to) soil water occur (Gibson et al., 2008). In some circumstances, the average isotopic composition of groundwater and the annual precipitation signature will differ due to seasonal biases in recharge (Clark & Fritz, 1997). This most commonly happens during spring recharge. Groundwater will be slightly depleted in ^{18}O and ^{2}H than the weighted mean precipitation when spring recharge is greater compared to other times of the year (Clark & Fritz, 1997). Isotopic enrichment of groundwater can result from recharge comprised of evaporatively-influenced waters from bare soil, leading to an offset below GMWL (Gat, 1996).

Biases between the weighted average annual precipitation and groundwater signature can be due to impact of climate (Clark & Fritz, 1997). In many areas of Canada, precipitation and groundwater data correspond well. In western coastal and eastern regions, the $\delta^{18}O$ of precipitation is mostly retained in the groundwater signature. In drier, Prairie regions of Canada, deviations of more than 3‰ are notable (e.g., local groundwater at Wynyard, Edmonton, The Pas, and Gimli are more depleted than precipitation) (Clark & Fritz, 1997).

Usage of isotope tracers for labelling water sources and interactions between the surface and subsurface have become a topic of many groundwater studies, such as: interactions between groundwater and surface water in coastal area of the Great Lakes (Huddart et al., 1999), mine and mineral deposit hydrogeology (Douglas et al., 2000; Sie & Frape, 2002), and groundwater as a climate archive (Remenda & Birks, 1999; Birks et al., 2000). Groundwater was used as an end-member in isotope hydrograph separation studies (Carey & Quinton, 2005; James & Roulet, 2009; Bansah & Ali, 2017)

2.5 Snow

Because of phase change (from liquid to solid) and shifts in continental air mass during winter, snowfall is generally more depleted in heavy isotope than rainfall (Falcone, 2007). Fractionation is a result of phase change (freezing or thawing), temperature (Rayleigh distillation), and the continental affect. Snow sublimation (solid to vapour) can cause additional isotopic fractionation within a snowpack prior to pack ripening and melt phases. St Amour et al. (2005) reported negligible fractionation during sublimation, while (Moser & Stichler, 1980) found fractionation of $\delta^{18}O$ during sublimation to be up to 3‰.

With increasing temperature, snowpack temperature rises while the heat deficit of the pack decreases. Melting happens after enough energy has been accumulated to change state from solid to liquid. When melting occurs slowly, the interaction of meltwater and the solid snow pack is minimal. A study conducted by Stichler et al., 1981, suggested that in the case of no additional rain-on-snow during melt, equilibrium fractionation will result between the solid ice and liquid meltwater phases. Exchange of the snowmelt with the open atmosphere will produce kinetic fractionation, which affects meltwater and residual snow packs (Stadnyk-Falcone, 2008).

2.6 Water yield

Water yield (WY) is expressed as the depth of runoff (R) from the watershed. Estimation of WY assessment of regional hydrological variability has been addressed by using isotope mass balance (IMB) (Gibson et al., 2002). A study conducted by Bennett et al. (2008) in wetland-rich terrain of northeast Alberta compared isotope-based approach for calculating average WY for moderate to large watersheds with Water Survey of Canada hydrometric data suggested similar values. It seems that isotopes are able to capture low water yields in flat, disconnected terrain and very high-water yield in areas connected to groundwater flow systems. Variations in water yield estimates can be affected by isotopic variations (Bennett et al. 2008; Gibson et al., 2010 a; Gibson et al., 2010 b). Gibson et al. 2017 observed positively-skewed water yield distribution in all six blocks of lakes, which was noticeably reflected by the predominance of lakes with lower than average runoff (water yield) (Gibson, et al., 2017). The cause might be due to variations in topography, lake order and drainage configuration (Sherry & Soranno, 2006). Gibson et al., 2017 reported the average water yield of 377 mm which is similar to one reported by Bemrose et al. (2009) of 285-490 mm).

2.7 Current State of Isotope Hydrology Research

In the last fifty years, in the area of catchment hydrology, storm hydrograph separation using stable water isotopes (isotope hydrograph separation – IHS) went through some major advances. Introducing stable water isotopes for separating storm hydrographs into event and pre-event water was of significant importance because the method is measurable, and based on components of the water itself (Klaus & McDonnell, 2013). The partitioning between event and pre-event water (Hrachowitz et al., 2011; James & Roulet, 2009) has been assessed together with catchment runoff coefficient for better insight into the runoff generation process. In cases when event water percentage is high and runoff ratios very low, "inferences of near-stream overland-flow control on the hydrograph volume have been made" (Klaus & McDonnell, 2013).

Most IHS studies after 1970 use ^{18}O or ^{2}H as a hydrograph separation tracer. The separation of a storm hydrograph can be performed if isotopic signature is distinct between the two end-members, using a mass balance approach:

$$Q_t = Q_p + Q_e \tag{2.14}$$

$$Q_t\ C_t = Q_p\, C_p + Q_e C_e \tag{2.15}$$

$$F_p = \frac{C_t - C_e}{C_p - C_e} \tag{2.16}$$

where Q_t is the streamflow, Q_p is the contribution from pre-event water, Q_e is the contribution from event water, C_t, C_p, and C_e are isotopic compositions of streamflow, pre-event and event water, and F_p is the fraction of pre-event water in the stream. We should define pre-event ("old" water as water that is stored in a catchment prior to the precipitation event that is contributing to streamflow (Klaus & McDonnell, 2013). The event ("new") water is the water from the current precipitation event, or in case of a snowmelt, is melt water from the snowpack and probably rain during rain-on snow conditions (Klaus & McDonnell, 2013). Accounting for additional contributing end-members resolved in a multi-component approach, such as:

$$Q_t = Q_1 + Q_2 + Q_3 + \cdots + Q_n \quad 2.17$$

$$Q_t\ C_t = Q_1C_1 + Q_2C_2 + Q_3C_3 + \cdots + Q_nC_{n2} \quad 2.18$$

where Q_n is the discharge of a particular runoff component and C_n is the tracer concentration of a particular runoff component.

In some systems, the standard IHS approach results in unrealistic component mixtures, either exceeding 100% or falling below 0% (McDonnell et al., 1991; Blume et al., 2008). Therefore, the use of a three-component hydrograph separation is necessary. Many studies showed usefulness of a three-component separation, especially at a hillslope scale (event water, bedrock groundwater, and the soil water formed hillslope runoff) (Iwagami et al., 2010), as well as in steep, humid catchments for the similar compositional blend (McGuire & McDonnell, 2010). In

the case of three flow component separation, it is necessary to establish an additional (second) tracer or a measurement of a flow component (Klaus & McDonnell, 2013). Additional tracers can be silica (McGlynn & McDonnell, 2003; Iwagami et al., 2010), chloride (Ogunkoya & Jenkins, 1993; Jenkins et al., 1994; McHale et al., 2002), DOC (James & Roulet, 2009), EC (Carey & Quinton, 2005; Muñoz-Villers & McDonnell, 2012). Three component mixing models have been usefully applied in a variety of different climates and regions, such as in tropical catchments for investigations on the impact of forest disturbance and quantifying mixing water occurrences in the landscape (Buttle & McDonnell, 2004), during spring freshet in the Canadian tundra and discontinuous permafrost (Gibson et al., 1993; Carey & Quinton, 2005; St. Amour et al., 2005; Carey et al., 2013) (estimated to be between 20% and 50% melt water contributing to the total hydrograph). IHS models were used in a low-relief fen-dominated catchment area in Manitoba, Canada, comparing two freshet periods (Metcalfe & Buttle, 2001). A difference in the contribution of snowmelt to peak discharge of 78% vs 28% between two years which was attributed to a difference in active layer thickness between years was found by the study.

Bansah and Ali (2017) conducted a two-component IHS study in the Prairie region of Canada (province of Manitoba) to evaluate the effect of end-member definitions and tracer choice (δ^2H and $\delta^{18}O$). Wide-ranging scenarios based on one "new" water and one "old" water end-member definition, and one tracer were evaluated. Eight potential definitions per end-member and two tracers were combined. Each combination of a "old", "new" end-member and a tracer formed a methodological scenario (total of 80, 40 based on δ^2H, and 40 based on $\delta^{18}O$) (Bansah & Ali, 2017). In general, fraction values of old water using $\delta^{18}O$ data were higher than ones using δ^2H across eight outlets. Some sites showed larger discrepancies versus others. The best agreement

between δ^2H and $\delta^{18}O$ fraction of "old" water was observed in early spring, when temperatures are cooler which leads to minimal isotopic fractionation (Bansah & Ali, 2017).

Some studies have proven the inability of a two component IHS to separate soil water and groundwater causing contribution of "old" water to exceed 100% or fall below 0% (Blume et al., 2008). This resulted in a three-component separation method that adds a geographic source component in addition to the time source (Bansah & Ali, 2017). When comparing two- and three- component IHS results, some studies reported similar results between the approaches (Carey & Quinton, 2005; Muñoz-Villers & McDonnell, 2012) while others found a discrepancy (approximately 10% difference in "old" water contribution between two methods) (Wenninger et al., 2004).

3 Data Collection Methodology

3.1 Climate Data

Canadian Prairie climate ranges from dry, semi- arid to somewhat dry, humid continental as classified by the Koppen-Geiger climate (*Dfb*) classification system (Chen & Chen, 2013). The regional climate of the Delta Marsh watershed is characterized as warm-summer humid continental, with short summers (mean temperature 20°C in July), and cold winters (mean temperature -20°) (Haig et al., 2020). Low and high average annual temperatures are -16.6°C and 18.5°C, respectively for Delta Marsh climate station and -17°C and 18°C for Brandon station (Figure 3.1). During the study period (approximately May to the end of October 2013-2016), mean temperature was 15°C, mean precipitation was 303 mm, and mean relative humidity was 78%. Precipitation across the Canadian Prairies is formed by any combination of orographic (originating from the Canadian Rockies), and frontal and convective uplifting mechanisms due to large spatial extent of the Prairie (Schellenberg, 2017).These annual averages were collected at Portage Southport station (climate ID: 5012324) (http://climate.weather.gc.ca/) since the records from meteorological stations installed by Ducks Unlimited did not include the data for a whole year, mainly for spring and summer months.

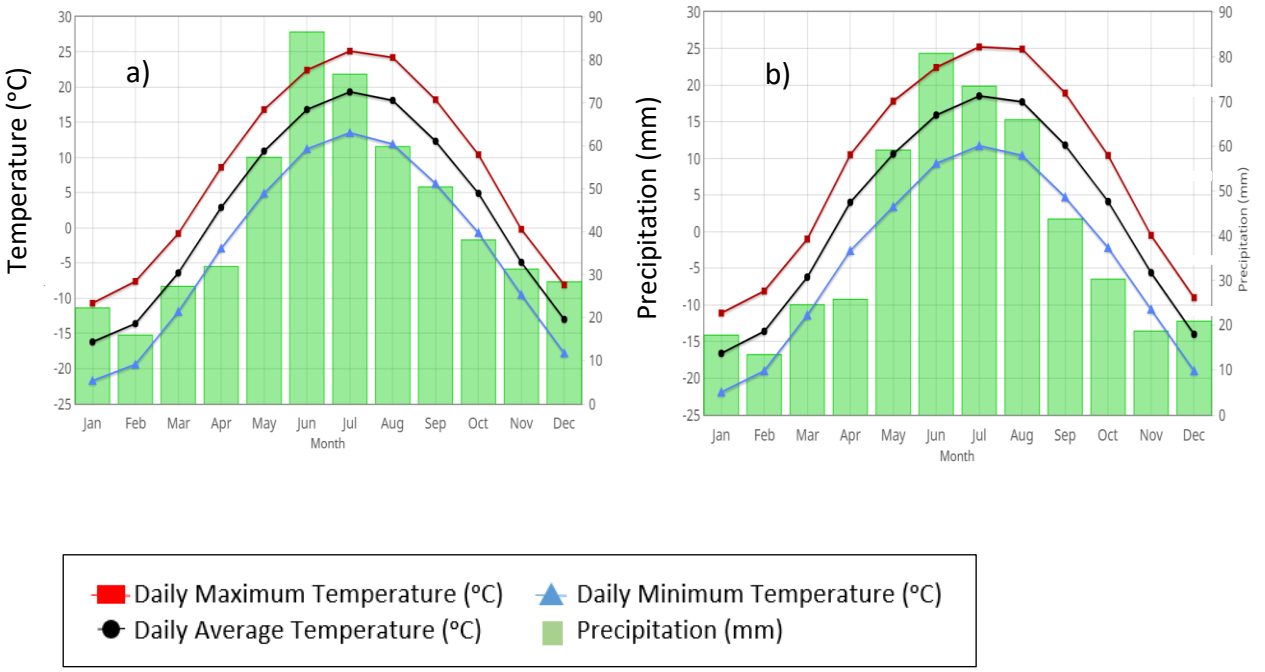

Figure 3.1 - Climate normals for a) Delta Marsh CS station (ID: 5040764, lat. 50°18'N, long. 98° 23' W) and b) Brandon(ID: 5010480,, lat. 49°54'N, long. 99° 57' W, located 150 km west of Delta Marsh) (http://climate.weather.gc.ca/).

This study covers only the area of the Marsh dubbed "East Marsh". For the purpose of this study, we separated the study area into West and East Marsh (Figure 3.2). This was done based on the hydraulic study (Aminian, 2015), which showed the Gap to be a connective channel between the two sections. West Marsh is comprised of Cadham Bay only (area between Delta Channel and the Gap), while East Marsh covers area east of the Gap and west of the Clandeboye Channel. The major exchange of water between our study area and Lake Manitoba is via Delta and Clandeboye Channels. Delta Channel carries 15% of inflow from lake Manitoba, while Clandeboye Channel 85% (Aminian, 2015).

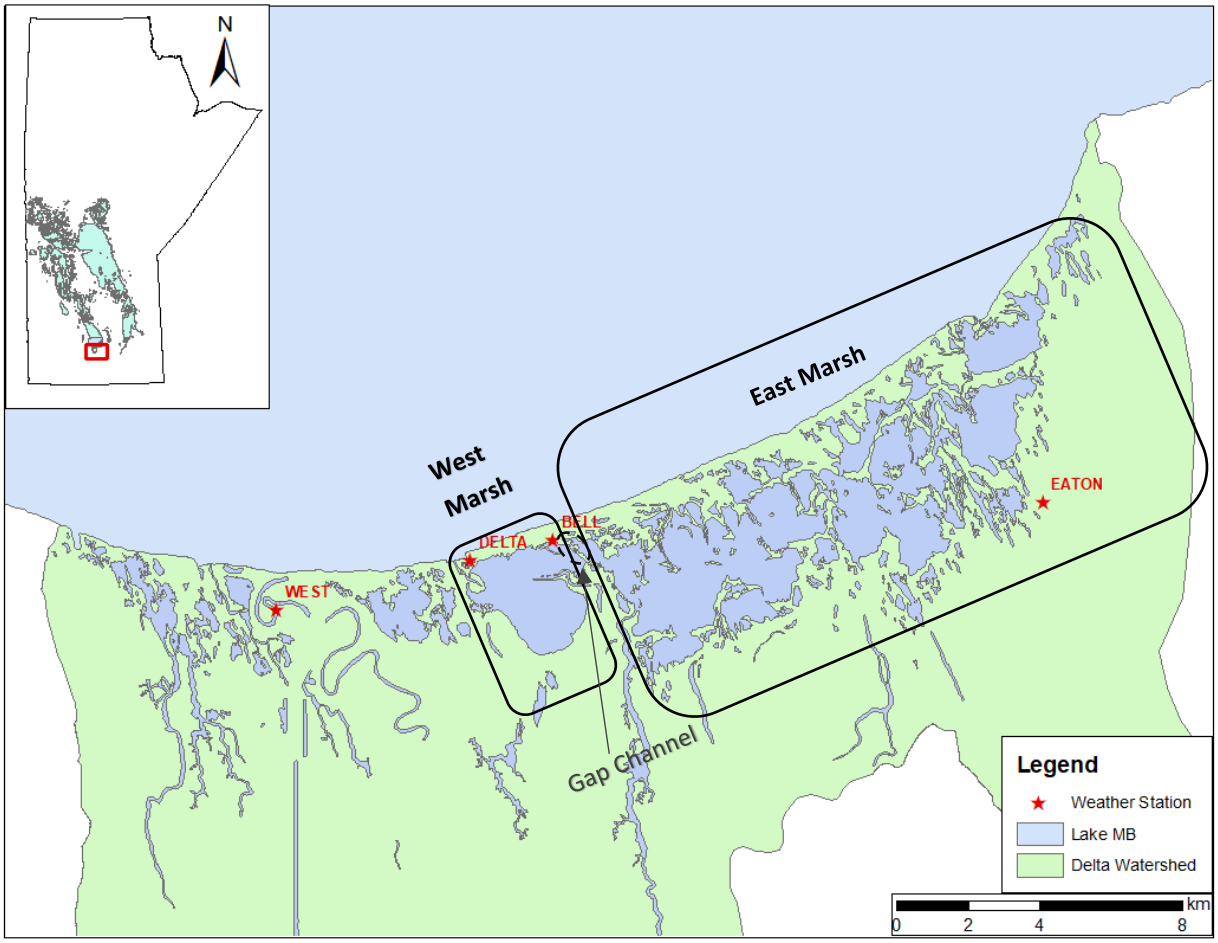

Figure 3.2 – Study site: West and East Delta Marsh

Over the course of the four-year study period, four meteorological (MET) stations were established and monitored (Figure 3.2). Data collected across the entire study domain consisted of: precipitation (mm), air temperature (°C), relative humidity (%), wind speed (km/h), wind direction (ϕ), wind gust (km/h), PAR (photosynthetically active radiation in µmol/m^2/s)) and evaporation using a class A evaporation pan (Figure 3.3). Data from the evaporation pan, was not used since it was not consistently installed at the start of the field season, nor were these data collected according to the National standard. The evaporation pan was monitored by the research station, and we were advised it was not being setup and monitored according to ECCC (Environment and Climate Change Canada) standards and that we should be careful with

utilizing these data. All other climate data were recorded every 15 minutes. Note that the wind direction (not wind speed) reading was erroneous all years prior to 2016, therefore wind data from Oak Point station were used.

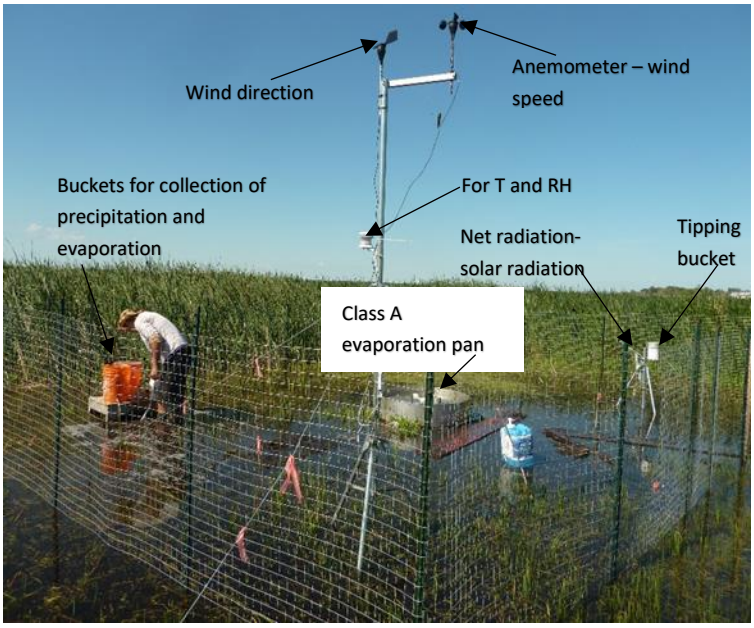

Figure 3.3 - Eaton Lodge weather station

In 2013 and 2014 two MET stations, Bell Landing and Eaton Lodge, were in operation (Figure 3.2,Table A.1). Due to a large storm on July 1, 2014 and subsequent flooding of the area, the Bell Landing station was relocated to Delta Station. In 2015 MET stations were located at Eaton Lodge and West Marsh. The West Marsh weather station was located just west of the Portage Diversion, near the old University of Manitoba field station. In 2016, three MET stations were operating - Eaton Lodge, Delta Station and West Marsh. Meteorological data from the stations located at Bell, Delta Station, and West station were used for West Marsh analyses; and Eaton Lodge was used for East Marsh analyses. MET stations were not installed at the same time, nor operated for the same period of time. Meteorological data were recorded every 15 minutes. In the

case of missing data from one station, data from the other were used to infill the station record. In the case of missing data from both stations, data from Portage Southport station (http://climate.weather.gc.ca/) were used to infill. Table 3.1summarizes total precipitation for period June 25 to October 31 for the four weather stations that were operated at Delta Marsh during 2013 to 2016 (as per correspondence with Bob Emery). On average, the 2015 field season had the highest amount of precipitation (325 mm), followed by 2013 (215 mm), 2016 (169 mm), and the least amount of rain fell in 2014 (104 mm).

Table 3.1 - Total precipitation for June 25 – October 31 (mm) for four weather stations during 2013 – 2016

	Precipitation in mm at Weather Stations			
Year	***Bell***	***Delta***	***Eaton***	***West***
2013	*226*		*204*	
2014	*96.1*	*119*	*97.3*	
2015			*278*	*370*
2016		*99.8*	*178*	*229*

3.2 Hydrologic and Hydraulic Data

In order to better understand the hydrology of Delta Marsh, surface runoff was monitored at several locations (streams and culverts) throughout the open water season of 2014-2016; with emphasis placed on the spring freshet in 2014 and 2015 (Schellenberg, 2017). The south to north flow from the watershed to the Marsh was measured at several culverts along provincial road PR 227 (Figure 3.2 at Schellenberg (2017)). Discharge was recorded using a SonTek Argonaut

Shallow Water Acoustic Doppler Velocimeter (ADV) and SonTek FlowTracker handheld ADV. For flow measurements at Portage Creek, the channel with the largest expected inflow contribution, an Argonaut device was used. More information on field monitoring methods and equipment can be found in Schellenberg (2017).

For the purposes of hydrodynamic modelling, hydraulic monitoring was also conducted during the 2013 and 2014 open water season. Water levels were measured throughout the Marsh using Solinst LeveLoggers, while velocity and discharge were measured at major channels. Velocity measurements were taken using two SonTek Argonaut Shallow Water ADVs, while for discharge measurements a SonTek River Surveyor M9 ADCP was used (Aminian, 2015). Discharge measurements were taken approximately bi-weekly at Delta Channel, Portage Creek, Crooked Creek, Fish Creek, and Waterhen Creek. Discharge was measured at Waterhen Creek. According to Aminian (2015), discharge at Waterhen Creek was multiplied by a factor of 1.42 in order to simulate the discharge from Clandeboye Channel. In both hydraulic and hydrologic data records and analyses, positive values denote flows *toward* the Marsh, and negative denotes flows *away from* the Marsh. In case of a connection channel within the Marsh (i.e., the Gap), positive flow was defined from west to east.

3.3 Isotope Data

Collection of stable water isotope samples was conducted together with collection of hydrological and hydraulic data. The stable water isotopes were collected over a period of four years, from 2013 to 2016, at over 103 sampling locations (Figure 3.4) in order to establish an isotopic framework and compare isotopic methods with a hydraulic approach. Stable water

isotope samples of precipitation, Marsh water, rivers (from upland sources), channels, groundwater, evaporation, and Lake Manitoba were collected by University of Manitoba graduate and summer students. A table with stable water isotope locations is shown in Appendix (Table A.1). Samples were collected mainly during the ice-free period, from May until the end of October with some under-ice marsh water, ice core, and snowpack samples collected during the winter and spring seasons. A narrow-mouthed 30 mL HDPE bottle was used for sample collection; bottles were filled to the top with water and immediately sealed and taped at the neck to ensure no evaporation or water loss occurred. Bottles were labeled with the full station number and date prior to wetting using the standard format:

[Type]-DELTA-[Location]-[Date]-[Sample Number]

Two samples from each site were collected, with the second one being labelled as a duplicate. A total of 2145 samples were analyzed with 4290 being collected using a gas source mass spectrometry instrument. During a two-year period (2013-14), 1774 samples were collected. Samples were sent to the Innotech Alberta Laboratory, British Columbia, for analysis with every 10^{th} duplicate included as a blind, quality control (QC) sample to ensure results were within analytical uncertainty. Analytical uncertainty for δD and δ^{18}O was 1‰ and 0.2‰, respectively. Any duplicate samples returned with error exceeding expected analytical uncertainty were reanalyzed by the laboratory. If results exceeding analytical uncertainty limits were once again returned, samples were removed from the dataset on account of presumed sample collection error. Isotope results were expressed in δ notation (in per mil, ‰) relative to Vienna Standard

Mean Ocean Water (VSMOW-2) such that $\delta_{sample} = 1000 \cdot (\frac{R_{sample}}{R_{SMOW}} - 1)$, where R = $^{18}O/^{16}O$ or R = $^{2}H/^{1}H$.

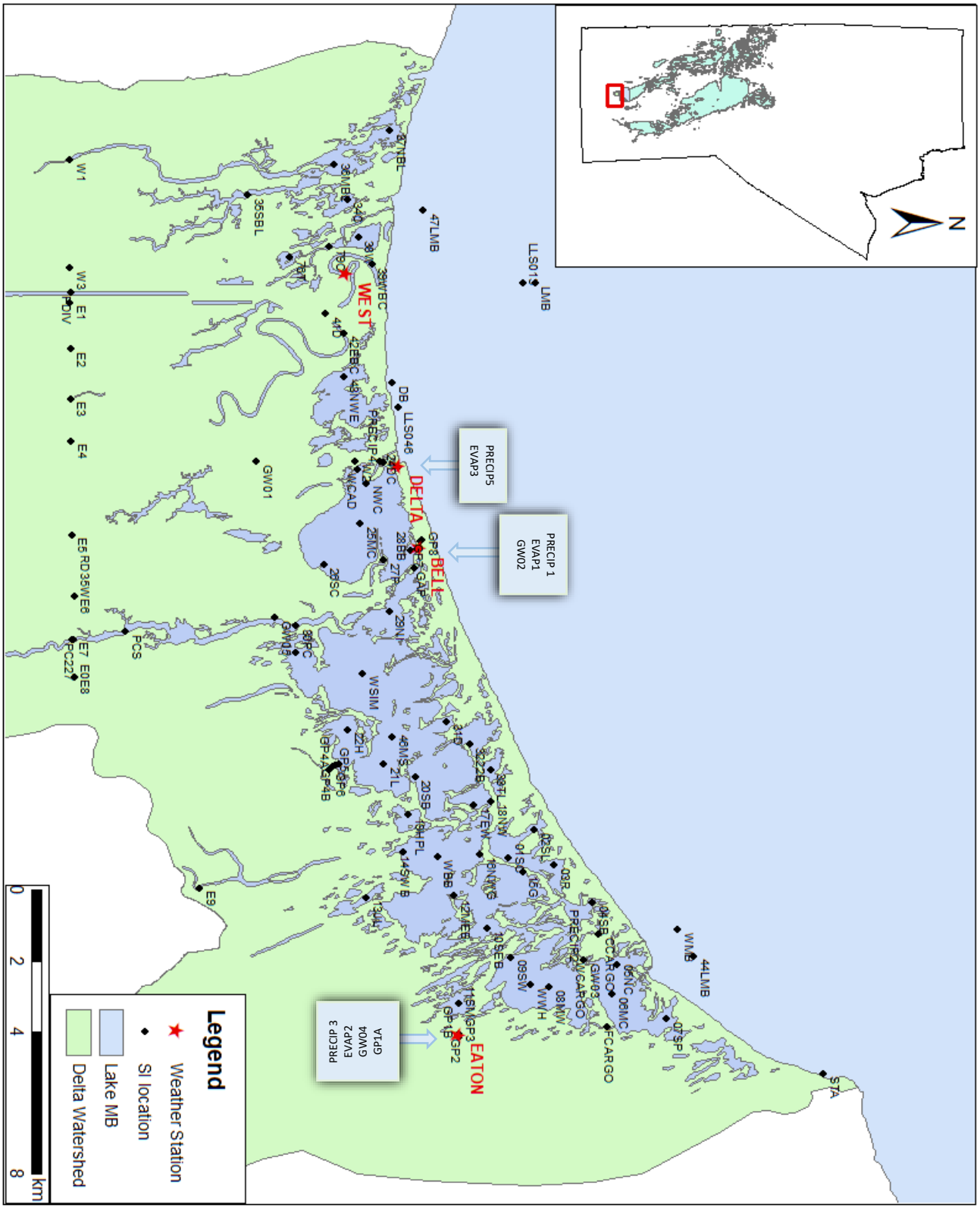

Figure 3.4– Stable isotope sampling locations

3.3.1 Precipitation Samples

For collecting stable isotopes in precipitation, two plastic 5-gallon buckets were installed per year at two different locations, one representing the East Marsh signature, and the other the West. Mineral oil was used to cover the bottom of the bucket and prevent evaporation of precipitation accumulating in the bucket. A tap was installed at the bottom of the bucket for easier sampling (and to avoid sampling the oil), and a mesh screen cover was placed on top to prevent debris accumulation or small animals from entering the bucket. The buckets were mounted on a platform (2 ft high) and secured with ropes to prevent tipping (Figure 3.5). Before sampling, the bucket was stirred to ensure a representative composite precipitation sample was taken and avoid oil mixing with the taken sample.

Figure 3.5 - Plastic bucket used for precipitation sample collection

Immediately after precipitation samples were taken, the remaining water in the bucket was emptied and a new layer of mineral oil was put on the bottom of the bucket. In 2013 and 2014

one bucket was placed at Bell station and the second at Waterhen Creek. In 2015 the two buckets were installed, one at Delta Channel and the other at Eaton Lodge, while in 2016, one was placed at Waterhen Creek and one at Delta station. Location of the buckets changed depending on logistic support for other components of the project (e.g. discharge measurement, TSS measurements) or just convenience. On average, composite precipitation samples were taken every 7-14 days from the beginning of May until the middle of October. Event-based precipitation sampling was not performed due to accessibility to the Marsh and the buckets. Table 3.2 shows precipitation samples collected throughout a four-year period. All precipitation sampling locations are presented in Table A.1.

Table 3.2 - Number of precipitation samples collected per year . "TOTAL" represents number of samples collected over a four-year period, "TOTAL with duplicates" represents number of samples with duplicates that were sent for analysis.

Precipitation Samples				
Location ID	**2013**	**2014**	**2015**	**2016**
PRECIP1	9	8		
PRECIP2	8	8		12
PRECIP3			15	
PRECIP4			14	
PRECIP5				16
TOTAL	**17**	**16**	**29**	**28**
TOTAL with duplicates	**17**	**18**	**32**	**34**
Number of sites	**2**	**2**	**2**	**2**

3.3.2 Evaporation Samples

For collecting stable water isotopes in evaporation, nearly identical buckets to those used for precipitation sampling were installed alongside the precipitation buckets (on the same platform). These buckets did not have a tap at the bottom, and were instead initially filled (with nearby marsh water) to the top, and were also covered with a mesh screen. No oil was added to these buckets. Before sampling, water was stirred by hand to ensure complete mixing through the water column, and then and a sample bottle was submerged and filled with water. These buckets were typically refilled with Marsh water once during the sampling season, but only after nearly all water had been evaporated from the bucket. Between 2013 and 2016, three buckets were installed for evaporation sampling. They were located each at one of the MET stations together with the precipitation buckets. In 2013 the evaporation bucket was installed at Bell Landing, in 2014 at Eaton Lodge, and in 2015 at Delta Station. Table 3.3 shows evaporation samples collected throughout the four-year period, used to help define the limiting maximum enrichment of the Marsh water for a given season. All evaporation sampling locations are shown in Table A.1.

Table 3.3 - Number of evaporation samples collected per year . "TOTAL" represents number of samples collected over a four-year period, "TOTAL with duplicates" represents number of samples with duplicates that were sent for analysis.

Evaporation Samples				
Location ID	**2013**	**2014**	**2015**	**2016**
EVAP1		9		
EVAP2			20	15
EVAP3				17
TOTAL	**0**	**9**	**20**	**32**
TOTAL with duplicates	**0**	**14**	**24**	**37**
Number of sites	**0**	**1**	**1**	**2**

3.3.3 Marsh Water Samples

Stable isotope samples were collected by our team from 24 sampling sites throughout the Marsh over the course of 4 years; with some sites added, relocated or shut down during this period (Table A.1). Several times during the winter period (on average, once per month) snow and ice sampling, together with under-ice water sampling was conducted at several locations per year to capture the end of season (baseflow) isotopic composition. In 2016, a synoptic survey of the Marsh was conducted six times during the summer season, which was coordinated by Professor Gordon Goldsborough's group of students from the Faculty of Science (Biology) for the purposes of surveying water quality across the Marsh (Table 3.4). A total of 27 sites (Table A.1) were sampled during the synoptic surveys (sampling locations 35SBL and 37NBL are listed under Marsh samples because they were sampled in previous years) (Table 3.4). Marsh water samples were collected using a narrow-mouthed 30 mL HDPE bottle filled to the top, sampled

from approximately 0.5 m depth below the surface to avoid the fractionated surface boundary layer. The bottle was sealed and neck taped to prevent evaporative fractionation post-sampling.

Table 3.4 - Number of Marsh samples collected per year together with 2016 synoptic survey . "TOTAL" represents number of samples collected over a four-year period, "TOTAL with duplicates" represents number of samples with duplicates that were sent for analysis.

	Marsh Samples				***Synoptic Survey***	
Location ID	**2013**	**2014**	**2015**	**2016**	**2016**	
01SC	*16*	*16*	*21*	*18*	**02SL**	6
04SB	*16*	*15*	*20*	*18*	**03R**	6
05NC	*10*	*7*	*11*	*19*	**07SP**	6
06MC	*10*	*10*	*12*	*19*	**08MW**	6
09SW	*9*	*10*	*11*	*12*	**10SEB**	6
11SM	*10*	*15*	*21*	*15*	**13JL**	7
12MEB	*16*	*16*	*20*	*19*	**14SWB**	6
16NWG	*9*	*9*	*11*	*11*	**15G**	5
17EW	*17*	*14*	*21*	*17*	**18NW**	1
20SB	*9*	*10*	*12*	*11*	**19HPL**	7
23TT	*9*	*8*	*12*	*14*	**21L**	5
25MC	*17*	*18*	*21*	*20*	**22H**	6
29NI	*10*	*10*	*11*	*11*	**26SC**	6
3222B	*10*	*9*	*11*	*11*	**27P**	2
46MS	*17*	*15*	*20*	*19*	**28BB**	6
NWC	*10*				**31D**	6
15G			*1*		**33TL**	*6*
35SBL	*5*	*6*	*2*	*6*	**34C**	6

37NBL	*5*	*6*	*2*	*6*	**36MBL**	6
38W	*3*	*6*	*2*	*6*	**39WBC**	1
43NWE	*1*	*4*	*3*	*6*	**42EBC**	1
SEC	*1*				**44LMB**	2
WBB-under ice		*1*	*1*	*1*	**45PCB**	6
WMB-under ice		*1*			**47LMB**	4
WSIM-under ice		*2*	*1*	*1*	**76T**	6
WWH-under ice		*2*	*1*	*1*	**TOTAL**	**132**
TOTAL	***210***	***210***	***249***	***255***	**TOTAL *with duplicates***	**147**
TOTAL with duplicates	***251***	***274***	***287***	***428***	**Number of sites**	**25**
Number of sites	***21***	***23***	***23***	***22***		

3.3.4 Lake Manitoba Samples

Lake Manitoba water was collected at four locations (Table 3.5). Lake Manitoba stable water isotope samples were collected by University of Manitoba students (close to Delta Beach), and by Manitoba Water Stewardship employees (all other sampling locations). On average three times per winter season, Lake Manitoba was sampled by University of Manitoba crew under ice at one location only (LLS013). All Lake Manitoba sampling locations are presented in Table A.1.

Table 3.5 - Number of Lake Manitoba samples collected per year . "TOTAL" represents number of samples collected over a four-year period, "TOTAL with duplicates" represents number of samples with duplicates that were sent for analysis.

Lake Manitoba Samples				
Location ID	**2013**	**2014**	**2015**	**2016**
LLS013	8	20	8	3
LLS046	7		1	
DB	1	5	3	
STA		5		
TOTAL	**16**	**30**	**12**	**3**
TOTAL with duplicates	**20**	**35**	**14**	**3**
Number of sites	**3**	**3**	**3**	**1**

3.3.5 River Inflow Samples

River and channel inflow samples were taken simultaneously with velocity and discharge measurements at corresponding sites. Primary flow paths connected Delta Marsh with Lake Manitoba and the surrounding watershed, which were defined as rivers; while channel flow paths were defined within the Marsh based on interconnected, narrow "channelized" areas. The number of samples per year per location, and total number of samples are shown in Table 3.6 and Table 3.7 for river and channel samples, respectively. Sampling locations (latitude and longitude) of river and channel samples are shown in Table A.1.

Table 3.6- Number of river samples collected per year . "TOTAL" represents number of samples collected over a four-year period, "TOTAL with duplicates" represents number of samples with duplicates that were sent for analysis.

River samples				
Location ID	**2013**	**2014**	**2015**	**2016**
24DC	24	16	22	18
30PC	17	15	20	16
41D	1	1	4	6
CCARGO	22	16	19	
FCARGO	22	12	19	
WCARGO	21	19	23	13
240CD		9	11	6
DELTAE0		2		
DELTAE1		1	3	1
DELTAE2		7	3	1
DELTAE3		5	2	1
DELTAE4		6	2	1
DELTAE5		1		
DELTAE6		1		1
DELTA E7			6	1
DELTAE8		1	3	1
DELTAE9		1		1
DELTAW1		6	5	1
DELTAW2		1		
DELTAW3		1	3	1
PC227		7		

PCS		1		
PDIV		9		
RD35W		6	3	
ROY		6		
TTCUL				1
TOTAL	**107**	**150**	**148**	**70**
TOTAL with duplicates	**119**	**177**	**163**	**79**
Number of sites	**6**	**23**	**16**	**16**

Table 3.7 - Number of channel samples collected per year . "TOTAL" represents number of samples collected over a four-year period, "TOTAL with duplicates" represents number of samples with duplicates that were sent for analysis.

Channel Samples				
Location ID	**2013**	**2014**	**2015**	**2016**
79C	3	6		6
GAP	9	8	11	5
18NW				5
27P				4
39WBC				5
42EBC				5
TOTAL	**12**	**14**	**11**	**30**
TOTAL with duplicates	**14**	**17**	**11**	**30**
Number of sites	**2**	**2**	**1**	**6**

3.3.6 Groundwater Samples

For the collection of groundwater, several wells were drilled over the course of the four-year study period, with one previously existing well also utilized for sampling (GW01); owned by the Rural Municipality of Portage la Prairie. The existing well was located approximately 0.5 km west of the PR 240 provincial road, which was approximately 7.3 m deep, and was equipped with a hose and a tap for municipal usage (and sampling).

The installed wells GW02-GW05 were approximately 1.5 m deep consisting of a PVC pipe (non-perforated) hand augured into the soil, with a pipe head extending above ground and capped with a metal lid. To extract water, a plastic hose with a hand pump was inserted through the pipe and samples were taken by pumping water through the hose. GW02 and GW03 were installed in 2014, and GW04 and GW05 in 2015. When water levels were low, samples could not be extracted.

Wells GP1A – GP8 were installed from the end of 2015 to the beginning of 2016 in order to expand groundwater monitoring efforts (Figure 3.6). On average, the depth of these wells was 1.5 m, with two deeper ones (approximately 2.2 m for GP1A and GP4A). Each well was equipped with a level logger. Before sample extraction, the logger was removed from the well, and the well was purged using a 5 cm diameter plastic bailer (1 m long with a stop ball). Depending on the well, water was purged on average 6-10 times (or until the water being removed was clearer and contained less grit) prior to sampling, to ensure representative (flowing) groundwater samples. Total number of groundwater samples collected over four-year period is shown in Table 3.8. All groundwater sampling locations are presented in Table A.1.

Figure 3.6 - A completed GP5 well installation. A plastic pipe with a lid sticking out of the ground. Contact person information were written on the white stick (beside the pipe).

Table 3.8 - Number of groundwater samples collected per year. "TOTAL" represents number of samples collected over a four-year period, "TOTAL with duplicates" represents number of samples with duplicates that were sent for analysis

Groundwater Samples				
Location ID	**2013**	**2014**	**2015**	**2016**
GW01	17	16	10	17
GW02		7		
GW03		4	15	9
GW04			4	
GW05			13	4
GP1A				10
GP1B				13
GP2				12
GP3				11
GP4A				15
GP4B				18
GP5				11
GP6				9
GP7				15
GP8				14
TOTAL	17	27	42	158
TOTAL with duplicates	18	33	46	173
Number of sites	**1**	**3**	**4**	**3**

3.3.7 Snow and Ice-on Samples

The winter sampling program for snow and ice started in February 2013. During all four winters monthly trips started in December (after competent ice formed) and finished in March (prior to ice breakup). Stable water isotopes for composite (Table 3.9) and depth-dependent (Table 3.10) snow packs were collected, while ice core samples were stratified (Table 3.11). Both, snow and ice core depth dependent samples were taken in 20 cm increments. In cases where snow depth was less than 20 cm, then increments were reduced to 10 cm intervals. For example, first sample was labeled as DD1 (depth dependent sample taken at first depth between 0-20 cm), second as DD2 (taken between 20-40 cm) and so on. DD1 refers as the first snow to fall or ice to freeze. Snow samples collected at certain depth were packed into bottles, taped at the neck and sent to the laboratory for analysis. Snow was left to melt in a bottle, meaning a bottle was not full once the ice turned to liquid. Ice cores were drilled using Kovacs Ice corer powered by an auger head. An ice core was cut into 20 cm long pieces, each representing certain depth, put into zip lock bag to melt and then transferred into a 30ml HDPE bottle. During some of the trips, Marsh and Lake Manitoba water was sampled under ice (when clean water could be obtained above the bottom sediment layer).

Table 3.9 - Number of snow composite samples collected per year . "TOTAL" represents number of samples collected over a four-year period, "TOTAL with duplicates" represents number of samples with duplicates that were sent for analysis.

Snow Composite Samples				
Location ID	**2013**	**2014**	**2015**	**2016**
NWC	1			
WCAD	1	4	3	2
TOTAL	**2**	**4**	**3**	**2**
TOTAL with duplicates	**2**	**5**	**3**	**3**
Number of sites	**2**	**1**	**1**	**1**

Table 3.10 - Number of snow dependent samples collected per year. "TOTAL" represents number of samples collected over a four-year period, "TOTAL with duplicates" represents number of samples with duplicates that were sent for analysis.

Snow Depth Dependent Samples				
Location ID	**2013**	**2014**	**2015**	**2016**
NWC	2			
SEC	3			
WCAD	2	8	7	2
TOTAL	**7**	**8**	**7**	**2**
TOTAL with duplicates	**7**	**9**	**8**	**2**
Number of sites	**3**	**1**	**1**	**1**

Table 3.11 - Number of ice core samples collected per year. "TOTAL" represents number of samples collected over a four-year period, "TOTAL with duplicates" represents number of samples with duplicates that were sent for analysis.

Ice Core Samples				
Location ID	**2013**	**2014**	**2015**	**2016**
NWC	2			
SEC	3			
25MC		11		3
WWH		10		3
TOTAL	**5**	**21**	**0**	**6**
TOTAL with duplicates	**8**	**24**	**0**	**6**
Number of sites	**2**	**2**	**0**	**2**

3.3.8 Laboratory Analysis

All isotope samples were sent to the Innotech Alberta Laboratory located in Victoria, British Columbia for analysis. A gas source mass spectrometry instrument was used for measuring isotopic ratios of light elements, including hydrogen, carbon, nitrogen, and oxygen. This instrument consists of three parts: (1) a source of positively-charged ions or molecules, (2) magnetic analyzer, and (3) ion collector. Analysis for deuterium was run using an established method on a Delta V Advantage mass spectrometer, and a GasBench II peripheral. Results are accurate to ± 0.2 per mille. Analysis for oxygen –18 was run using an established method on a Delta V Advantage mass spectrometer, and a HDevice peripheral. Results are accurate to ± 1 per mille. For a description of this methodology, see Nelson (2000). The results of deuterium and oxygen-18 mean values, together with standard deviation for every 10^{th} sample and two runs of

analysis (second run was done for each 10^{th} sample) were sent back to us in an Excel spreadsheet.

3.4 Summary

Over the course of the four-year study, 103 stable water isotope sampling locations were established across Delta Marsh, with 1774 samples collected during the 2013-14 period and 2145 during 2013-16. Representative source water and hydrologic "end point" samples were collected from precipitation (rain and snow), evaporating water, ice, groundwater, open Marsh water (and under ice cover), rivers from upland source areas, and channels into and out of (and within) the Marsh. Lake Manitoba water was also sampled. A total of 4290 samples (with duplicates) were collected over the entire study period (2013-2016). Some sampling locations were added, moved or terminated due to logistical support, access and necessity to the sampling program.

4 Development of Isotope Framework

4.1 Introduction

The conceptual dual isotope framework, or $\delta^{18}O$-$\delta\ ^{2}H$ plot, incorporates all isotope samples and was used for better understanding the Marsh water balance and relative importance and contribution of water balance components. A box-whisker plot was created to better understand the statistical spread of the samples, number of unique end members (source water components), and relative geographical position of influence for end member components.

4.2 Methodology

The box-whisker plot was created using all samples collected from the Marsh (along with "*river*" and "*channel*" samples – defined in Chapter 3.3.5), Lake Manitoba, groundwater, and precipitation from the four-year study period. The plot in Figure 4.1 shows distribution of $\delta^{18}O$ (deuterium was also plotted and behaved similarly, not shown) from 2013-2016. Sampling locations were ordered longitudinally from west to east. A two-year box whisker plot was created to give a better perspective on marsh statistics between the two- and four-year periods (the former is presented in Figure A.2 in Appendix A). Duplicate samples are excluded from both the framework and box-whisker plots.

The study site encompasses an area from Delta Channel on the west to Clandeboye Channel on the east. The Gap is considered to be a dividing point (based on hydraulic portion of the larger Delta Marsh study) between the two subsections.

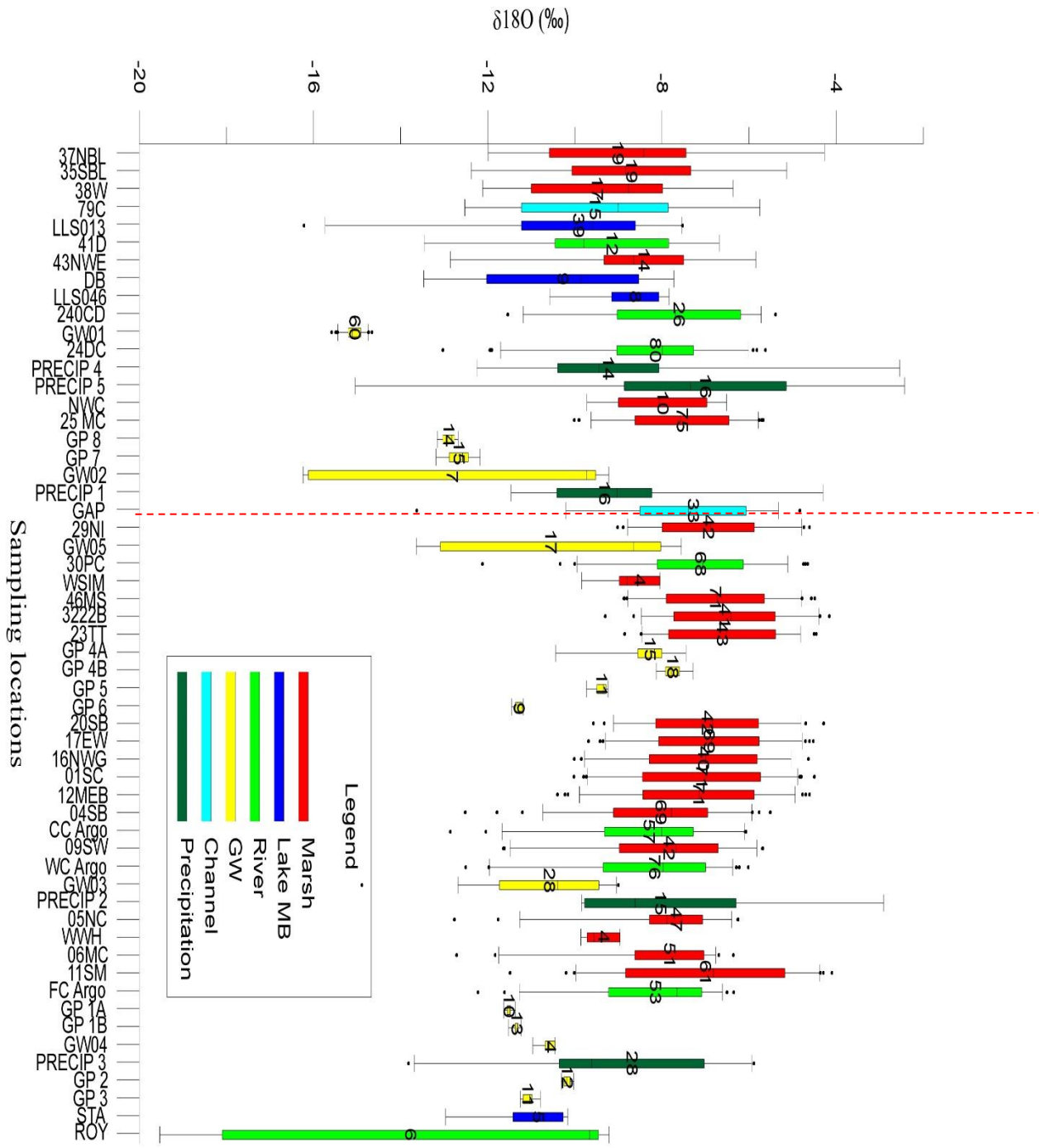

Figure 4.1 - Box-whisker plot of variability in $\delta^{18}O$ across Delta Marsh for period 2013 – 2016. Stations ordered longitudinally from West to East. Numbers in the middle of each bar represent number of samples collected over period of four years. The black dots represent outliers.

The solid bars in each box represent the station median, with upper and lower limits of the bars representing the upper and lower quantiles. Upper and lower whiskers represent 5^{th} and 95^{th} percentile, and IQR (interquartile range) are 25 and 75, and outliers were calculated at 1.5 times IQR. The box-whisker plot shows almost uniform median among the Marsh samples in the East Marsh, while there are some fluctuations in the West due to more inflow captured by the river samples. Similar trends are observed in box-whisker plot analysis over the two-year period, suggesting that it was a representative period of sampling for longer-term conditions and end member sources. The stable isotope signature over four years is slightly more enriched (0.5 per mille) compared to period from 2013-2014.

Marsh stable isotope composition varies from east to west across the Marsh, influenced by distinct end member (source water) components, and evaporation. The influence of evaporation is most apparent mid-marsh (approx. 46MS), where there is little influence from rivers or Lake Manitoba, and the isotopic composition is on average 2-3 per mille more enriched than the eastern and western sections of the Marsh, which show greater influence of Lake Manitoba inflows. Spatial variability of open water stable isotopes ($\delta^{18}O$) collected over the four-year study period is presented in Figure 4.2. Data were temporally averaged across the four-year period, which likely smoothes isotopic variability in some degree. We can see a uniform, more enriched signature across middle section of the Marsh (approximately -6.55 ‰ for $\delta^{18}O$). West and east sections, which are more connected to Lake Manitoba, show more pronounced depletion in isotopic signature, suggesting influence of the lake itself; or groundwater which is similarly depleted. Given their similar isotopic compositions, it is difficult to distinguish groundwater from Lake Manitoba influence. Far east section (in orange/red) shows the most depleted

signature (approximately -11.40 ‰ for $\delta^{18}O$) although there is no direct connection with Lake Manitoba. Ridge separating the lake and the Marsh is sand, allowing lake water coming through and hence we see pronounced depletion in signature. Old timers suggest that there are 'springs' in the Marsh (anecdotal). Spatial variability of deuterium (δD) is shown in Appendix A (Figure A.3).

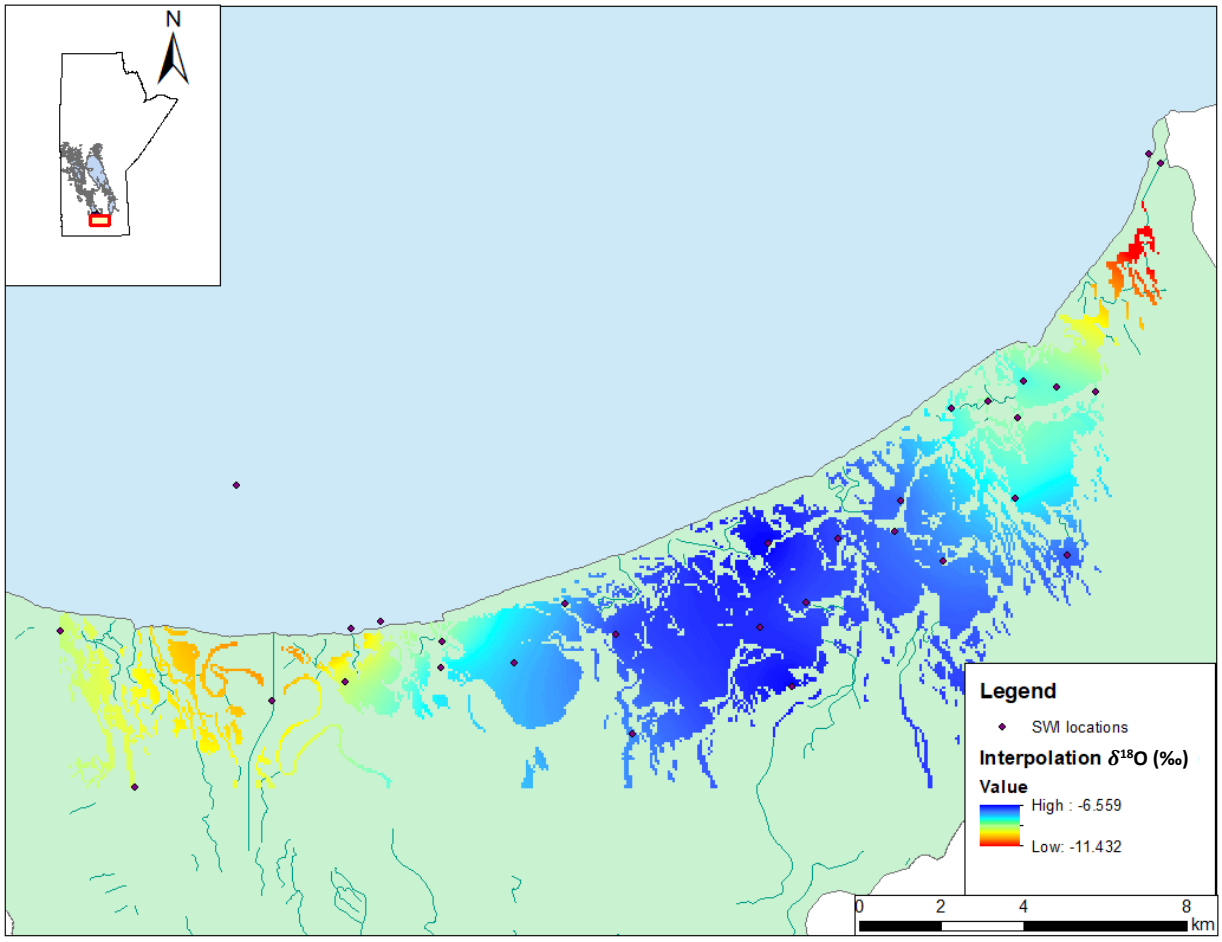

Figure 4.2 – Spatial mapping of $\delta^{18}O$-seasonal average for period 2013-2016. More uniform signature across middle section of Delta Marsh with pronounced depletion toward west and east sections.

From the box-whisker plot (Figure 4.1), end members associated with precipitation (meteoric water), groundwater, Marsh inflows (including rivers and Lake Manitoba), and evaporation are

observed to impact the composition of Marsh water geographically. A more detailed analysis of the sampling methodology and temporal variation in each significant end member identified above follows.

4.2.1 Meteoric Water

The global meteoric water line (GMWL), expressed as $\delta^2H = 8\ \delta^{18}O + 10$, represents linear variations between hydrogen and oxygen (Craig, 1961). The isotopic framework with identified distinct end member end points is presented on Figure 4.3. In Delta Marsh, the local meteoric water line (LMWL) (Figure 4.3) represents temporal variability in isotopic composition of local precipitation (rain and snow). The LMWL was derived using flux-weighted rain and snow data from two (2013-2014) stations. Rain and snow were accumulated by day from 15 min records. Slopes of the LMWL for the two-year (2013-2014) and four-year (2013-2016) study periods are 7.8 and 7.7, respectively. LMWL was derived by regression through weighted rain and snow samples. The values of LMWL obtained in our study agrees with (Birks & Edwards, 2009) for Gimli and The Pas of 7.78 and 7.62, respectively. For each station, the amount-weighted isotopic composition of an end point ($\delta_{P\,(aw)}$) was calculated by weighting the isotopic composition of precipitation to seasonal (from May – October) precipitation amount via:

$$\delta_{P(aw)} = \frac{\sum_{i=1}^{n} \delta_{P(i)} P_i}{\sum_{i=1}^{n} P_i}\ (‰) \qquad 4.1$$

where $\delta_{P(i)}$ represents the isotopic composition of precipitation integrated over a period when the sample was collected and P_i is the amount of precipitation falling during the period *i.* The

precipitation end points were amount-weighted as they were expected to mimic seasonal average source water to the Marsh (Gibson et al., 2008). Derivation of the local evaporation line and all other framework endpoints are discussed in the following sections.

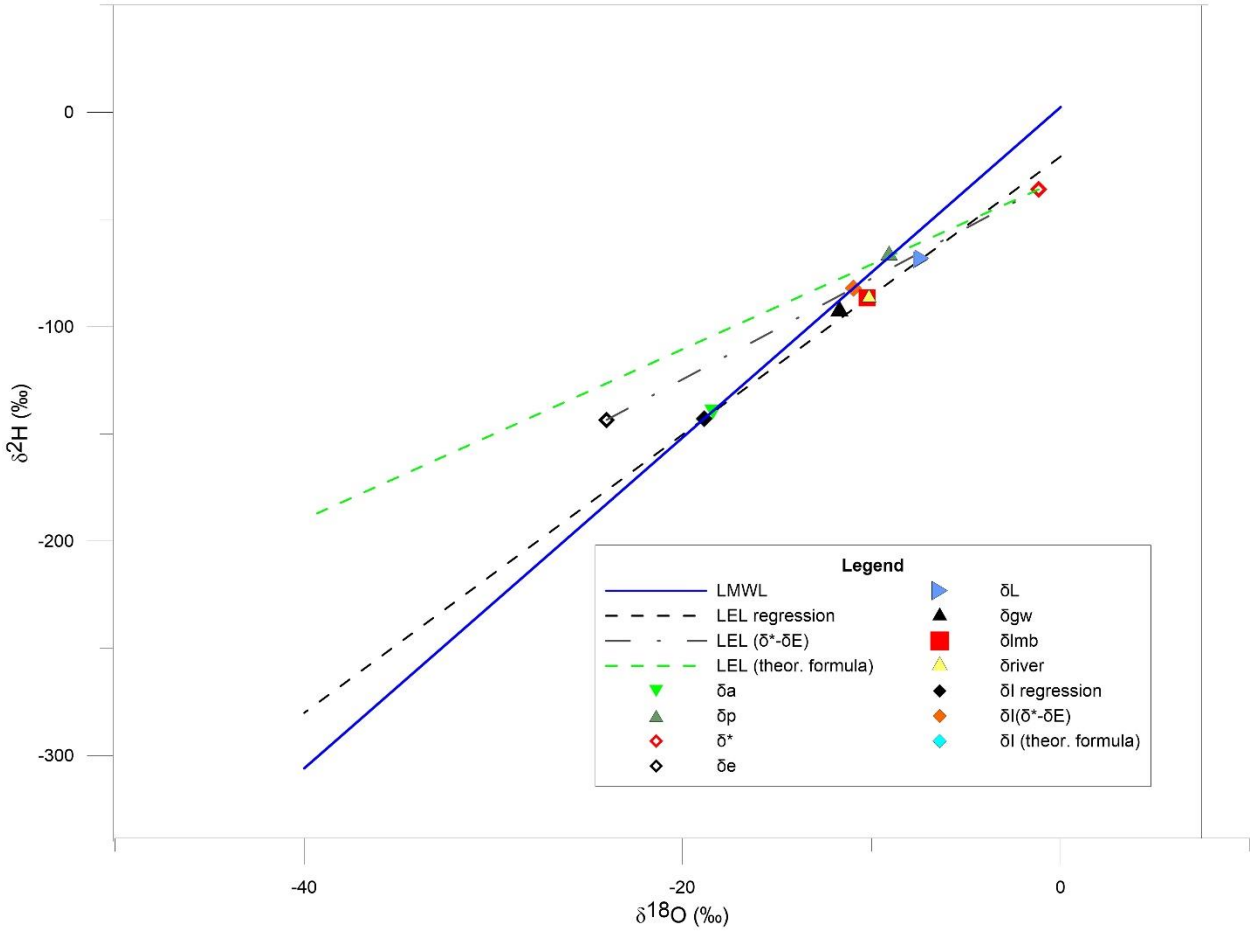

Figure 4.3 - Isotope framework for period 2013 -2016. LMWL is local meteoric water line, LEL – local evaporation line was presented using three different methods (regression, as a slope between δ and δe end points, and using theoretical formula), δa is an evaporation flux weighted end point of atmospheric vapour, δp is precipitation flux weighted end point of precipitation samples, δ* is an evaporation flux weighted end point of limiting isotopic enrichment, δe is an evaporation flux weighted end point of evaporative flux, δL is an amount weighted mean of all marsh samples, δgw is an amount weighted mean of all groundwater samples, δriver is an amount weighted mean of all river samples, δlmb is an amount weighted mean of Lake Manitoba samples. δI is an isotopic composition of inflow as an intersection between LMWL and LEL. δI (theor. formula) overlaps with δp and therefore is not visible on the graph.*

4.2.2 Atmospheric Moisture and Water Vapour

The isotopic composition of atmospheric moisture upwind of the Marsh was assumed to be in equilibrium with precipitation (Gibson et al., 2015a). This assumption was tested using a wind diagram from Oak Point, which predominantly showed a south-easterly wind direction; meaning the Marsh would be upwind of evaporated moisture (Appendix A: Figure A.4). Therefore, the isotopic composition of atmospheric vapour (δ_A) (Figure 4.3) was calculated based on the following formula (Gibson et al., 2008; Gibson et al., 2015a):

$$\delta_A = \frac{(\delta_p - \varepsilon^*)}{(1 + 10^{-3}\varepsilon^*)} \quad (‰) \tag{4.2}$$

where δ_p is isotopic composition of precipitation sample, $\varepsilon^* = (\alpha^* - 1) \cdot 1000$ was the equilibrium isotopic separation, and α^* was the equilibrium isotopic fractionation factor (in per mille) based on Equations 2.11 and 2.12 (Horita & Wesolowski, 1994). Isotopic composition of atmospheric moisture over a lake can be also directly measured in samples of atmospheric moisture collected over a study system (Yamanaka & Shimizu, 2007; Good et al., 2012), derived from evaporation pan data (Gibson et al., 1999; Rozanski et al., 2008), and the use of an index lake approach (Gibson & Reid, 2014).

The isotopic composition of precipitation was collected at two locations yearly (the third station was omitted since samples were only collected in 2015). The δ_P end point was derived by amount-weighting individual precipitation samples collected from each MET station. The two distinct end points (one for each station) were averaged to get a yearly value of δ_P. Four end

points over a four-year period were amount-weighted to derive the 2013-2016 δ_P end point; and similarly, for the two-year period (2013 -2014). A similar methodology was applied to derive end points for δ_A, δ_E, δ^*, except that samples were evaporation flux-weighted instead. The evaporation flux weighting approach considers development of isotopic signals under seasonally varying evaporative conditions (Gibson & Edwards, 2002). At mid-to-high latitudes, like the Delta Marsh study site, evaporation (E) varies seasonally under different environmental conditions influenced by changing weather (Gibson et al., 2008), therefore δ_A is evaporation flux weighted to simulate annual variability in δ^2H – δ^{18}O space. Evaporation flux weighting was done as follows:

$$\delta_{x(ew)} = \frac{\sum_{i=1}^{n} \delta_{x(i)} E_i}{\sum_{i=1}^{n} E_i} \ (‰) \qquad 4.3$$

where $\delta_{x(i)}$ represents the time varying isotopic composition of atmospheric moisture (δ_A), vapour composition of the evaporate (δ_E), and δ^* integrated over a period when a sample was collected, whereas P_i and E_i are the amounts of precipitation and evaporation over the period *i.*

The isotopic concentration of evaporate was calculated based on the formula of (Craig & Gordon, 1965), presented in detail in Section 2.3 (Equation 2.10) . δ_L was derived as the arithmetic mean of all Marsh samples collected in any given time step from open water areas (i.e., not including rivers).

Given the size of the Marsh, precipitation samples from both MET stations and Marsh samples were not often collected on the same day; moreover, precipitation samples were collected every 7-14 days (as composite samples). To derive the isotopic composition of δ_P for a given day, the mean between two composite precipitation samples (from each MET station, with possibly two composite sampling periods) was used that spanned the date Marsh water sampling was conducted. All variables were substituted into Equation 2.10 to derive a daily δ_E value. Isotopic concentration of evaporate for a year was calculated by evaporation flux-weighting daily δ_E based on estimated daily evaporation using the Penman–Monteith method (Schellenberg, 2017). To derive the end point value of δ_E, either for the four year or two-year study period, seasonal evaporation flux-weighting was performed. δ_A and δ_E were evaporation flux-weighted in order to obtain similar long term (end point) values. For δ_E, relative humidity was constrained to less than 88%; for relative humidity higher than 88% diffusion becomes dominant and the mathematical formulation of Craig and Gordon (1965) becomes invalid. This methodology follows the recommendations of Gibson et al. (2008) who suggested that atmospheric fluxes should be evaporation flux-weighted, and water fluxes should be amount-weighted (Gibson et al., 2015a).

Inflows to Delta Marsh come from Lake Manitoba, groundwater contributions, and from the upland watershed in a form of overland flow and river inputs. For the dual isotope framework analysis, input composition to the Marsh, δ_I, was defined using three methods explained in the following sections.

4.2.3 Groundwater

Groundwater was sampled at several locations across the Marsh. GW01 was the deepest well, and the only well that was sampled continuously over the four-year period, and there is no variation in isotopic signature (Figure 4.4). The median value of $\delta^{18}O$ over the two- and four-year study periods is therefore the same at approximately -15 ‰. Groundwater wells GW02 – GW05 were installed for this study using metal pipes (no perforation) hammered into shallow, wet soils, to not more than 1.5 m depth. These wells often ran dry given their shallow depth, and the wells were not purged prior to sampling. This resulted in sampling of more evaporated soil water isotopic compositions, or water that was meteorically-connected. GW02 was sampled only in 2014 with a total of 7 samples being collected. GW02 was located close to Lake Manitoba and was relocated (and renamed) in 2014, likely during the flood event of 2014 (not recorded in the field book). In 2014, GW02 responded to the June 2014 heavy precipitation event and inundation of Lake Manitoba waters into the Marsh, resulting in a significantly depleted groundwater sample (more depleted than GW01).

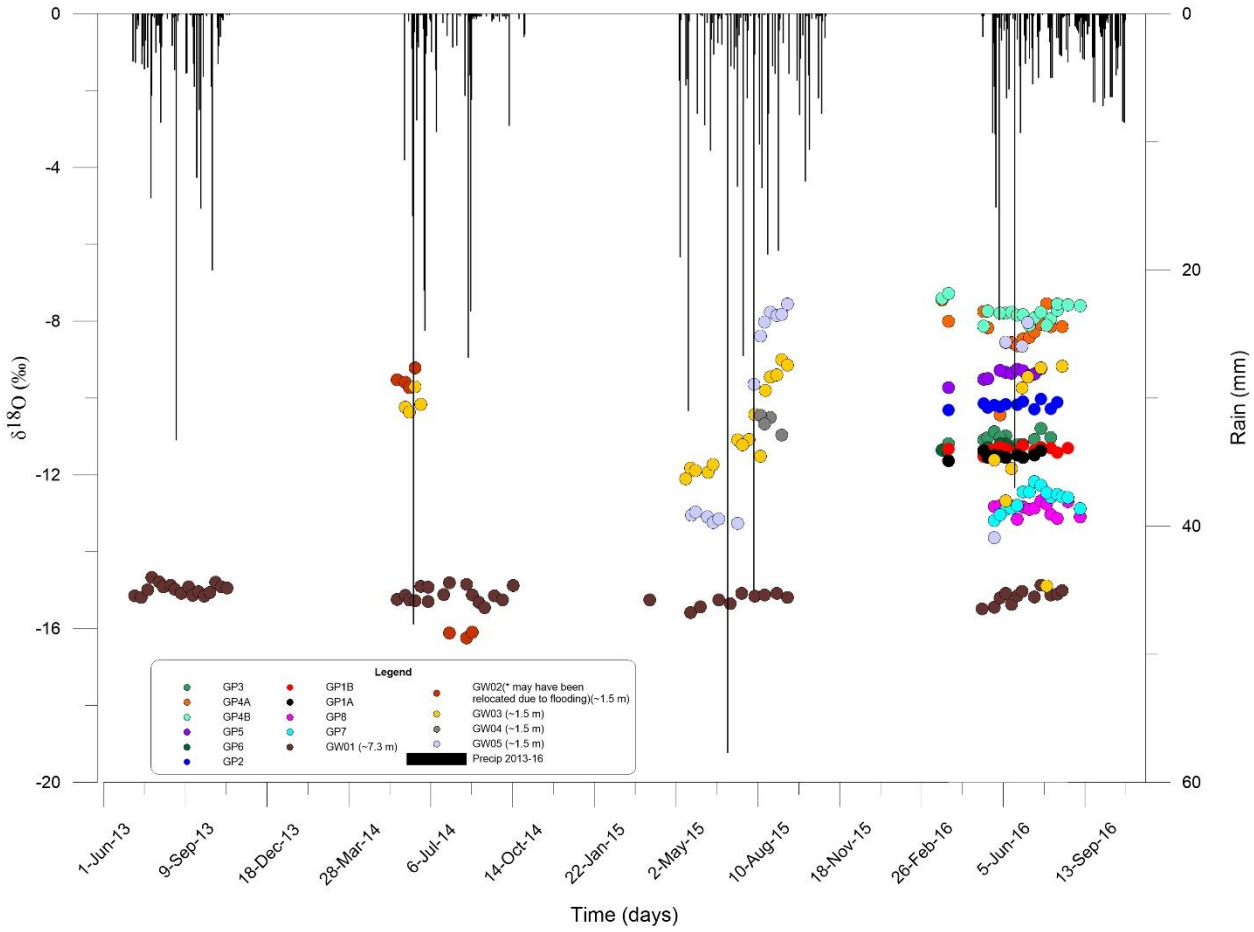

Figure 4.4 - Groundwater stable isotopic signature of $\delta^{18}O$ and precipitation amount (2013 -2016). GW01 is the deepest and the most sampled well over the course of four years. There is no variation in isotopic signature of the well. GW02 – GW05 are the wells that respond to meteoric water. GP1 – GP8 have different signatures due to different depths and locations but the signature for each well was fairly consistent over the 2016 season.

Groundwater well 03 (GW03) (yellow dots in Figure 4.4) was sampled in 2014, 2015, and 2016. Samples from GW03 in 2015 indicate significant enrichment closer to the end of the season, reflecting the higher evaporation rates in the late summer/fall period across the Marsh. The one exception is a much more depleted sample collected on July 28th 2016, for which the exact cause is unknown.

GW04 was sampled in August 2015 only (dark grey dots in Figure 4.4), with 4 samples being collected of almost uniform signature during that month. GW05 (light grey dots in Figure 4.4) was sampled in 2015 and 2016, and also indicates connectivity with the atmosphere, indicating later season enrichment. There are very few GW05 samples collected in 2016 (four in total) since often times water was not extracted from the well due to low ground water table.

Wells sampled across multiple years indicate more variation in isotopic signature than the ones sampled only for one season (as expected), with the exception of the GW02; reflecting the seasonal variability in shallow groundwater compositions that exist for the Marsh. The isotopic signature for each GP well was pretty uniform, and there was no cross over between the various GP well signatures indicating they were sampled from different depths (aquifers) and were not meteorically-connected. On the box-whisker plot (Figure 4.1). GP1A and GP1B were located in near proximity to Eaton MET station (approximately 50 m west) together with GP2 and GW04 (at the enclosed Eaton station site) (Figure 3.4), approximately 900m east from the closest Marsh site 11 SM). Although wells were drilled at different depths (approximately 1.8 m and 2.6 m for GP1A and GP1B, respectively) there was almost no difference in isotopic signature between two wells (mean value if –11.5 and -11.3 respectively). It seems that these wells were not prone to influence from either of the Marsh or precipitation, suggesting a different, more isolated aquifer layer.

GP2 (approximately 1.8 m deep) had fairly uniform signature throughout the season with prominent depletion probably due to above mentioned large precipitation event. GP3 (approximately 2.2 m deep) showed more variability than GP1A, GP1B and GP2, which is also

likely occurring due to well being often dry. This suggests the well is much more directly connected to meteoric influences and responds to wet and dry periods.

GP4A and GP4B (approximately 0.8 m and 2.3 m deep, respectively) were very close to the Marsh sampling site 23 TT at Simpson Bay (approximately 100m south from 23TT). GP4A and GP4B carry isotopic signatures very similar to that of the Marsh (mean of -7.78 ‰ for GP4A, -8.17 ‰ for GP4B and -6.50 for 23TT), which was reasonable considering their close proximity to the open Marsh area. These numbers are mean values, and may not represent actual similarity; however, from Figure 4.1 it is obvious that groundwater samples closely follow the trend in the Marsh samples. These wells are likely influenced by the Marsh itself (or vice versa). Precipitation is another parameter that influences groundwater signatures. On June 19, 2016 there was a heavy rain event (approximately 40 mm recorded at Delta and 34 mm at Eaton MET) having $\delta^{18}O$ of -8.42 ‰. GP4A isotopic signatures recorded in the following sampling period (three and 10 days later) were very close to the heavy precipitation signature (-8.65 and -8.47 ‰ respectively), suggesting flushing of the groundwater well with meteoric water, while GP4B not as much (-7.84 and -7.83 ‰ respectively).

GP5 (approximately 1.0 m deep) was located approximately 70m south from GP4A and GP4B. GP5 was located in between GP4A/GP4B and GP6 and have isotopic mean composition of -9.35 ‰. This well also reacted to the heavy precipitation event in June 2016 by showing a depletion dip in its signature. GP6 was located approximately 140 m south east from GP5 and it carried isotopic signature almost identical to GP1B (mean of -11.3 ‰). This similarity is probably not due to similar depths. GP6 was dry very often

GP7 and GP 8 (approximately 1.2 m and 1.0 m deep, respectively) were closest to Lake Manitoba of all GP wells and most depleted (located close to Bell MET (Figure 3.4) with mean signatures of -12.6 and -12.8 ‰ respectively (Figure 4.1). We can only suspect higher influence of Lake Manitoba on these wells, and therefore such depleted signatures. The most variability in isotopic signature was recorded in these two wells. Heavier rain was recorded on June 19 and the only well that was influenced by this rainfall (showed depletion in signature) was GP7. GP wells did not show enrichment throughout the season (mostly uniform isotopic signature) and therefore were not influenced by evaporation or precipitation.

The isotopic signature of groundwater (mean of -11.70‰ for oxygen – 18, number of samples - 244 was more depleted than the samples collected over the open water area (mean of -7.28 for oxygen – 18, number of samples 922), but the degree of depletion varied with groundwater well depth and sampling duration. During the wetter (flooded) year (2014), groundwater was more influenced by Lake Manitoba (Figure 4.5), mixing between these two sources was pronounced, which was the reason why an old and new water IHS separation would be expected to fail (will be discussed in Chapter 5).

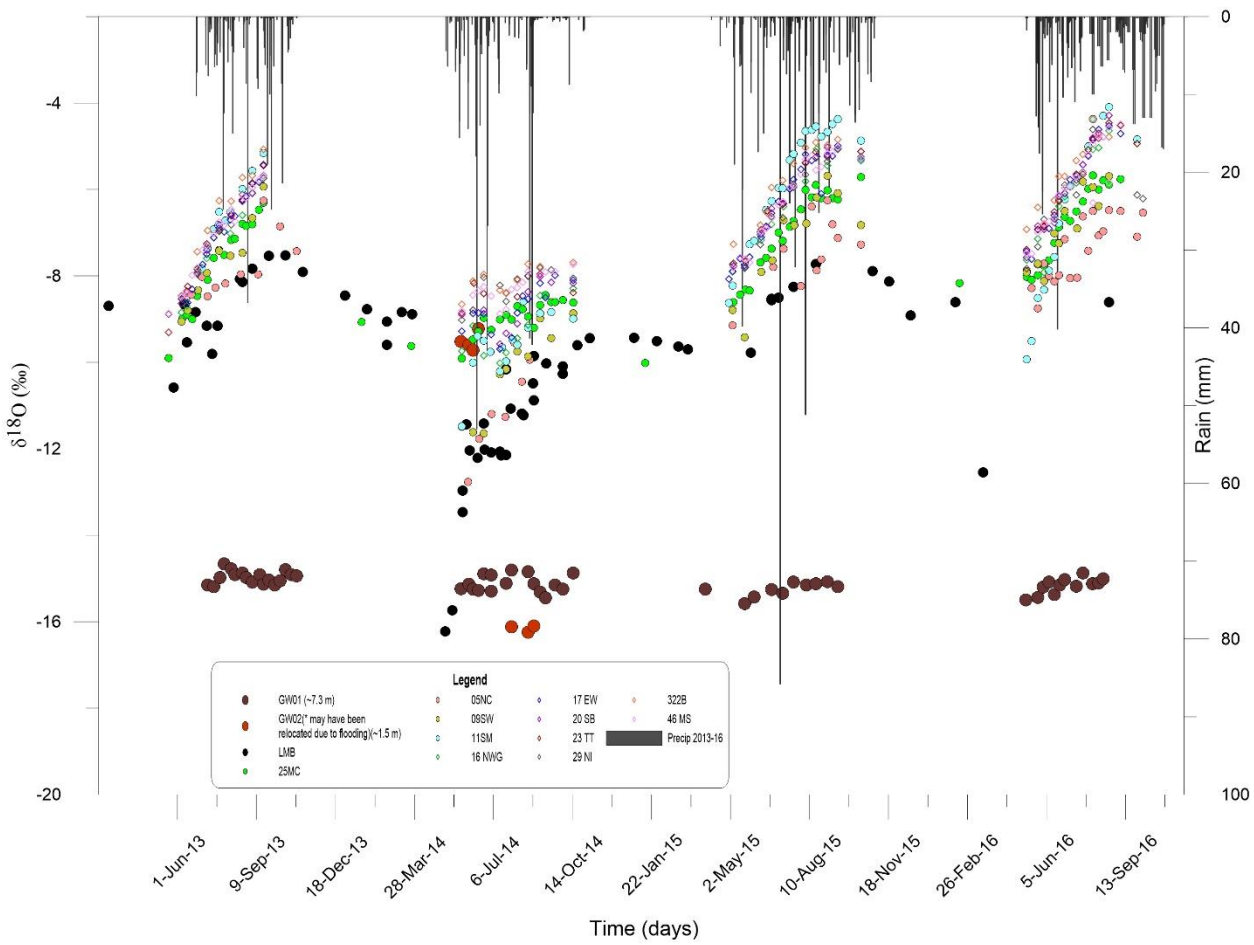

Figure 4.5 - Oxygen-18 isotopic signature of the Marsh, Lake Manitoba and groundwater wells (GW01 and GW02).

4.2.4 Upland flow – Rivers and Runoff

Overland runoff was not directly sampled. It was assumed that the isotopic composition of overland runoff was the same as precipitation, which is accurate given relatively short travel times from origin to the Marsh (during snowmelt or rain events). River sampling was opportunistic; samples were collected when there was flow or a location was accessible to reach (e.g., low Marsh level and high vegetation growth on the Marsh bottom prevented movement of a boat and those locations were not sampled). All collected data were arithmetically averaged to represent an end point on the framework. River samples close to connection points with Lake

Manitoba (e.g Roy and 41D location) were more depleted in signature compared to open water marsh locations. For other locations, the isotopic signature of river samples was very similar to the Marsh composition, suggesting significant influence of the Marsh. This suggest that far east and west river location points have higher interaction with Lake Manitoba, while middle channels (Waterhen Channel, Fish Creek,) are inter-connected with the Marsh.

4.2.5 Lake Manitoba

Lake Manitoba carries more depleted isotopic signatures (mean of -9.971 ‰ for $\delta^{18}O$) compared to Delta Marsh (mean of -7.266 ‰ for $\delta^{18}O$). Lake Manitoba sites were sampled opportunistically resulting in inconsistent frequencies of sampling, not commensurate with the Marsh sampling. For the framework end point, samples were arithmetically averaged. The lake influence over the Marsh is dominant during wetter (flooded) years (2014), which appears as a "dip" for 2014 compared to other years (Figure 4.5).

4.2.6 Local Evaporation

The local evaporation line (LEL) represents surface water undergoing evaporation (Figure 4.3). It can be estimated using three methods:

1. Regression through surface water data (i.e., local mixing line, LML)
2. Calculating the slope of the line between end points δ^* and δ_E
3. Using theoretical formula (S_{LEL}) for calculating the slope of a local evaporation line

4.2.6.1 Local Mixing Line (LML)

This method regressed a line through only the Marsh data (i.e., evaporatively-influenced, non-upland samples – river samples were excluded). Slopes of the local mixing line for 2013-2016, and 2013-2014 using this approach were both approximately 6.5 (Figure 4.6), indicating very similar evaporative conditions in the Marsh over both periods, and that the smaller two-year period was representative of conditions across the entire four-year period. The slope was higher than expected (closer to meteoric water) since here, it was assumed that the LML was an approximation of total evaporative fractionation with the system (or that LML ~ to LEL). This approach neglected the influence of upland contributing areas and includes groundwater inflows, which are not evaporatively influenced. This method relied entirely on sample data and did not utilize theoretical approaches.

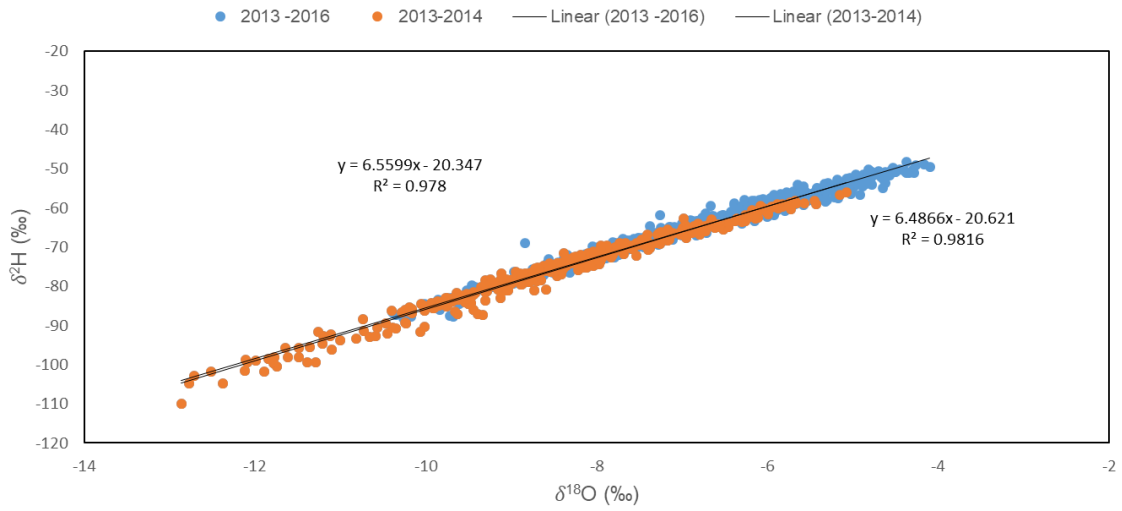

Figure 4.6 - LML for 2013-2014 and 2013-2016 based on regression through the Marsh data.

4.2.6.2 Slope Between δ^* and δ_E

The second method calculated the LEL as the line between the two end points derived from theoretical equations and sample data, δ* and δ_E. The isotopic composition of a desiccating water body would approach δ^* as it dries up, which represents a theoretical end point or limiting enrichment (reflective of specific atmospheric conditions). It can be calculated using a rearrangement of the Craig and Gordon Equation 2.10 (Gibson et al., 2016):

$$\delta^* = \frac{(\mathrm{h}\delta_A + \varepsilon_K + \frac{\varepsilon^*}{\alpha^*})}{\mathrm{h} - 10^{-3} \cdot (\varepsilon_K + \frac{\varepsilon^*}{\alpha^*})} (‰) \quad 4.4$$

Isotopic composition of evaporate (δ_E) was calculated using Equation 2.10. Evaporation samples that were collected for period 2014-2016, and are presented in Figure 4.7, along with the theoretical maximum evaporative enrichment (δ^*). Note that δ^* was a theoretical value, derived from average long-term weather conditions. When samples fall beyond the theoretical value of δ*, it was because weather conditions on that day were more conducive to higher evaporation loss (i.e., higher temperature and lower relative humidity).

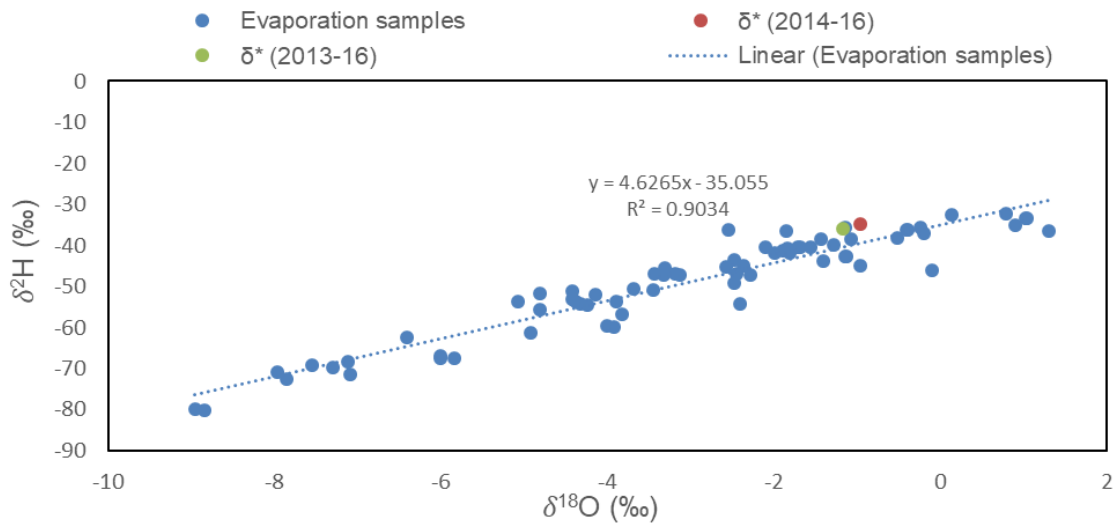

Figure 4.7 - Evaporation samples collected over period 2014 – 2016. Presented in $\delta^{18}O$- $\delta^{2}H$ space with δ^{*} end points for 2013 – 2016 (green dot) and 2014 -2016 (red dot).

The slope of LEL calculated using this method was ~ 4.7 for both the two- and four-year periods, which corresponds to previous estimates of the Boreal region (Gibson et al., 2008). It was noted that this was significantly more enriched than the LML approach, which was expected, as it does not rely solely on the Marsh water samples, that contain a proportion of non-evaporated (less enriched) water. This method, alternatively, extracts the slope of the LEL by joining the long-term average end point of the theoretical maximum enrichment to that of the composition of water vapour (δ_E), assuming all water along the line has undergone some degree of evaporation.

4.2.6.3 Using Theoretical Formula for SLEL

The slope of LEL (S_{LEL}) of lake waters fed by local precipitation predicted by the Craig-Gordon model can be estimated via:

$$S_{LEL} = \frac{\left[\frac{\mathrm{h}(\delta_A - \delta_P) + (1 + \delta_P)(\varepsilon_K + \frac{\varepsilon^*}{\alpha^*})}{h - \varepsilon_K - \frac{\varepsilon^*}{\alpha^*}}\right]_2}{\left[\frac{\mathrm{h}(\delta_A - \delta_P) + (1 + \delta_P)(\varepsilon_K + \frac{\varepsilon^*}{\alpha^*})}{h - \varepsilon_K - \frac{\varepsilon^*}{\alpha^*}}\right]_{18}} \quad 4.5$$

This equation was evaluated based on δ_A and δ_P assuming that lakes were fed by precipitation-derived water (Gibson et al., 2015a). S_{LEL} was equal to ~4.0 for both the two- and four-year study periods. The formula yielded a result that suggested Marsh water is even more evaporated than under the other two methods. This was not unexpected given this third method relied most heavily on meteorically-driven processes, assuming fully turbulent (i.e., ideal) evaporation was possible through the entire season. In reality, Marsh evaporation would be reduced by seasonal vegetation growth and water uptake, diffusive (high humidity) conditions, and changing Marsh water compositions (i.e., that δ_L deviates from meteoric input, δ_P). This formula has been previously used for predicting slopes of LEL in small, local systems; but has not been applied regionally or globally due to complexities with deriving an accurate value of atmospheric moisture (δ_A) composition (Gibson et al., 2008).

Since precipitation samples were collected on weekly and bi-weekly basis, mineral oil was poured on the bottom of the precipitation buckets to prevent evaporation loss and enrichment. Nevertheless, there is the possibility that some degree of evaporation occurred (or additional (re)evaporation of raindrops) that may alter the estimated slope of the LEL for Method 3. Method 2 serves as a reality check for Method 3 as the two methods are similar and should not yield entirely different results.

4.3 Synoptic Surveys

Synoptic surveys of the Marsh open water areas were conducted in 2016, every three weeks from May – October. In this survey broader locations (the one that were not sampled on a regular basis) (Table 3.4) were sampled mainly in one day, sometimes two depending on the weather and logistics. The survey was conducted by Prof. Goldsborough's group using air boats (much faster than the regular boats that were used for sampling purposes). The purpose of these surveys was to look at the spatial and temporal differences over the Marsh and it showed temporal (approximately between -5 to -8.5 ‰) and spatial (approximately between 4 ‰ difference) variation over the Marsh. All samples showed the same trend – increasing enrichment throughout the season resulting from evaporation of surface water (Figure 4.8 and Figure 4.10). Maximum enrichment was reached beginning of August (the last survey shown no change in composition). A plot with deuterium concentrations is shown in Appendix (Figure A.5).

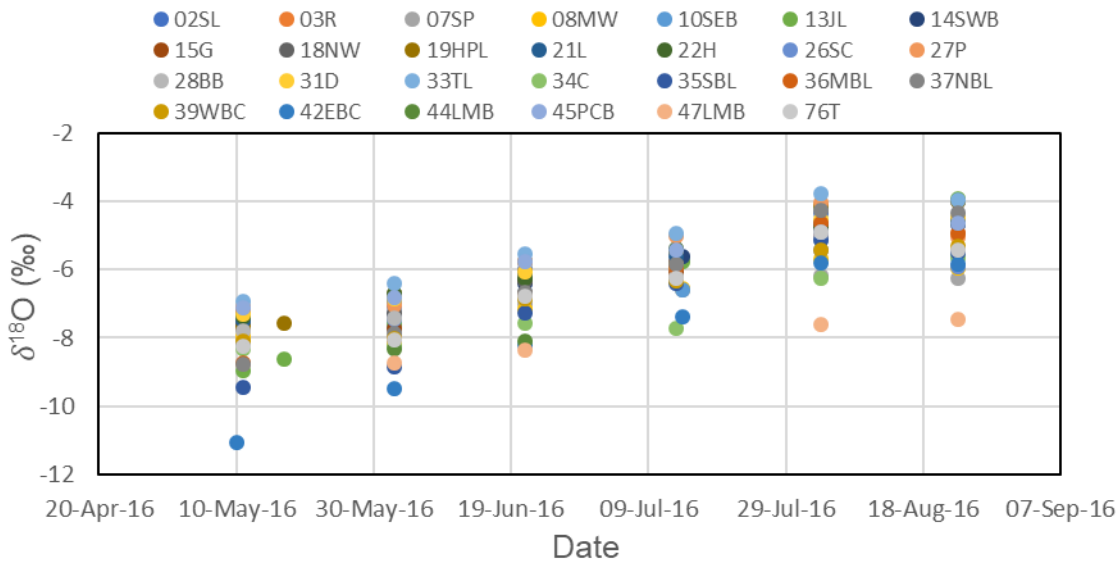

Figure 4.8 – Spatial difference in $\delta^{18}O$ (Synoptic surveys of Delta Marsh in 2016). Dots represent different sampling locations.

The variability observed across the Marsh from the average of all synoptic surveys (Figure 4.9) represents a snap shot in time (2016) of the correlation between sites, compared to a four-year variability plot (Figure 4.2). The plot shows the highest enrichment in the central east section of the Marsh (in blue), while central part of the Marsh (yellow to red section) as well as eastern and western areas (in yellow to orange) showed more depleted signatures. Sampling point 42EBC showed the highest depletion during the season due to being located in a channel connected with the watershed, and possibly receiving a large amount of very depleted snowmelt – at least early in the season, which would influence the first two synoptic surveys. It is also a possibility that there is a more permanent and direct connection with groundwater in this region, which is an anecdote suspected by locals that during higher stage, groundwater seeps through the sand ridge in that area ("center" according to Figure A.1), which may also contribute to a more depleted signature at 42EBC. This could be confirmed with further monitoring.

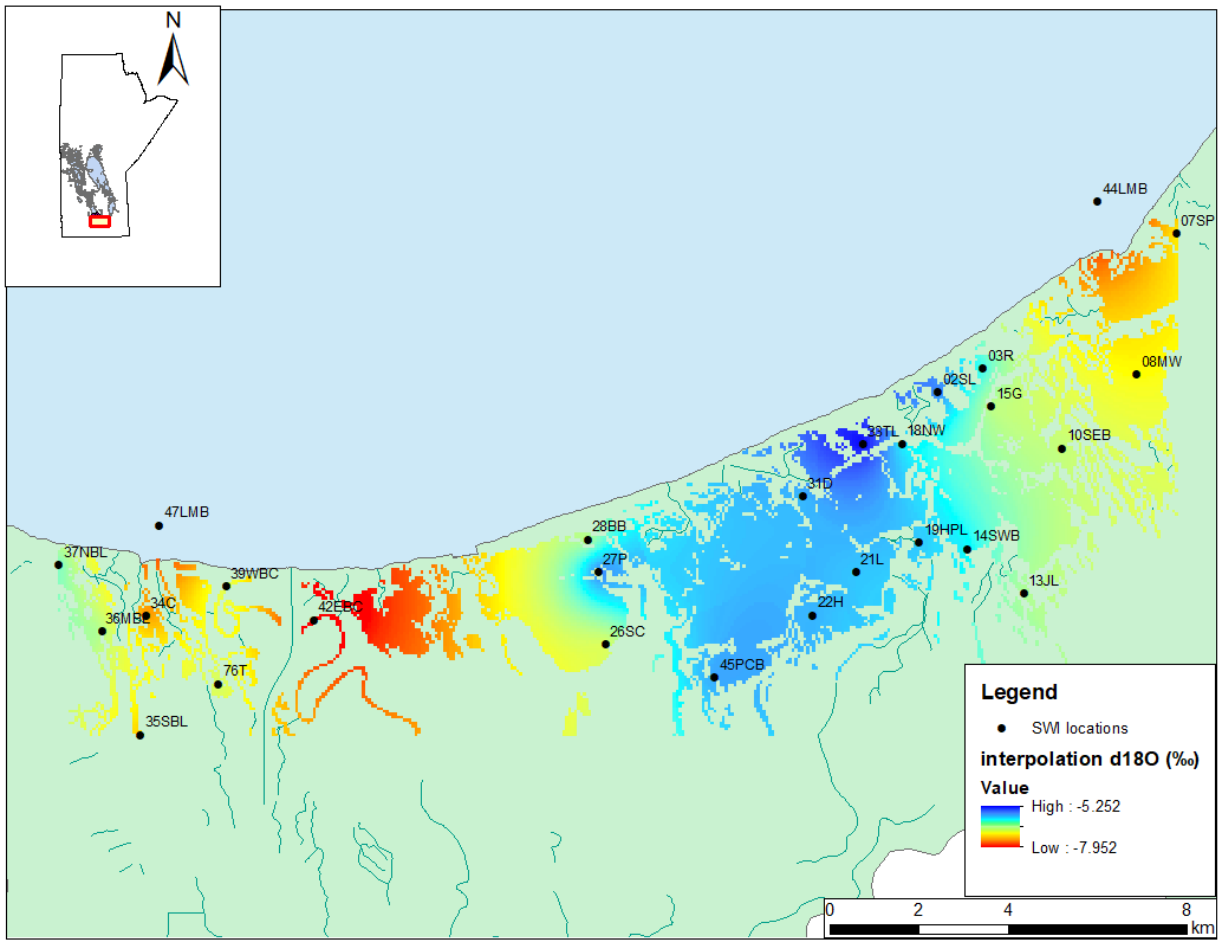

Figure 4.9 – Variability plot of synoptic survey of the Marsh in 2016.

Variability across the Marsh for each individual synoptic survey is presented in a box-whisker plot (Figure 4.10). The solid bars/numbers in each box represent the station median/number of samples, with upper and lower limits of the bars representing the upper and lower quantiles. Upper and lower whiskers represent 5th and 95th percentile, and IQR (interquartile range) are 25 and 75, and outliers were calculated at 1.5 times IQR. Based on the plot, we can say that the variability across the Marsh remains about the same within each survey. There is pronounced enrichment throughout the season, presumably due to less influence of snowmelt and more

influence of evaporation, also visible on the plot in the relationship among survey median values.

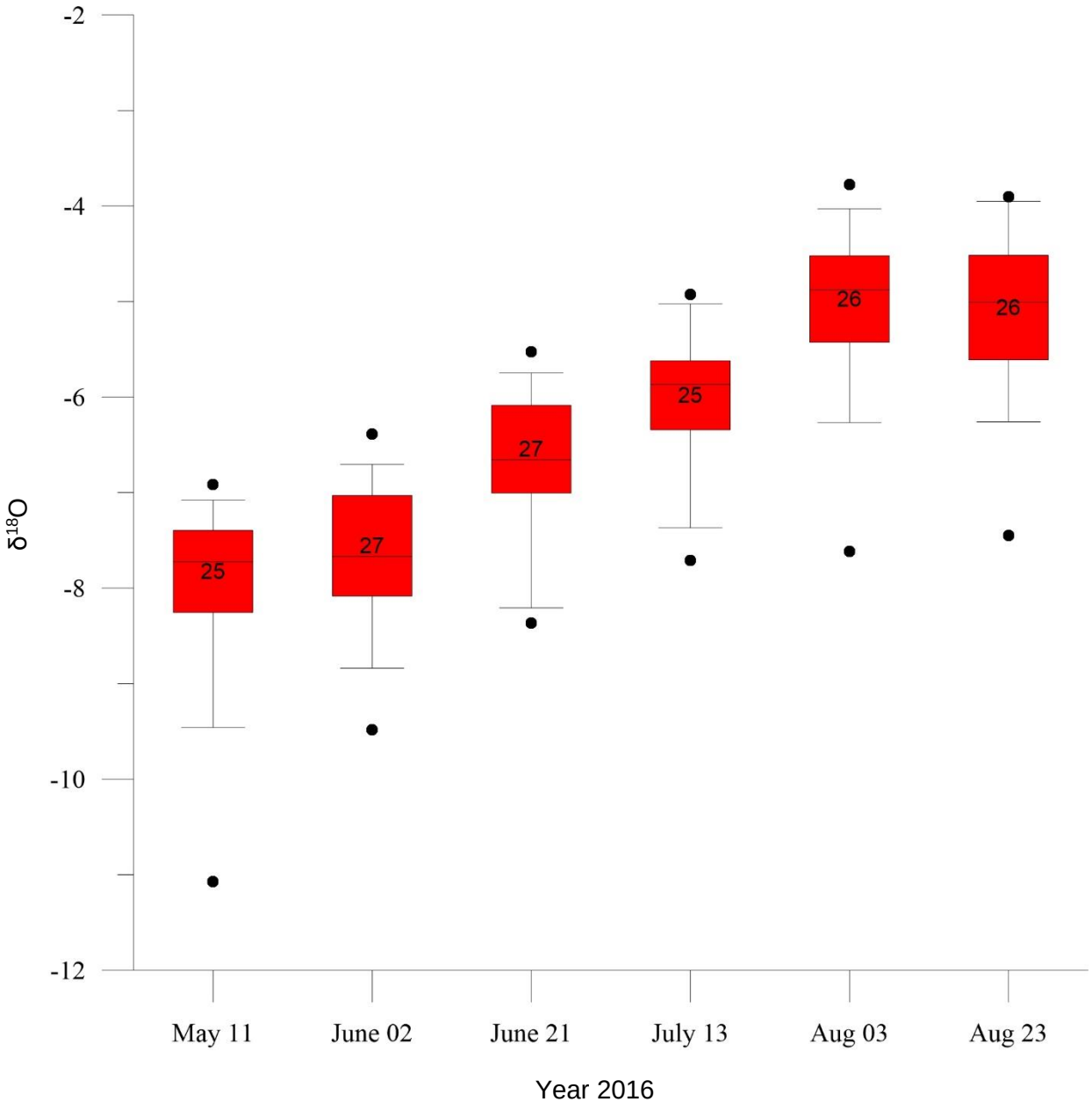

Figure 4.10 – Box – whisker plot - variability across the Marsh for each individual synoptic survey in 2016 . Each bar represents one synoptic survey.

4.4 Results & Discussion

Using the samples collected and methodology described above, a dual isotope framework for the entire study period (2013-16) and shorter study period (2013-14) was developed (Figure 4.3 and Figure 4.11, respectively). By looking at the slopes of LMWL, LEL lines and end points we can conclude that there was no difference between both frameworks, meaning the two-year period was representative of longer term hydrometerological conditions. All end points for the two study periods 2013-2014 and 2013–2016 are presented in Table 4.1. All end points for a four-year period were more enriched compared to a two-year period, which was expected considering higher amount of evaporation over four years. The difference in end points between two periods is approximately 10% and lower for both deuterium and oxygen-18 with exceptions for GW (on average 15% difference). A groundwater endpoint had a higher difference between two periods due to having more wells in 2016 and a dominating GW01 well for the first two year as having the most depleted signature.

Table 4.1 - Framework end points (δ^*, δ_E, δ_A, δ_{GW}, δ_L) for 2013-14 and 2013-16 periods. Atmospheric components (δ^*, δ_A, δ_E) were evaporation flux weighted, meteoric component (δ_P,) was amount flux weighted, and liquid components (δ_L, δ_{GW}) were averaged.

	2013 - 2014		**2013 - 2016**	
	δ^2H (‰)	δ^{18}O (‰)	δ^2H (‰)	δ^{18}O (‰)
$\boldsymbol{\delta^*}$	-40.20	-1.74	-35.99	-1.17
$\boldsymbol{\delta_E}$	-153.1	-25.75	-143.5	-24.01
$\boldsymbol{\delta_A}$	-144.4	-19.17	-139.7	-18.39
$\boldsymbol{\delta_P}$	-70.02	-9.20	-65.68	-9.07
$\boldsymbol{\delta_{GW}}$	-106.6	-14.17	-92.60	-11.70
$\boldsymbol{\delta_L}$	-74.49	-8.28	-67.77	-7.28

Temporal variation over a four-year period (Table 4.2) represents variation between framework endpoints over a four-year period. The most depleted end points occur in 2014 compared to all other years except groundwater, which included two more wells (Table 3.8) in 2014, which contributed to a more enriched signature. In 2014, there was an overland flooding and all isotopic signatures were depleted due to amount of depleted water coming from Lake Manitoba.

Table 4.2 - Individual yearly values for δ^*, δ_E, δ_A, δ_P, δ_{GW}, δ_L

	2013		**2014**		**2015**		**2016**	
	δ^2H (‰)	δ^{18}O (‰)	δ^2H (‰)	δ^{18}O (‰)	δ^2H (‰)	δ^{18}O (‰)	δ^2H (‰)	δ^{18}O (‰)
$\boldsymbol{\delta^*}$	-39.08	-1.71	-41.39	-1.79	-33.19	-1.03	-25.47	-1.00
$\boldsymbol{\delta_E}$	-137.4	-23.31	-167.0	-28.38	-126.3	-20.55	-147.3	-25.96
$\boldsymbol{\delta_A}$	-142.6	-18.93	-146.3	-19.43	-141.6	-18.58	-134.4	-17.05
$\boldsymbol{\delta_P}$	-67.72	-8.09	-72.01	-10.16	-62.95	-9.52	-61.93	-8.18
$\boldsymbol{\delta_{GW}}$	-110.8	-14.97	-103.9	-13.67	-93.89	-11.73	-88.37	-11.01
$\boldsymbol{\delta_L}$	-68.38	-7.34	-80.10	-9.14	-63.09	-6.51	-61.38	-6.39

The LMWL from 2013–2016 can be approximated by $\delta^2\mathrm{H} = 7.7\ \delta^{18}\mathrm{O} + 2.4$ versus, $\delta^2\mathrm{H} = 7.8\ \delta^{18}\mathrm{O} + 5.4$ for the period 2013–2014. Evaporated waters often cluster around LEL that was offset from the LMWL and having a slope from 4-6 (Gibson & Edwards, 2002).

All three methods for calculating LEL gave slightly different slopes (i.e., 4.0, 4.7, and 6.5) for the reasons noted in the methodology section; however, all methods agree over both the longer and shorter time periods. Methods 2 and 3 yielded similar LELs, suggesting evaporation plays a significant role in the hydrologic cycle of the Marsh and that it varies seasonally (ET was higher

than precipitation from Table 3.1; 378 mm in 2013 and 365 mm in 2014). Therefore, evapotranspiration will be looked in more detail in later chapter. This was supported by the deviation of the LML approach from the slope of the LMWL, which occurred because of evaporation post-rainfall prior to sampling. The fact that Method 1 (i.e., the LML approach) yielded a different result from Methods 2 and 3 (i.e., theoretical approaches) suggest that inflow contributions to the Marsh (i.e., groundwater, upland flow and Lake Manitoba) were also a significant component in the Marsh annual water budget.

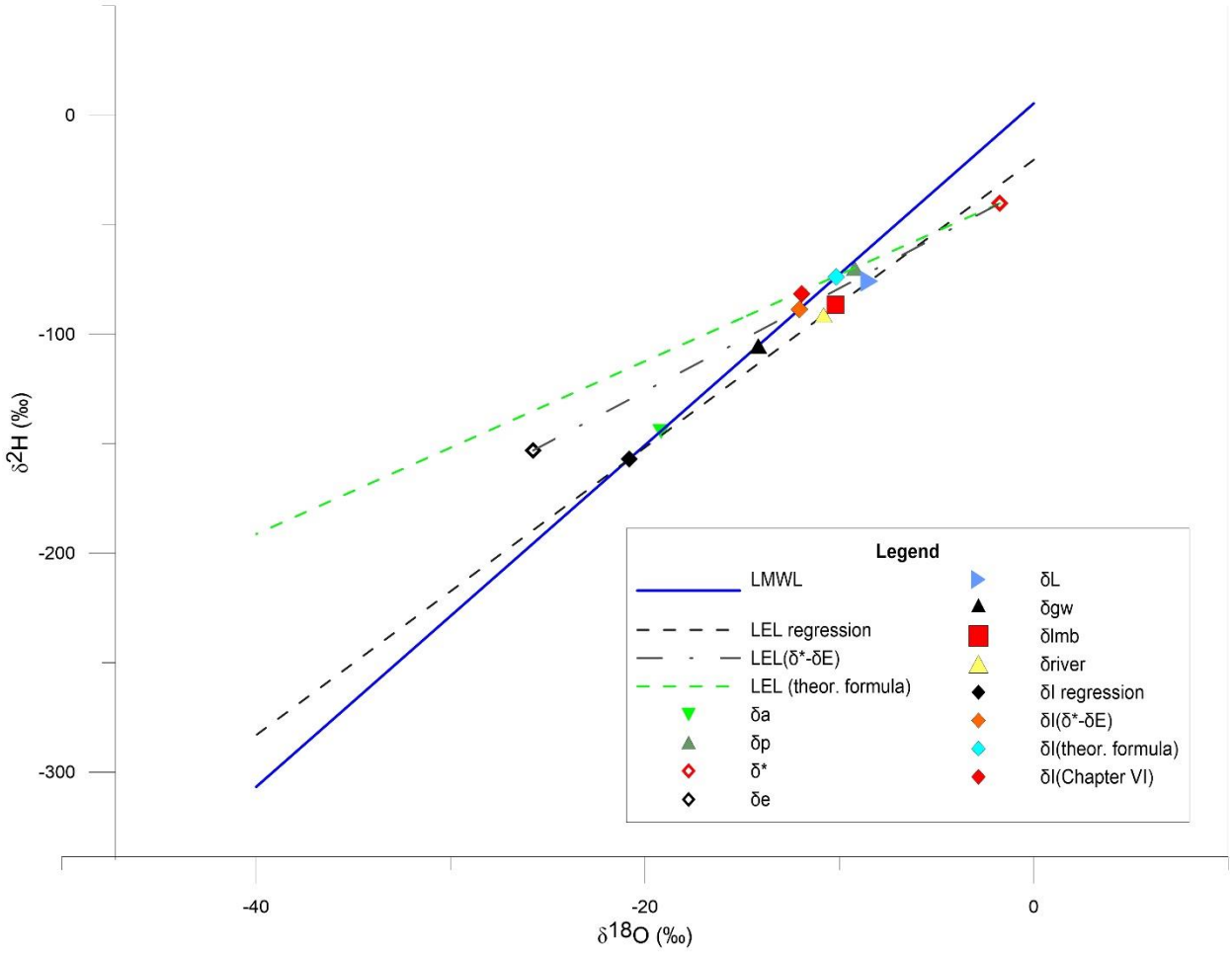

Figure 4.11 - Isotope framework for period 2013 -2014. LMWL is local meteoric water line, LEL – local evaporation line was presented using three different methods (regression, as a slope between δ and δe end points, and using theoretical formula), δa is an evaporation flux weighted end point of atmospheric vapour, δp is precipitation flux weighted end point of precipitation samples, δ* is an evaporation flux weighted end point of limiting isotopic enrichment, δe is an evaporation flux weighted end point of evaporative flux, δL is an amount weighted mean of all marsh samples, δgw is an amount weighted mean of all groundwater samples, δriver is an amount weighted mean of all river samples, δlmb is an amount weighted mean of Lake Manitoba samples. δI is an isotopic composition of inflow as an intersection between LMWL and LEL.Here are presented four δ_I's (from three methods of calculating LEL) and the one that is calculated in Chapter VI using water balance approach under assumption of non-headwater system with significant upland contribution.*

In general, the intersection between the LMWL and LEL was representative of the isotopic composition of the inflow (δ_I), hence the three methods (for calculating the LEL) yield three different estimates of δ_I. This indicated significant variability in the isotopic composition of the

Marsh inflow, which can occur from either different source waters (end members) contributing at different times, or varying compositions of each end member through time, or both. From the intersection between LMWL and LEL, the composition of δ_I was significantly more depleted relative to the other two methods (Table 4.3) suggesting there is a significant hydrologic contribution from 'other' sources that was not captured by the Marsh itself (e.g., upland watershed area), and/or substantial contributions and mixing with more depleted source waters (e.g., Lake Manitoba, groundwater or residual snowmelt).

The other two methods for calculating the LEL yield similar slopes, and therefore resulted in similar values of δ_I (Table 4.3). Methods 2 and 3 capture only precipitation, atmospheric moisture and evaporatively-enriched Marsh data, giving more enriched LEL slopes and δ_I compositions. Both methods were representative of the evaporation loss within the system, and the impact to isotopic compositions.

Table 4.3 - Stable isotope input concentrations (δ_I) using three methods for calculating slope of LEL.

	Regression method		**δ^* - δ_E method**		**Theoretical S_{LEL}**	
	δ^2H (‰)	δ^{18}O (‰)	δ^2H (‰)	δ^{18}O (‰)	δ^2H (‰)	δ^{18}O (‰)
2013-2014	-142.5	-18.96	-88.71	-12.06	-73.83	-10.16
2013 -2016	-138.1	-18.32	-82.17	-10.98	-67.65	-9.08

4.5 Summary

Delta Marsh is a very dynamic system with several significant end members, and inflow contributions, including from Lake Manitoba, groundwater and upland flow. Comparison of the

two- and four-year study periods show that, on average, the two-year period accurately captured or reflected the longer-term system variability. The shorter two-year period (2013-14) was representative of longer-term conditions, but it would be beneficial to confirm this statement with additional sampling collected over an even longer time frame. This assumption was also derived over a sufficiently short period that long-term climate variability is not a significant factor; as conditions over the Marsh change, this framework and the basis for the assumption will also change. A framework was developed that gives a good understanding of correlation between (and significance of) end members influencing the Marsh hydrologic change.

The Marsh end point (δ_L) (Figure 4.3) suggested that the Marsh is not in hydrologic steady state and that inflows are greater than outflow (the Marsh is gaining water). Position of the Marsh end point (δ_L = -68.74, -7.42 ‰) implied that over the longer-time period, the Marsh was highly influenced by inflows. Evaporation process played a significant role in the Marsh water balance during this time. Some groundwater wells were influenced by rainfall (enrichment during receiving enriched precipitation signature), suggesting a direct connection of meteoric water (recharge) to the groundwater system, and therefore a relatively short-term and responsive groundwater geology. This implies vulnerability to droughts, since groundwater is not primary input to the Marsh (impacts on Marsh low flows). Groundwater and Lake Manitoba end points fall very close to framework, suggesting direct inter-connection between the two.

5 Time-Series Modelling

In Chapter 5 we use the water balance approach to perform time-series modelling to establish a model that is capable of predicting isotope mass balance when sampling may not be available. This can help establish a method for examining changes in Marsh hydrology in the future, and for verification of evaporative losses. The Marsh was divided into two compartments (east and west, as defined in Section 1.4) and inflows and outflows for each compartment were separated.

Application of steady state models has been successful in the estimation of long-term evaporation and outflow (Gibson et al., 1993). For short term periods (weeks or months) non-steady state models are generally more suitable (Gibson, 2002).

Enrichment in $\delta^{18}O$ and $\delta^{2}H$ happens during the ice-free period when a lake is well-mixed (Gibson, 2002). For a shallow and well-mixed lake during the ice-free period, the water balance and isotope mass balance can be expressed as:

5.1

$$\frac{dV}{dt} = I - Q - E$$

$$V\frac{d\delta_L}{dt} + \delta_L\frac{dV}{dt} = I\delta_I - Q\delta_Q - E\delta_E \quad 5.2$$

where V is the volume of the Marsh, dt is the time increment the mass balance is evaluated over, dV is the change in volume over time interval dt, $I = P + I_{GW} + I_S + I_{OLF}$ is the instantaneous inflow consisting of precipitation (P), groundwater inflow (I_{GW}) , surface water inflow (I_S), and overland flow inflow (I_{OLF}),$Q = Q_{GW} + Q_S + Q_{OLF}$ is the instantaneous outflow consisting of groundwater outflow (Q_{GW}),surface water outflow (Q_S),and overland flow outflow (Q_{OLF}), E is the evaporation, and δ_L, δ_I, δ_Q, and δ_E are the isotopic compositions of the Marsh, inflow, outflow and evaporative flux, respectively. I_S comprises inflows from all channels: Delta Channel, the Gap, Portage Creek and Clandeboye Channel. For a well-mixed lake (shallow, open fetch, and subject to mixing through wind turbulence), we can assume that isotopic composition of the outflow is the same as isotopic composition of the Marsh ($\delta_Q \sim \delta_L$) (Gibson, 2002).

Rearranging Equation 5.1 and Equation 5.2 gives:

$$\delta_I = \frac{\delta_S I_S + \delta_G I_G + \delta_P P + \delta_{OLF} I_{OLF}}{I} \quad 5.3$$

where δ_S, δ_G, δ_P, and δ_{OLF} are isotopic signatures of surface water, groundwater, precipitation, and overland flow, respectively. δ_E is very difficult to measure directly (Gibson, 2002), and therefore, based on the linear resistance model of Craig and Gordon (Craig & Gordon, 1965) presented using Equation 2.10.

All inflow components from channels, groundwater and overland flow were modelled (Aminian, 2015; Schellenberg, 2017) and corresponding isotopic compositions were sampled. In case of the non-availability of surface water and groundwater isotopic compositions, we can assume for a well-mixed lake that $\delta_S = \delta_G$, which is also approximately equal to δ_L (Gibson, 2002). Due to the non-concurrent sampling schedule of all input components, an equal (step-wise) value between two sampling periods is assumed. Flux values were recorded on an hourly time step. Rearranging the water balance (Equation 5.2 and Equation 5.3), assuming well-mixed conditions, yields:

$$V\frac{d\delta_L}{dt} + \delta_L\frac{dV}{dt} = I\delta_I - Q\delta_L - \frac{E}{1-h+10^{-3}\cdot\varepsilon_K}(\delta_L - h\delta_A - \varepsilon) \quad 5.4$$

where $\varepsilon = \varepsilon^* + \varepsilon_K$ is the total isotopic fractionation incorporating both equilibrium (ε^*) and kinetic (ε_K) fractionation components. According to (Gibson, 2002), Equation (5.4) can be further simplified depending on the water balance scenario (fraction or time dependent modelling). Fraction dependent or volume dependent models have been used in cases when the isotopic composition is either constantly enriching and there is a significant volume reduction (i.e. desiccating ponds or evaporation pans), or depleting in case of a volume increase (i.e. flooded ponds), respectively (Gibson, 2002):

$$\delta_L = \delta_{SS} - (\delta_{SS} - \delta_0)f^{\left[\frac{-(1+mx)}{1-x-y}\right]} \quad 5.5$$

where δ_L is the change in isotopic composition of the Marsh with change in the remaining fraction of water, $\delta_{SS} = (\delta_I + mx\delta^*)/(1+mx)$ is the steady state isotopic composition of the

Marsh, δ_0 is the initial composition of the Marsh, x is the evaporation to inflow ratio (E/I); and y is the outflow to inflow ratio (Q/I), $m = (h - \frac{\varepsilon}{1000})/(1 - h + \frac{\varepsilon_k}{1000})$ is an enrichment slope, as defined by (Welhan & Fritz, 1977). Time-dependent models can be used when isotopic changes are negligible and there is no significant change in lake volume over time (i.e. I = Q +E). Assuming $\frac{dV}{dt} = 0$ in Equation 5.5 yields (Gonfiantini, 1986):

5.6

$$\frac{d\delta_L}{dt} = -[(1 + mx)\delta_L - \delta_I - x\delta^*](\frac{I}{V})]$$

where $x = E/I$ is the fraction of the Marsh water lost by evaporation, and $1 - x = Q/I$ is the fraction of the water lost due to outflow. Integrating and using mean values of δ_I, δ_A, ε^*, ε_K, h, V, I, Q and E over the given period of analysis yields (Gonfiantini, 1986):

$$\delta_L = \delta_{SS} - (\delta_{SS} - \delta_0)\exp[-(1 + mx)\left(\frac{It}{V}\right)] \quad 5.7$$

δ^* was evaluated in Chapter 4. Theoretically speaking, both models were "applicable" (at different times of the year) for the Marsh environment and were rigorously tested. Due to mathematical constraints, the fraction dependent model was deemed inappropriate and time dependent model was henceforth applied, producing acceptable results. Plots for fraction dependent model for $\delta^{18}O$ and δD are shown in Appendix A (Figure A.6 - Figure A.9).

5.1 Model Set-up

This particular model looks at the Marsh as two continuous-flow stirred tank reactors (CFSTRs) representing the West and East Marsh (Figure 5.1). CFSTRs are well-mixed tanks with defined inflow and outflow streams, and one of the simplest systems to use for modeling natural water bodies (Chapra, 2008). Here we assume that all contents in the receiving water body are well-mixed and uniformly distributed (Chapra, 2008), since the Marsh is shallow and a relatively steady wind applied across the surface of the system (transporting moisture down gradient). CFSTRs can be connected in two general ways: feedforward and feedback. Water never flows twice through a feedforward system, while in feedback systems, the flow is bi-directional (Chapra, 2008). We consider the Marsh as a feedback CFSTR, meaning flow between compartments can be bi-directional.

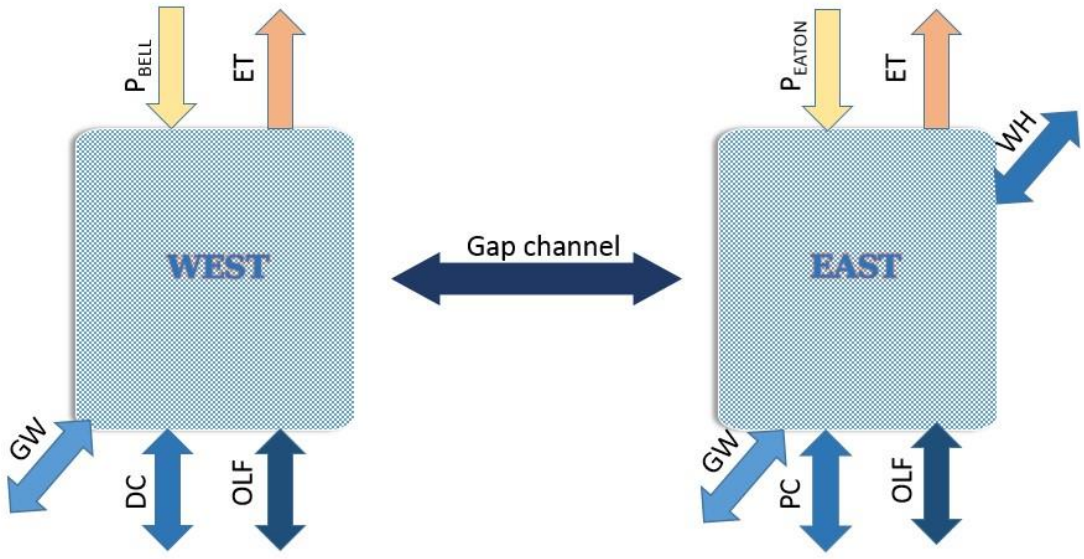

Figure 5.1 - Delta Marsh presented as two CSTR's with all inflows and outflows. Two-directional arrows represent flows in two directions (to and out of the Marsh) and from west or east part of the Marsh (for Gap Channel).

The model was setup for 2013 and 2014 using Microsoft Excel®, based on the availability of isotope analyses at the time of model setup. Based on CFSTR theory, the Marsh was divided into two tank reactors having average open water surface areas of 6.9 km^2 for the West Marsh and 39.3 km^2 for the East Marsh. Channel Gap was determined as the dividing point (based on hydraulic modelling by Aminian (2015) between the two tanks. Flows within the Marsh are bi-directional (into and out of the Marsh). Based on hydraulic and hydrologic models developed by Aminian (2015) and Schellenberg (2017), the flow convention was defined as positive for inflow and negative for outflow. The flow through the Gap in a west to east direction was considered positive.

Groundwater (GW) and overland flows (OLF) were calculated by the hydrologic model (Schellenberg, 2017), while river flows by hydraulic model (Aminian, 2015). Evapotranspiration was calculated using Penman-Monteith method (details on the evapotranspiration calculations are found in Schellenberg (2017)). Discharge was combined with stable water isotope concentrations for corresponding water balance components. The isotopic composition of OLF (i.e., runoff) was assumed to be the same as precipitation, meaning transit time was sufficiently fast and there was no additional evapotranspiration along the flow path for OLF. Overland runoff represents excess precipitation that is carried towards rivers, lakes and eventually the oceans.

The model computational timestep was daily. Since stable water isotopes were sampled weekly or bi-weekly, corresponding parameters were calculated for the same sampling periods (δ^*, δ_a, δ_E, m); inputs were therefore presented as step-wise values on a daily computational time step. Based on the box whisker plot analysis (Chapter 4.2), suitable reference points for Equation

(5.7) were determined to be 25MC and 46MS for the West and East Marsh, respectively. One location per Marsh section was assumed to be representative of the whole section, and therefore referred to here as "reference points". Averaging across the section would have smoothened the temporal variations, which would not have been as desirable for calibrating or validating a model.

Precipitation for the West Marsh came from Bell station (P_{Bell}). Surface water inflows originated from Delta Channel, the Gap, and overland flow; while groundwater inflow was taken from GW01 well. For the East Marsh, precipitation came from Eaton station (P_{Eaton}). Surface water inflows were from Portage Creek Channel, the Gap, Clandeboye Channel, and overland flow; while groundwater inflow was taken from GW03 well. Precipitation and evapotranspiration were estimated in mm per day and discharges in m^3/s. To calculate overall inflow in mm, discharges were converted into mm (fluxes were divided with a surface area of the marsh, per daily time step).

There was a discrepancy between sampling periods and of the commencement of seasonal modelling with respect to groundwater. In 2013 GW01 was sampled from July 9 until October 30, with modelling starting on June 20. To gap fill these data, we regressed a second order polynomial ($R^2 = 0.297$) through observed data from 2013-16 using Julian days. We extracted the missing data between June 20-July 8 2013 for the West Marsh. There were no samples collected for GW03 (the well was not established) in 2013, but only from 2014-2016. In order to extract the missing data for 2013, we linearly regressed trough GW03 data for period 2014-2016 ($R^2 = 0.253$) and used Julian days to extract data for the missing field season. In 2014, GW01

was sampled throughout the field season and therefore the measured values were used for the West Marsh. GW03 was sampled between June 5 – June 24 (assumed uniform signature until July 2nd). For the period of missing data (between May 28 – June 5 and July 3 – Oct 31), the linear regression approach was used as explained above for GW03 well.

5.2 Results and Discussion

The water balance was found to not close (i.e., inputs did not equal outputs) during each of the two modelling periods since the model was set-up for only a five to six-month period during ice off conditions (Appendix A:Table A.3). The time dependent model assumes negligible or no change in storage and in our case, volume change was not significant (less than 5 %). Model results for $\delta^{18}O$ for both compartments in 2013 and 2014 are presented in Figure 5.2a) and b) and. Similar trends were captured by δD. Plots of δD are shown in the Appendix (Figure A.10). Measured values are presented using blue circles with error bars representing analytical uncertainty of ±0.2 ‰. In general, there would be modelling uncertainty (from hydrologic and hydraulic models) as well that would add to these bars. That means, in reality, these error bars would be even larger, not smaller. The influence of uncertainty in hydrologic and hydraulic models is discussed in more detail in subsequent sections.

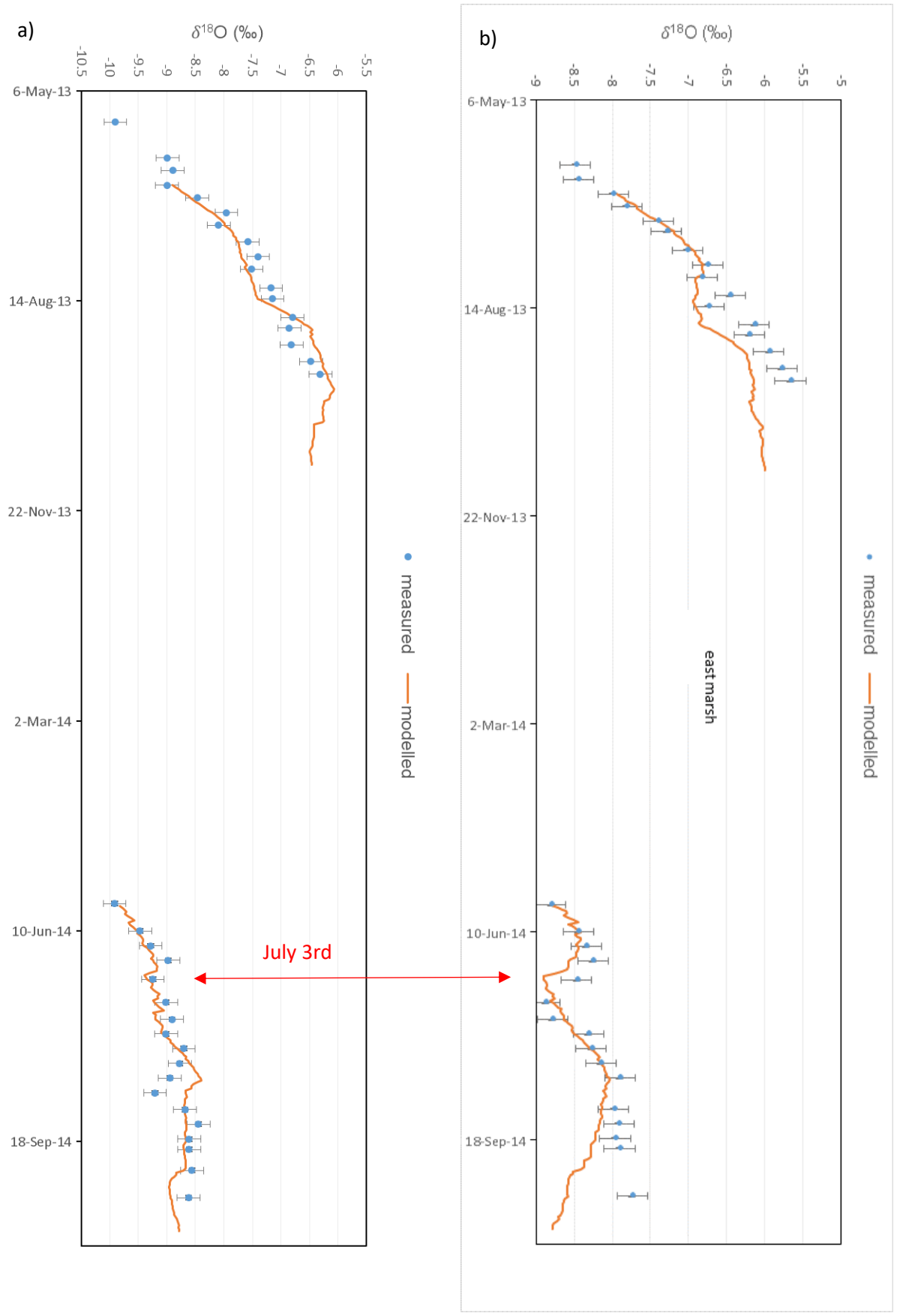
a)
b)
δ18O (‰)
-10.5
-10
-9.5
-9
-8.5
-8
-7.5
-7
-6.5
-6
-5.5
-5
6-May-13
14-Aug-13
22-Nov-13
2-Mar-14
10-Jun-14
18-Sep-14
measured
modelled
east marsh
July 3rd

Figure 5.2 – Time dependent model for 2013 and 2014; comparison of measured and modelled isotopic composition of $\delta^{18}O$ of for a) west and b) east CFSTR. Measured values are represented in blue circles with error bars representing analytical uncertainty of +/- 0.2 ‰, while orange line represents model results

In general, the trend is similar between measured and modelled isotopic concentrations in 2013, with slightly more depleted values for the western CFSTR. There is a clear seasonal enrichment signal in both sections of the Marsh, with an evident temporal variation between the two compartments. Isotopes are ideally suited for modelling or tracing evaporation loss. On the other hand, estimated evapotranspiration (ET) from the Penman-Monteith method is found to be inaccurate when compared to modelled evaporative enrichment due to the inclusion of the transpiration component (non-fractionating isotopically). Here, we use proxy validation to estimate the proportion of Penman-Monteith estimated ET actually occurring across the Marsh since we do not have measurements of evaporation. This assumes all other components of the Equation (5.7) are well estimated, and hence we calibrate δ_L using evaporation loss until it matches the observed isotopic compositions.

At the beginning of the season, the model matches well with the observed isotopic data (when the majority of ET is also E), while later in the season, it begins to diverge and either overestimates (west 2013 and 2014 (middle of the season), east 2014) or underestimates (west 2014, east 2013 and 2014) the observed isotopic data. In the middle of the season in 2013 (approx. July 17 –Aug 22), the model underestimates ET, while later in the season it overestimates ET for the western compartment and underestimates it for the eastern CFSTR. In general, in the beginning of the season evaporation is a more dominant process since there is no developed vegetation (transpiration ~ 0), while later in the season, with plant growth, transpiration becomes more dominant and a higher proportion of ET. Evaporation loss is higher

in eastern section of the East Marsh due to larger open water surface areas. In general, dominant emergent vegetation cover is Typha with no significant variation between in density and amount between East and West Marsh (Baschuk, 2011). Grassland and shrubland cover are more dominant in East Marsh (P. Kowal, personal correspondence, April 2020) and we assume that could further influence evapotranspiration. However, the ET might not be the only parameter that impacts δ_L. δ_L is a function of several parameters (i.e., temperature, relative humidity, volume) including the inflow components.

In 2014, significant differences in the trend of measured and modelled data between two compartments is noticeable, as well as variability in over/under-estimation of ET throughout the season. For the period July 3–July 22, there is a significant depletion in the East Marsh, likely due to extensive flooding from the use of the Portage Diversion. On July 3rd, the fail-safe on the west dike of the Portage Diversion began spilling (Emery & Wrubleski, 2015) . It is possible that the water flow had been partially blocked with debris during the course of the storm which may had restricted water flow from Lake Manitoba into Delta Marsh through Delta Channel (B. Emery, personal conversation, December 13, 2019). After July 3rd, the West Marsh underwent enrichment, while the east compartment further depleted, suggesting either a faster transit time for the western section of the marsh (i.e., water flushed out in less than ten days), and/or more depletion due to water entering the eastern compartments due to additional connectivity during high water conditions. According to Fig. 6:16 from Aminian (2015), it was estimated that that 85% of the water that enters Delta Marsh from Lake Manitoba does so through Clandeboye Channel, and only about 15% of the water that enters Delta Marsh does so through Delta Channel. Furthermore, it was observed that the magnitude of discharge exceeds that from Delta

Channel (Aminian, 2015), further explaining depletion of the East Marsh. Although it looks like the dilution factors (how much water enters certain section of the Marsh) would be the same between the east and west, this is not the case because the influence of the Portage Diversion outflow entering Lake Manitoba, and then entering the Marsh through the Delta and Clandeboye Channel was not directly accounted as inflow, but would differentially impact each section.

June 25–July 3, 2014 period had less rain, but saw a single, highly depleted sample recorded at Eaton (at Eaton: 27 mm of rain, isotopic composition -99.1 (δD) /-13.7 ($\delta^{18}O$) ‰; at Bell: 78 mm of rain with an isotopic composition (-75.0 (δD) / -10.9 ($\delta^{18}O$) ‰). In general, heavy rains have more depleted isotopic signatures (Gonfiantini, 1986), but may also vary from 'normal' rainfall signatures due to the different origin of the air masses. For example, large rainfall events can carry more enriched isotopic signatures associated with an air mass originating from the tropical regions of the Pacific Ocean, whereas more depleted rainfall signatures can be associated with air masses originating from the North Pacific and Arctic Ocean (St. Amour et al., 2005). During this period there were two days of heavy/medium rainfall recorded at Bell station, and only one medium rainfall at Eaton. Composite sampling of precipitation was recorded for a period of nine days; hence we can only assume the isotopic signature of those single events. Prolonged depletion for the most eastern section of the marsh versus enrichment in the west could perhaps be explained by the significant impact of depleted flooded Lake Manitoba water entering the Marsh on the east side (Clandeboye Channel). It seems that the western CFSTR was not affected by these flood waters in the same way as the eastern portion of the Marsh, and hence the need for spatially distributed modelling is necessary.

First, on July 1st Portage Diversion was breached on the west side (fail safe is on the west side) so water did not enter the Marsh area east of Portage Diversion directly. This was done to avoid all water directly entering Lake Manitoba. Second, water was flowing through the box culvert bridge at the channel, although it was possible the water flow could have been partially blocked with debris during the course of the storm which may have restricted water flowing from Lake Manitoba into Delta Marsh at Delta Channel (B. Emery, personal correspondence, December 13, 2019). It should be noted that between July 3 and August 26, 2014, the precipitation signature at Bell station was sampled four times compared to only one sample collection at Eaton station due to accessibility issues. During that period, rain compositions sampled at Bell were progressively enriching. There was no significant difference in temperature and relative humidity between the two stations, suggesting different sources of meteoric water that were also captured by the Marsh signature (depletion in east, enrichment to the west).

From August 5 - 26, 2014 there was also a noticeable difference in isotopic signature, with pronounced depletion in the West and enrichment in the East Marsh (Figure 5.2). During that period the precipitation signature in the east was not recorded (only one composite precipitation sample was recorded at Eaton, versus four at Bell station). Although, between July 15 – August 20, very little rain fell (approx. 18 mm at both stations), and each composite sample (3 samples collected) at Bell was more depleted than the previous (approximately -0.6 ‰ for $\delta^{18}O$). The amount of rain that fell onto the West Marsh was much higher than at the East Marsh, especially between August 20-26 (105 mm at Bell, 20 mm at Eaton) with the depleted precipitation signature at Bell compared to a sample that was recorded seven days previously. Those two very depleted signatures at Bell, with very little rain, implied that rainfall sources had changed,

meaning very depleted re-evaporated moisture (during drier conditions) contributed to rain formation.

Inflow fluxes were derived from hydrologic and hydraulic models, as previously mentioned. The uncertainty of the hydraulic model was generally found to be low (NSE above 0.6; Aminian, 2015), however, was higher for hydrologic modelling (NSE = 0.35) with percent deviation of –6.9 %, indicating modelled streamflow was underestimated relative to observed streamflow (Schellenberg, 2017). It should be noted that there were limited observed data with which to calibrate and validate the hydrologic model. To examine the impact on the isotope modelling, a 6.9% decrease in inflow was applied to the time dependent model, which resulted in an increase in overall modelling error. Overall, the modeled values became more depleted using reduced inflows, temporally varying throughout from 3-5 ‰ for deuterium, and 0.002-0.4 ‰ for oxygen-18 from the beginning until the end of the season, respectively. This would yield higher ET values calculated by the model for the sensitivity analysis, meaning Penman-Monteith estimated ET would need to be increased even more for modelled isotope compositions to match with observed values (Section 5.3).

Evapotranspiration is a dominant process in the Marsh environment. Here evapotranspiration was calculated over an open water surface area (i.e., 46.2 km^2). As stated previously it was estimated using Penman-Monteith method, which was found to be inaccurate in estimating the seasonally varying transpiration process, meaning perhaps the parameters used in the method did not correctly account for actual ET from the Marsh. Transpiration is a dominant process in a

wetland environment during plant growing season. We therefore applied isotopes to conduct a sensitivity analysis of estimated ET using modelled versus observed δ_L.

5.3 Sensitivity Analysis and Statistics

Sensitivity analysis was conducted in order to define a better approximation of evapotranspiration (ET) in the both sections of the Marsh. The analysis was conducted for the range of 0.5 ET – 2 ET with different increments depending on the results. This range was chosen based on the observed data range (Figure 5.3 and Figure 5.4). Plots for δD are shown in Appendix A (Figure A.11 and Figure A.12). Nash Sutcliffe efficiency (NSE) and root mean square error (RMSE) were chosen as metrics to evaluate model performance with respect to time and offset of peak performance (NSE), the mean offset of simulated and observed values (RMSE). These metrics are commonly used to evaluate isotope simulation (Stadnyk & Holmes, 2020).

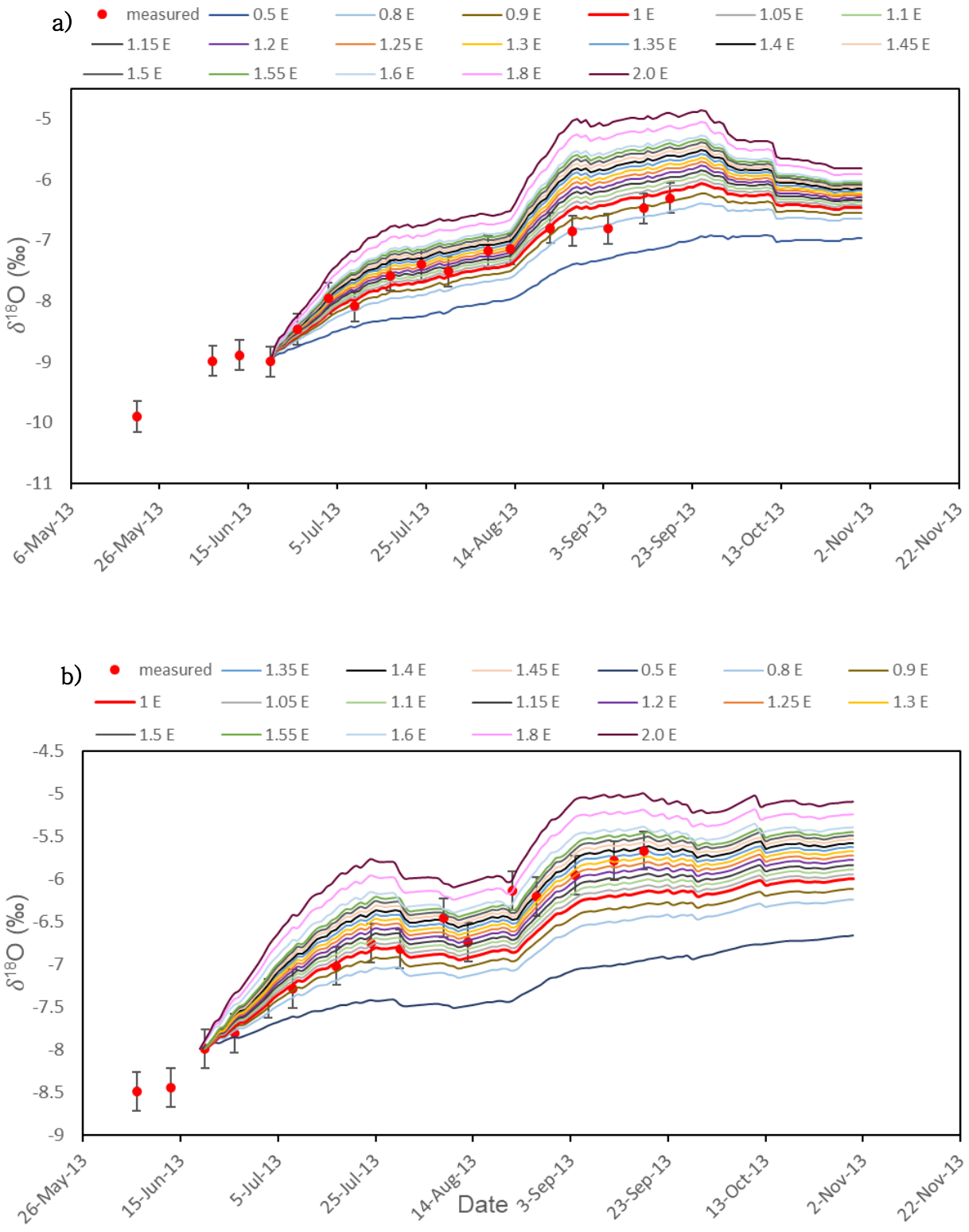

Figure 5.3 - ET sensitivity graphs for (a) West and (b) East Marsh in 2013 ($\delta^{18}O$). Red dots are measured values with error bars representing analytical uncertainty of $\pm$ 0.2 ‰, lines represent percentage difference for ET (range 0.5 – 2.0 ET) with different increments of ET.

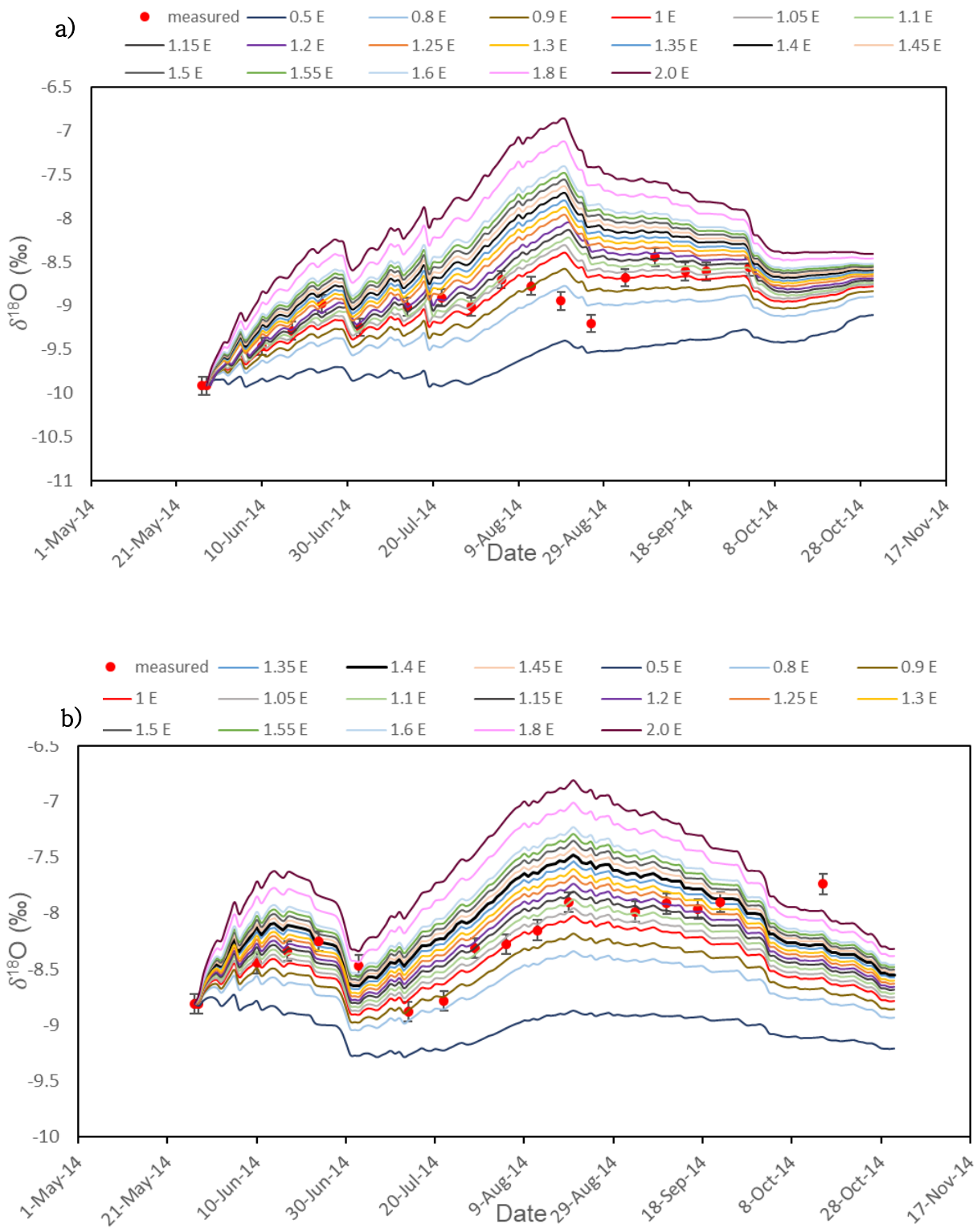

Figure 5.4 ET sensitivity graphs for $\delta^{18}O$ for (a) West and (b) East Marsh in 2014 ($\delta^{18}O$). Red dots are measured values with error bars representing analytical uncertainty of ± 0.2 ‰, lines represent percentage difference for ET (range 0.5 – 2.0 ET) with different increments of ET.

NSE is a normalized statistic for assessing the goodness of fit of hydrologic models (Nash & Sutcliffe, 1970; McCuen et al., 2006). It provides a quantitative measure how well the simulated model output fits with the observed data. An NSE corresponding to 1 represents a perfect match between the modelled and observed data, whereas an NSE of 0 indicates that the model predictions are not any more accurate than the mean of the observed data. NSE is calculated as:

$$\mathrm{NSE} = 1 - \frac{\sum_{i=1}^{n}(OBS_i - SIM_i)^2}{\sum_{i=1}^{n}(OBS_i - \overline{OBS})^2} \quad 5.8$$

where OBS represents observed data, SIM is modelled, and OBS is an average value of measured data. NSE and RMSE were calculated for both stable water isotopes. Each metric was calculated individually for each value of ET for both years. These two statistics were then combined into a minimization function using $(1 - NSE + RMSE)/2$, which was then averaged across both isotopes (Table 5.1). Values of the minimization function in 2013 were 8.64 and 0.55 for West and East Marsh, respectively, and in 2014 0.79 and 0.86. Our model therefore showed that ET is overall underestimated by Penman-Monteith method, and a mean value of 1.25 ET for 2013 and 1.18 ET for 2014 is needed to provide the best statistical performance of the isotope timeseries model to observed data. A table with complete set of values for NSE, RMSE and minimization function is shown in Appendix A (Table A.4).

Table 5.1 - Results of ET sensitivity analysis for 2013 and 2014 for both Marsh compartments and averaged yearly values. Reported are result of minimization function using N (NSE) and R(RMSE) as a mean of both isotopes.

Year	Compartment	Min((1-N)+R)/2	ET sensitivity analysis result	Average
2013	WEST	8.639	1.05 ET	**1.25 ET**
	EAST	0.550	1.45 ET	
2014	WEST	0.786	1.15 ET	**1.18 ET**
	EAST	0.860	1.2 ET	

The computed Marsh composition, or δ_L, was compared to the measured isotope data using the full Penman-Monteith estimated ET. Simulated δ_L lines were generated using different scaling factors applied to estimated ET and compared to the observations (red dots) to evaluate when there was more or less than the Penman-Monteith-estimated ET.

In general, in 2013, at the beginning of the season the model (1 ET) does a good job at estimating the observed isotope values, especially in the East Marsh. Later in the season, in the western model indicates that ET tended to be overestimated by Penman-Monteith, whereas it was generally underestimated in the eastern part. This discrepancy could arise because of the difference in size between two compartments, leading to more evaporation from a bigger water body surface area, and/or more transpiration across an area due to a larger plant population. At the end of the season, in the East Marsh simulated a best match (to observed isotope data) for 1.3-1.35 x ET; and ~0.8 x ET for the West Marsh.

In 2014, at the beginning of the season the Penman-Monteith estimated ET was generally underestimated. In the period after flooding (mid-July), however, the modelled results indicate differentiation between the East and West Marsh. Actual evaporation appears to have been higher than that estimated by Penman-Monteith for the West Marsh (~1.15 ET), but lower (or suppressed) in the East (0.85 ET). Signature of depleted water that enters East Marsh through Clandeboye Channel weakens evaporation signal and therefore suppressed ET.

Overall, final estimated evaporation across each study season was found by averaging the values from both compartments, arriving at 1.25 ET for 2013 and 1.18 ET for 2014. These adjusted estimates of Penman-Monteith evaporative losses were carried forward through the remainder of analyses in this study.

5.4 Separation of Streamflow Components and Uncertainty Analysis

5.4.1 Streamflow Separation

Separation of Marsh volume into 'old' and 'new' water components using stable water isotopes was attempted using two-component separation based on the method presented by St. Amour et al. (2005). Here we applied the separation on a volume basis instead of using streamflow. Snow, groundwater, and surface water are typical source waters in cold climates (St. Amour et al., 2005). Based on mass and isotope balance equations, the mixing ratio of source water components is determined in a two-step process. The first step involves separation between new and old water, where new water represents direct snowmelt and old water is baseflow, which is

comprised of groundwater and surface water inflow. Direct precipitation also contributes to total runoff but is assumed negligible since precipitation mainly recharges to groundwater or enters via surface runoff. This is especially valid in case of rain-free periods (St. Amour et al., 2005). In that case

$$Q = D + R \tag{5.9}$$

$$\delta_Q Q = \delta_D \mathrm{D} + \delta_R \mathrm{R} \tag{5.10}$$

where Q is total streamflow or runoff volume, D is new water (direct snowmelt), R is baseflow, and δ values and subscripts refer to isotopic signature of respective components.

Substitution of Equation (5.10) into (5.9) and rearranging yields

$$\frac{D}{Q} = \frac{\delta_Q - \delta_R}{\delta_D - \delta_R} \tag{5.11}$$

$$\frac{R}{Q} = \frac{\delta_Q - \delta_D}{\delta_R - \delta_D} = 1 - \frac{D}{Q} \tag{5.12}$$

which are proportions of new and old water volumes during the freshet period, respectively. In this study, the first step in the separation process was not conducted due to temporal differences in collection of these data (groundwater sampling started in June/July).

The second step in partitioning includes separation of the old water component from Equation (5.12) into surface water and groundwater, given by the mass and isotope balance:

$$R = R_{GW} + R_{SW} \quad 5.13$$

and

$$\delta_R R = \delta_{GW} R_{GW} + \delta_{SW} R_{SW} \quad 5.14$$

where R (m^3) is baseflow volume (old water), R_{GW} (m^3) is groundwater volume, and R_{SW} (m^3) is surface water plus rain volume, δ_R, δ_{GW}, δ_{SW} are isotopic compositions (‰) of baseflow, groundwater and surface water plus rain, respectively. By substituting Equation (5.16) into Equation (5.15) and rearranging yields

$$\frac{R_{SW}}{R} = \frac{\delta_R - \delta_{GW}}{\delta_{SW} - \delta_{GW}} \quad 5.15$$

$$\frac{R_{GW}}{R} \approx \frac{\delta_R - \delta_{SW}}{\delta_{GW} - \delta_{SW}} = 1 - \frac{R_{SW}}{R} \quad 5.16$$

where $\frac{R_{SW}}{R}$ and $\frac{R_{GW}}{R}$ represent the surface water plus rain and groundwater contributions, respectively.

Finally, we can compute the fraction of the new water volume contributing to the Marsh in any given time step using

$$R_{SW} = \frac{\delta_R - \delta_{GW}}{\delta_{SW} - \delta_{GW}} \cdot R \quad 5.17$$

Separation of runoff components was accomplished for 2013 and 2014 using a step-wise method. As a reference value for δ_R, Marsh water under ice was taken (two samples were taken on February 28, 2013 and six in total in 2014 – two in January and four in March). δ_R and δ_{GW} were constant for every time step (mean value of all samples in a specific year), while δ_{SW} and R were time step dependent. Total volume was calculated as a sum of volumes for east and west compartments. For each compartment, volume was calculated as a product of water depth (modelled water level for a reference point minus bed level ~ 246.0 m) and surface water area. The fraction of old water, or R_{GW} , was calculated as $R - R_{SW}$.

5.4.2 Uncertainty Analysis

An uncertainty analysis was applied to the two-component tracer-based separation to quantify uncertainties in old and new water fractions (Genereux, 1998). Hydrograph separation is one method of analyzing stream response to a given new water, or input event. In this research, the isotope component gives additional data on actual sources of water, thus allowing separation into two or more components based on isotopic difference between components end members.

Based on (Genereux, 1998), uncertainty in isotope hydrograph separation (IHS) can be determined as:

$$W_{f1} = \sqrt{\left[\frac{\delta_{SW} - \delta_S}{(\delta_{SW} - \delta_{GW})^2} \cdot W_{Cgw}\right]^2 + \left[\frac{\delta_S - \delta_{GW}}{(\delta_{SW} - \delta_{GW})^2} \cdot W_{Csw}\right]^2 + \left[\frac{-1}{(\delta_{SW} - \delta_{GW})^2} \cdot W_{Cs}\right]^2} \quad 5.18$$

Where W_{Csw}, WC_{gw}, and W_{Cs} were uncertainty components in surface water plus rain, groundwater and surface water only, respectively, represent the standard deviation plus the analytical uncertainty associated with each component. δs is isotopic concentration of only surface water (sampled marsh water). Hydrograph separations included analytical uncertainty for δD and δ18O of 1‰ and 0.2‰, respectively.

Table 5.2 shows the separation of surface and groundwater components (in percentage). In 2013, there was a significant contribution of surface (new) water at the beginning of the season due to the contribution of snow melt, or groundwater piston-like flow as a result of the spring freshet. With time, the surface water contribution decreases and groundwater (old) component contributions gradually increase. This behavior is anticipated as the bulk hydrologic 'new water' volume in cold regions is typically the snowmelt at the start of the season.

In 2014, due to a very wet year and large rainfall event (peak hydrologic flow that year) in late spring that coincided with the end of snow melt, surface or new water contributions remained near 100%, with contributions from groundwater being negligible. The component separation resulted in surface water contributions exceeding 100% in several time steps in 2014, yielding negative groundwater contributions. In these cases, surface water contribution was set to 100% and groundwater to 0%. This was likely a numeric artefact of the two-component separation method assumptions being violated in 2014, specifically due to the significant contribution of snowmelt and/or flood waters entering the Marsh simultaneously with rainfall (i.e., a third

component that would have been analyzed in a three-component separation analysis). In this study, sampling of snowmelt did not coincide with groundwater sampling and hence a three-component separation method was not possible. Overall, in 2013 average surface water contributions were found to be 59.8% (or 40.2% for groundwater). In 2014, average surface water and groundwater contributions were 91.82% and 8.18%, respectively. Uncertainty was calculated using Equation 5.18, which yielded overall uncertainty estimates of 31% for two years (20% in 2013 and 26 % in 2014) (Table 5.3).

Table 5.2 - Separation of surface water (new) and groundwater (old) components. Separations were calculated using both stable water isotopes (δD and δ^{18}O), with the final value calculated as the mean of both two values. NOTE: in time steps where surface water contribution exceeds 100%, it was set to 100%, and groundwater to 0%. Columns labelled as "SW" and "GW" under "Final" represent a mean values of percentage separation calculated using δD and δ^{18}O for a corresponding component.

$$Rsw = \frac{(\delta_R - \delta_{GW})}{(\delta_{SW} - \delta_{GW})} \cdot R$$

					Final (%)	
2013	**Surface water (SW) (%)**		**Groundwater (GW) (%)**		**SW**	**GW**
	δD	**δ^{18}O**	**δD**	**δ^{18}O**		
20-Jun-13	71.28	83.40	28.72	16.60	***77.3***	***22.7***
27-Jun-13	58.51	71.52	41.49	28.48	***65.0***	***35.0***
3-Jul-13	58.01	70.20	41.99	29.80	***64.1***	***35.9***
17-Jul-13	55.12	67.32	44.88	32.68	***61.2***	***38.8***
24-Jul-13	54.33	68.69	45.67	31.31	***61.5***	***38.5***
30-Jul-13	53.18	64.34	46.82	35.66	***58.8***	***41.2***
7-Aug-13	56.25	69.74	43.75	30.26	***63.0***	***37.0***
13-Aug-13	53.56	63.70	46.44	36.30	***58.6***	***41.4***
22-Aug-13	56.65	67.87	43.35	32.13	***62.3***	***37.7***
27-Aug-13	48.44	58.39	51.56	41.61	***53.4***	***46.6***
4-Sep-13	45.45	57.66	54.55	42.34	***51.6***	***48.4***
12-Sep-13	46.34	57.17	53.66	42.83	***51.8***	***48.2***
18-Sep-13	51.46	62.43	48.54	37.57	***56.9***	***43.1***
9-Oct-13	46.63	56.33	53.37	43.67	***51.5***	***48.5***
2014						
	δD	**δ^{18}O**	**δD**	**δ^{18}O**	***δD***	***δ^{18}O***
17-Jun-14	102.46	118.34	0.00	0.00	***100.0***	***0.0***
24-Jun-14	96.00	104.23	4.00	0.00	***100.0***	***0.0***
03-Jul-14	118.09	137.56	0.00	0.00	***100.0***	***0.0***
12-Aug-14	89.51	96.49	10.49	3.51	***93.0***	***7.0***
19-Aug-14	80.68	88.97	19.32	11.03	***84.8***	***15.2***
26-Aug-14	75.63	87.64	24.37	12.36	***81.6***	***18.4***
03-Sep-14	78.42	88.13	21.58	11.87	***83.3***	***16.7***
10-Sep-14	94.13	110.13	5.87	0.00	***100.0***	***0.0***
17-Sep-14	78.22	85.89	21.78	14.11	**82.1**	**17.9**
22-Sep-14	96.71	109.37	3.29	0.00	**100.0**	**0.0**

Table 5.3 - Uncertainty in surface water and groundwater component separations.

	δD (%)	δ^{18}O (%)	AVERAGE (%)
2013	20	20	20
2014	25	26	26
OVERALL	32	31	31

From the isotope hydrograph separation (IHS) analysis, the two-component seasonal separation method appears to work in 2013, which was a more 'normal' hydrological year (Figure 5.5). At the beginning of the season, surface water dominates due to the contribution of snowmelt and rainfall derived runoff and channel inflows. Surface water and groundwater contributions subsequently begin to converge as the season goes on, which is expected by the late fall as baseflow (groundwater) begins to dominate. Had sampling continued into winter, it is anticipated that groundwater contributions would exceed surface contributions and tend toward 100% as ice cover prevents new water, or surface runoff, contributions.

In 2014 (Figure 5.6) conditions were surface water dominated. We did not use event-based sampling, which would be recommended especially for capturing the third component for separation analysis, which contributed to the breakdown of the methodology.

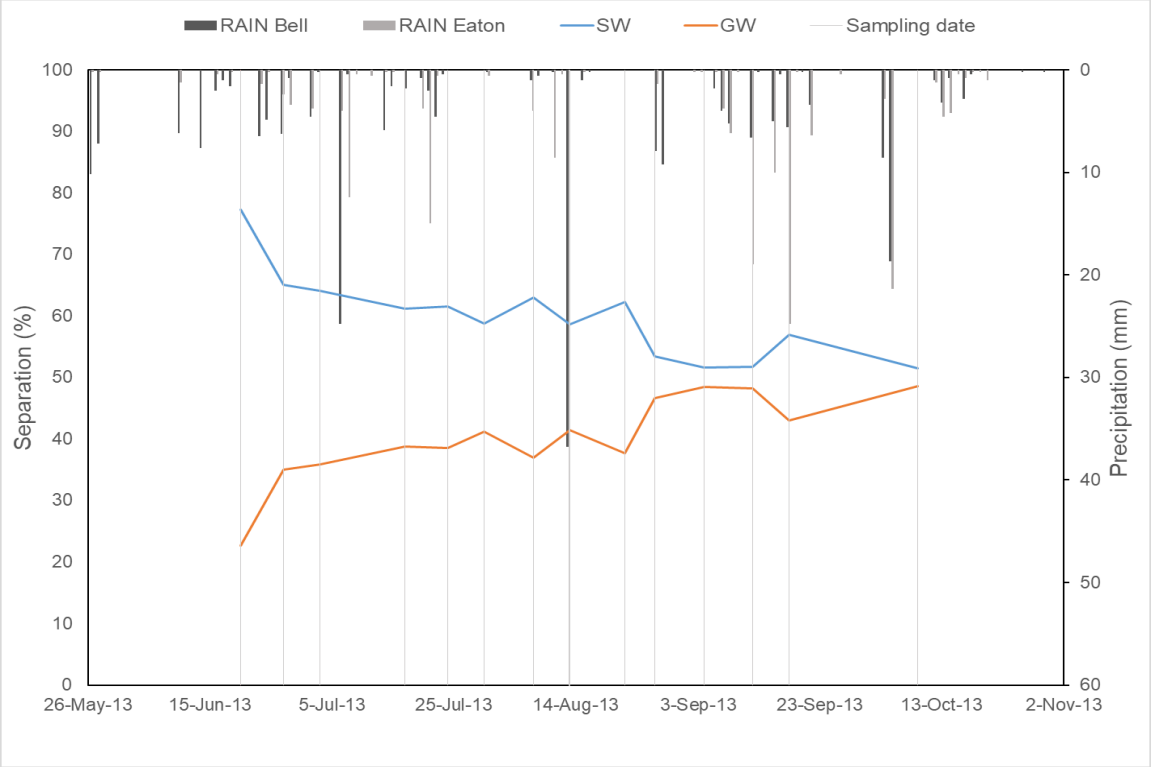

Figure 5.5 - Separation of surface water (with rain) and groundwater in 2013. Vertical light gray lines show dates when precipitation samples were collected. Precipitation bars are presented on the second x-axis with corresponding amounts (in mm) on the second y-axis

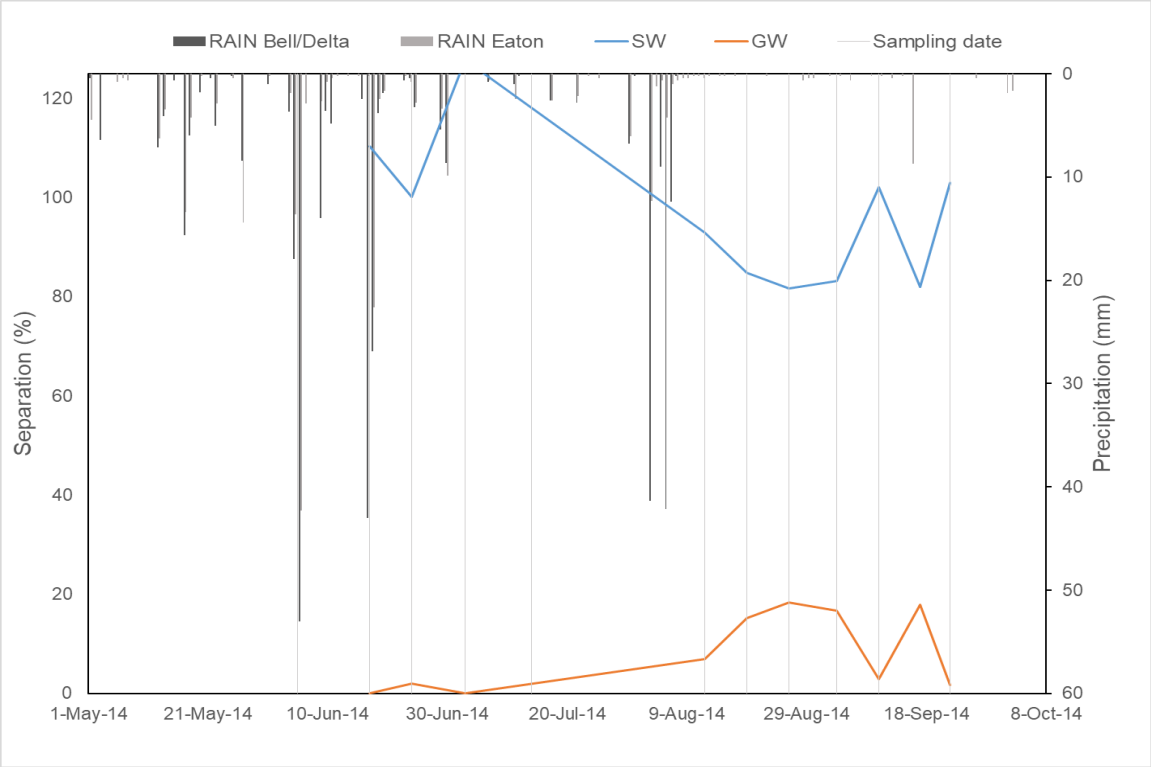

Figure 5.6 - Separation of surface water (with rain) and groundwater in 2014. Vertical light gray lines show dates when precipitation samples were collected. Precipitation bars are presented on the second x-axis with corresponding amounts (in mm) on the second y-axis

5.5 Summary

Based on the dual framework analysis and corresponding end points, it was shown that the Marsh is not in a hydrologic steady state (inflows are higher than outflows) over the 2013-2014 study period, which was also confirmed by Aminian (2015). Isotope mass balance shows the extent of the impact the evaporation component of the water cycle has on the seasonal water balance. On the other hand, it was shown that the Penman-Monteith method does not accurately capture the evaporative water loss across the Marsh, perhaps owing to the seasonal plant growth affecting open water area and evapotranspiration partitioning (relative contribution of the transpiration component). There is also significant spatial variability in ET loss (impact on water balance). Based on a sensitivity analysis, we conclude that evapotranspiration was generally

underestimated by the Penman-Monteith method. Separation of streamflow components was conducted using two component isotope separation. Old water component was separated into groundwater and surface water. Two component separation is applicable in 2013 ("normal" hydrologic year) while the method breaks down in the flood dominated year (2014) due to significant contribution from a third component that was not captured by our analysis (Lake Manitoba or snowmelt).

Due to significant difference in processes (ET) in time (2013 and 2014) and space, it is suggested that spatially distributed models be used to examine the variations in water budget across the Marsh. We need to look more closely at time varying water balance components.

6 Volume Dependent Model

In Chapter 6, a volume-based modelling approach is applied to estimate the Marsh residence time, water yield and water losses due to evaporation. All these components are important for defining overall hydrologic behavior and response of the Marsh over the long-term. Long-term baseline conditions were assessed for 2013-14 period and can be used in future look of water balance over the Marsh as well as in climate change assessment.

6.1 Methodology

Here it was assumed that the Marsh is in isotopic and hydrologic steady-state over the long-term, allowing the water balance to be presented as:

$$I = Q + E\ (m^3\ ) \tag{6.1}$$

$$I\delta_I = Q\delta_Q + E\delta_E\ \ (m^3‰) \tag{6.2}$$

where I, Q, and E are the Marsh inflow, outflow and evaporation with corresponding delta values ($\delta_I, \delta_Q, and\ \delta_E$) were in ‰, respectively. The Penman-Monteith method estimates ET, though the isotope model requires an estimation of open water loss, E. An assumption is made that the

ET calculated in Chapter 5, Section 5.3 (scaled value of Penman-Monteith) represents seasonally-averaged E for the Marsh, such that 1.25 ET (2013) and 1.18 ET (2014) were used. In steady-state, the isotopic composition of outflow was assumed identical to the Marsh composition ($\delta_Q = \delta_L$). Rearranging Equation 6.1 to $Q = I - E$ and substituting into Equation 6.2, we can estimate the fraction of water loss by evaporation, or the evaporation to inflow ratio (x):

$$x = \frac{E}{I} = \frac{\delta_I - \delta_L}{\delta_E - \delta_L} \text{ (dimensionless)} \quad 6.3$$

Water and isotopic mass balance are calculated for the Marsh as one system, unlike in Chapter 5 (i.e., where the Marsh was divided into two CFSTR). The surface area of the Marsh is approximated to be 46.2 km^2, on average. The Gap, or the connecting channel between western and eastern compartments, is disregarded from our inflow calculations in this methodology since we deal here with the Marsh volume as one unit. Therefore, for the inflow calculation, only inflows from Portage Creek, Delta Channel, Clandeboye Channel, overland flow, and ground water were considered. Using Equation 6.3 and the δ_I conditions mentioned below (Equations 6.10 and 6.11), the evaporation to inflow ratio is calculated on a daily time step and then averaged across the period of analysis (i.e., kept the same as from Chapter 5).

Three methods were used to calculate the isotopic composition of inflow, with each method presented in detail in Chapter 4, Table 4.3. In general, since we cannot state which method is better for estimating the inflow to the Marsh, therefore we apply all three as a sensitivity analysis of the Marsh response to changing inflow. Here it is assumed that the Marsh is a non-headwater system (i.e., downstream within the drainage order), and therefore inflow was not solely derived

of meteoric origin, but rather influenced by upland surface water flows and drainage (Haig, 2018). Accounting for upstream inflow (J), and assuming negligible change in total Marsh volume (-72 mm in 2013, 260 mm in 2014) over the sampling interval, a simplified mass balance can be presented:

$$I = P + R + J\ (m^3) \tag{6.4}$$

where P (mm/day) is precipitation, R (m^3/day) is runoff, and J is upstream inflow from Lake Manitoba and the watershed (m^3/day). Precipitation was arithmetically averaged between two meteorological stations and converted to m^3/day by multiplying with the surface area of the whole marsh (46.2 km^2) and divided by a daily time step.

Considering the isotopic signature of these sources, Equation 6.4 can be expanded to reflect the dual isotope mass and water balance:

$$\delta_I = \frac{P\delta_P + R\delta_R + J\delta_J}{P + R + J}\ (‰) \tag{6.5}$$

where δ_I, δ_P δ_R, and, δ_J are the isotopic compositions of the inflow, precipitation, runoff, and upstream inflow, respectively (‰). δ_P was calculated as an arithmetic average of precipitation samples collected at both meteoric stations, Eaton and Bell. To estimate runoff, it was assumed $\delta_R \approx \delta_P$, or limited fractionation along the flow path due to turbulence (Gibson & Reid, 2014). Rearranging Equation 6.4 and using Equation 6.3, runoff can be written as:

$$R = \frac{E}{x} - P - J\ (m^3) \tag{6.6}$$

Substituting Equations 6.3 and 6.4 into Equation 6.5, the inflow composition, δ_{I}, for the Marsh can be calculated to incorporate inflow along the flow path:

$$\delta_I = \frac{-J\delta_J\delta_L + \mathrm{E}\delta_P\delta_E - \mathrm{E}\delta_L\delta_P + \mathrm{J}\delta_P\delta_L}{\mathrm{E}\delta_E - \mathrm{E}\delta_L - \mathrm{J}\delta_J + \mathrm{J}\delta_P}\ (‰) \tag{6.7}$$

where J is the sum of all the inflows into the Marsh, including (in this study) inflows from Lake Manitoba, δ_j is the flux-weighted average, well-mixed isotopic concentration of all the inflows in any given timestep, δ_{L} is the mean isotopic composition of all measured open water Marsh samples across the Marsh at any given time step, δ_{E} is daily isotopic signature of the evaporative flux, over a period of analysis. δ_j (‰) is calculated based on a mixing model theory:

$$J\delta j = DC \cdot \delta_{LMB} + PC \cdot \delta_{PC} + OLF \cdot \delta_{OLF} + GW \cdot \delta_{GW} + CC \cdot \delta_{LMB} \tag{6.8}$$

$$\delta j = \frac{DC \cdot \delta_{LMB} + PC \cdot \delta_{PC} + OLF \cdot \delta_{OLF} + GW \cdot \delta_{GW} + CC \cdot \delta_{LMB}}{J} \tag{6.9}$$

where DC, PC, OLF, GW, and CC are water fluxes from Delta Channel, Portage Creek, overland flow (m^3/s), ground water (m^3/s), and Clandeboye Channel (m^3/s), respectively. δ_{PC}, δ_{OLF}, δ_{GW} are corresponding isotopic signatures (‰), with δ_{LMB} representing the isotope concentration of Lake Manitoba from the sample locations close to Delta Channel on the west and Clandeboye Channel on the east. Isotopic compositions were assumed constant between two sampling periods. In 2013 Lake Manitoba samples were collected at Delta Beach (location DB and

LLS046) on the west side, and about 5 km northwest from Delta Beach (location LLS013). DB was sampled only once and LL046 eight times. Only isotope samples collected at Delta Beach were used in the δ_j calculation for Delta Channel and Clandeboye Channel as well. Since sampling on the eastern side of Lake Manitoba was not performed, we assumed the same isotopic composition as LLS046 and DB across the whole Marsh. Samples from the location further north (LLS013) were disregarded since samples collected at DB would be more representative of the inflow concentration that Delta Channel would see. In 2014, however, samples were collected at DB and close to Clandeboye Channel on the east side (location STA); the ones collected at DB were used for Delta Channel, and the ones collected at STA were used for Clandeboye Channel. Results for $\delta_I$and x are presented in Table 6.1.

It is necessary to mention that, here, δ_{E} was calculated on a daily time step using Equation 5.4, relative to a weekly or bi-weekly basis as was used in Chapter 5 for time-series modelling. The isotopic composition of precipitation and all Marsh samples was held constant for the period of time between sampling, while temperature and relative humidity changed daily. Temperature (T) and relative humidity (RH) were averaged (on a daily basis) between the two meteorological stations since the analysis was for the entire marsh. RH was constrained to less than 88%, as per the International Atomic Energy Agency (IAEA) working group recommendations (IAEA, 2018) to ensure a turbulent, non-diffusive boundary layer for evaporative fractionation (δ_{E}). Beyond RH's of 88%, fractionation ceases and the Craig and Gordon model no longer applies (IAEA, 2018) as transport is defined by diffusion through the atmosphere rather than by turbulence.

Isotopic composition of the inflow was calculated using Equation 6.7. In some time steps, the isotopic composition of the Marsh was more depleted than the inflow, which is generally not

possible according to the dual framework analysis. This can occur in reality, however, due to a time lag along the flow path between the (observed) Marsh composition and the (calculated) upstream inflow composition. Therefore, we set the following conditions mathematically:

$$if\ \delta_I < \delta_L\ then\ \ \delta_I \tag{6.10}$$

$$if\ \delta_I > \delta_L\ then\ \ \delta_L \tag{6.11}$$

This can be further clarified by the fact that, in the case of a big rainfall event, the composition of the Marsh can be more depleted than that of the inflow. Due to incomplete mixing present in reality, it takes some time for the isotopic composition of the Marsh (δ_L) to adjust.

Chemical content, biological properties as well as ecosystem function of lakes are strongly affected by residence time (Haig, 2018) . Residence time is considered as one of the most commonly estimated outputs of isotopic mass balance calculations (Brooks et al., 2014; Gibson et al., 2016). In Aminian (2015), it was reported that residence time using a conventional hydrologic or hydraulic approach has not been calculated due to the complicated bi-directional flow within the Marsh. Here, we have accounted for that by separating inflows from outflows based on sign convention, as defined in Chapter 5.

In general, water yield and overland flow can be estimated using stable water isotopes (Haig, 2018). Runoff at the hillslope and catchment scale are controlled by factors integrated from isotope mass balance (Bennett et al., 2008; Gibson et al., 2017, 2015b, 2010a). Large snow accumulation and quick melt over frozen and water-saturated soils produce larger runoff

(Pomeroy et al., 2007; Coles et al., 2017; Coles and McDonnell, 2018). Gibson et al. (2015b) suggested there is strong correlation between high water yield (i.e., runoff) and areas of thawing permafrost. This is also relevant for snowmelt-dominated, frozen soil environments. Delta Marsh lies along the boundary region between Prairie and Boreal Plain, hence the findings of Gibson et al. (2015b) are applicable to our study region.

Residence time (or transit time, τ) of a reservoir is the time that a parcel of water spends in a reservoir (Dingman, 2015). It is estimated as follows:

$$\tau = \frac{V}{I} = x\frac{V}{ET} \quad 6.12$$

where V is the mean volume of the Marsh (m^3), I is the inflow (m^3/s), ET is total evapotranspiration over the study period (mm/day), and *x* is evaporation to inflow ratio. ET was converted to m^3/s by multiplying by the whole Marsh area. Residence time results using the conventional hydraulic and isotopic approach are presented in Table 6.2.

Water yield (WY (mm/year)) is expressed as the depth of runoff R (m^3) from the watershed (Gibson et al., 2015b) as follows:

$$WY = \frac{R}{WA} \cdot 1000\ (\frac{mm}{year}) \quad 6.13$$

where, WA is the watershed area (m^2). Since the watershed area that is contributing to the Delta Marsh study region was difficult to delineate because of changing wetland structure (based on seasonal water levels), flat terrain, and lots of tiny channels; it was estimated from a long-term steady state in ArcGIS and found to be 348.2 km^2. We also considered a range of contributing watershed area between 300-400 km^2 to develop a sense of how water yield varies seasonally or inter-annually (ranging between 324 - 243 km^2 in 2013 and 320 - 240 km^2 in 2014).

As addressed by Gibson et al. (2019)**,** the isotope mass balance (IMB) determines water yield variability of lakes on the Boreal Plain. In that study, the mean value of water yield based on IMB was 130 mm/year, which was similar to the average WY value of 137 mm/year estimated from hydrometric gauges in their study. Good agreement between water yield determined from IMB and Water Survey hydrometric gauging stations was reported by Bennett et al., (2008) for the Fort McMurray region, demonstrating that isotopes can be used as surrogates for hydrometric estimates of WY and residence time in regions that are ungauged but having isotope data.

When mean WY is less than total annual precipitation this means that a fraction of annual precipitation falling within the watershed did not enter the study lake area (Haig, 2018). In Delta Marsh, Portage Diversion, groundwater and Lake Manitoba all contribute to the water yield calculation, with the only exception being precipitation (Table 6.2). When water yield exceeds precipitation that means there is more components contributing to runoff which is generally a long-term unsustainable system. This is caused likely because of high water levels on Lake Manitoba relative to thirty-year historical levels.

6.2 Results and Discussion

In Table 6.1 are presented the results for δ_I estimated using the Haig (2018) approach and x using both the hydrometric formula (τ=V/I) and the isotopic approach.

Table 6.1 – Isotopic composition of the inflow (δ_I), and evaporation to inflow ratio (x) using isotopic and conventional hydraulic approaches.

	δ_I (‰)		$x = \frac{\delta_I - \delta_M}{\delta_E - \delta_M}$ (%)			$x = \frac{E}{I}$ (%)
	δD	**δ^{18}O**	**δD**	**δ^{18}O**	**Mean(σ)**	
2013	-73.46	-13.65	23	20	22 (54)	187
2014	-89.52	-10.21	29	19	24 (28.1)	337

Mean *x* values using the IMB approach were lower in 2013 (μ = 22 %, σ = 54 %) and were slightly higher in 2014 (μ = 24%, σ = 28.1%). Big deviations in both mean and variability were present in these data.

On the other hand, the standard hydrological or physical measurement method gave significantly higher mean values, 187% and 337% for 2013 and 2014, respectively. Since E/I ratios exceeding 100% would result in outflows that exceed inflows, and therefore Marsh isotopic compositions that approach δ^* on the framework, these values are considered to be non-realistic. Based on the framework analysis, *x* should be less than 0.5, which was in fact the case for isotopically-derived values of *x*. Isotopes respond to the evaporation component of the water balance most significantly, making them good for estimating E/I ratios.

In Phillips (1976) it was shown that transpiration can exceed 75% of total ET at analyzed sites. More recently, Jasechko et al. (2013) reported that 80 to 90% of total terrestrial ET flux globally can be attributed to transpiration. In this study we assumed a negligible long-term transpiration component, but it is likely a more significant component of ET estimated by the Penman-Monteith method toward the mid to end of summer and throughout the fall when vegetation cover is more prominent. This assumption in our methodology, therefore, likely generates unrealistically high values of x (assuming ET $\approx$ E) for the hydrologic approach. Based on Jasechko et al. (2013) and account for 80% of total terrestrial ET flux as transpiration, 37.5% for 2013 and 67.5% for 2014 for contributed to evaporation (20% of total *x* calculated using hydraulic approach). As stated in Chapter 5, the Penman-Monteith method is not well designed to estimate ET over relatively large open water and wetland surface areas. This method was selected for this research for two reasons; first, we wanted to be consistent with the hydrologic model (Schellenberg, 2017) that was used as part of the Delta Marsh study; and second, each method for estimating evapotranspiration has its own flaws, and no one method is specifically better than the other one. Additionally, the water balance during our seasonal study periods (approximately five to six months) did not close, and in fact suggested there was more inflow in the system (than outflow), which was not captured by the standard hydraulic approach.

Bortulouzzi (2013) estimated the residence time for Cadham Bay using two approaches. She found that residence time estimates ranged from 4.5 to 166 days, with an average of 25 days. Cadham Bay area is approximately six time smaller than our study area encompassing the majority of the Marsh. Assuming everything is scalable (which is not always the case hydrologically), we end up we a similar residence time values as derived by isotopic method in

our study, 99 days in 2013 and 140 days in 2014 (Table 6.2). In Table 6.2, results were presented for mean precipitation and mean inflows to the Marsh; as well as total precipitation, total evaporation, residence time (τ), total runoff (R), and water yield (WY). Residence time was calculated for deuterium and oxygen-18 separately, and then averaged. Water yield exceeded precipitation, implying additional watershed or marsh storage must be contributing to runoff on an inter-annual basis.

Table 6.2 - Total precipitation and evaporation, average of all inflows (mean J), and runoff. Residence time (τ) calculated using isotopic and conventional hydraulic approaches and water yield (WY) range using isotopic approach. WA (water surface area); ranges between 300-400 km^2, long term estimated WA is 348.2 km^2.

	2013	***2014***
sum P (mm)	*188*	*263*
sum P (m^3)	8,714,590	12,158,079
sum E (m^3)	23,006,990	26,102,915
mean J (m^3)	603,693	882,000
$\tau = \frac{V}{I}$ ***(days)***	117	102
$\tau = x\frac{V}{ET}\ (\delta D)$***(days)***	106	168
$\tau = x\frac{V}{ET}\ (\delta 18O)$ ***(days)***	92	112
$\bar{\tau}$ ***(days)***	99	140
R = E/x - P-mean J (m^3)	97,248,171	96,120,905
WY (mm) (WA = 300 km^2)	324	320
WY (mm) (WA = 348.2 km^2)	**279**	**276**
WY (mm) (WA = 400 km^2)	243	240

Haig (2018) made a similar comparison between gauged data and a non-headwater IMB model for all years (twelve) and lakes (seven inter-connected) within the Qu'Appelle River basin. She

estimated a mean E/I of 15.3 % using IMB, which was very close to that estimated from instrumental data (15.0 %); both of which are close to the results presented here for the IMB approach (~ 20 %). Haig (2018) reported a residence time of 0.56 year (~ 204 days) over a 637.2 km^2 surface area, which can be considered representative of runoff in Prairie environments. Components that contribute to the residence time calculation must be considered uniquely, however, this offers a deeper understanding of the difference in spatial and temporal variation between two studies, sizing of the watersheds (52 000 km^2 vs 580 km^2), water body surface area, meteorology, and hydrology (inter-connected lakes vs. marsh environment).

If we accounted for uncertainties that were carried forward from the hydraulic and hydrologic models (i.e., simulated inflows), this would result in slightly higher residence time values using the conventional hydraulic approach (126 days in 2013 and 109 days in 2014). Therefore, these modelling uncertainties alone do not account for the inaccuracies when using this method to compute residence time. This uncertainty does affect the residence time, water yield and evaporation to inflow ratio (x) calculated from the isotopic method. This method also results in slightly higher residence time values of 108 days in 2013 and 158 days in 2014. The evaporation to inflow ratio increases by 2 to 3 % (24 % in 2013, and 27 % in 2014) and water yield decreases (253 and 241 mm/year in 2013 and 2014, respectively).

6.3 Summary

In Chapter 6 evaporation to inflow ratio, residence time, and water yield were estimated using the stable water isotope approach and compared to hydraulic metrics. E/I using IMB method was found to be 22% and 24% for 2013 and 2014, respectively. The hydraulic-based approach gives

unrealistic values, which are not commensurate with the evidence obtained by our sampling program and fails as a result of assuming steady state hydraulic conditions. Caution should be used when applying these methods in the future. Isotope methods should consider preferable as they account for evaporation loss. Evidence from the isotope framework derived in Chapter 4 and from Aminian (2015) demonstrate that the Marsh is not in hydrologic steady state over this study period. Water residence time using IMB was found to be 99 days in 2013, and 140 days in 2014, which is close to the average residence time estimated using Cadham Bay (Bortulozzi, 2013), assuming everything is scalable by contributing area. An average yearly water yield is similar for both years (approx. 280 mm) and ranges between 240 and 325 mm.

7 Conclusions and Recommendations

7.1 Conclusions

Delta Marsh is one of the largest freshwater wetlands in North America, spanning approximately 185 km^2 (Ducks Unlimited Canada, 2013). Delta Marsh Watershed (DMW) extends along the southern shore of Lake Manitoba (Ducks Unlimited Canada, 2013). A total open water surface area of the Marsh is 46.2 km^2, with 6.9 km^2 belonging to the West Marsh (between Delta Channel and the Gap) and 39.3 km^2 to the East (between the Gap and Clandeboye Channel). Over the course of fifty years, the health of the Marsh has deteriorated, resulting in an increase in cyanobacterial blooms, intrusion of invasive fish and plant species, and consequently a decrease in flora and fauna and a loss of productive recreational use of the marsh. Several studies have been conducted in order to address these concerns: studying the wet – dry cycle in prairie wetlands (Murkin et al., 2000), the impacts of common carp on water quality, sedimentation, algae and submerged vegetation (Hertam, S.C., 2010; Badiou, 2005; Badiou & Goldsborough, 2014), and patterns in hydrology and water chemistry of the marsh and impact of Lake Manitoba hydrology (Bortoluzzi, 2013). The hydrology of DMW (Schellenberg, 2017), and hydrodynamic modelling within Delta Marsh and Lake Manitoba, along with discharge estimation (Aminian, 2015), together with this study, are part of the *Delta Marsh – Restoring the Tradition Project* that

has been conducted by the Department of Civil Engineering at the University of Manitoba. Each of these project components contribute to a better understanding of the lake-marsh-watershed system.

Stable water isotopes of precipitation, Marsh and Lake Manitoba water, groundwater, evaporation, snow, and ice were collected over a four-year period from 2013-2016. A total of 2145 samples were analyzed and a dual isotopic framework was established to understand source water contributions to Delta Marsh.

An isotope framework was established for a two- and four-year period. The slope of the local meteoric water line (LMWL) for the two-year period (2013-2014) was 7.8 and for the four-year period (2013-2016) is 7.7, indicating a relatively constant meteorological response. Hence, we find consistency in the origin of precipitation for the Marsh during both the shorter duration study period, and longer-term study period. Air masses over the prairie region vary from the tropical region of the Pacific Ocean to air masses originating from the North Pacific and Arctic Ocean (St. Amour et al., 2005), and that is captured by the isotope in precipitation signature over the study period. We were able to capture heavy rainfall with highly depleted isotopic signatures, suggestive of a different air mass origin for large storm events. A very small rainfall event with a highly depleted isotopic signature was also being captured, implying that source moisture can be derived from re-evaporated moisture across the Marsh. This can be very important in monitoring long-term hydrometeorologic conditions for the Marsh, particularly under changing climates and during periods with no rain or very little rain.

A dual isotope framework analysis was performed to determine the framework end points. The framework showed that the Marsh was not in a hydraulic steady-state, and that inflows are generally greater than the outflows based on the positioning of the marsh endpoint, δ_L (closer to δ_I). If the Marsh was in hydrologic steady state, δ_L would have been closer to the mid-section of the LEL and near the steady state composition (δ_{SS}), or half way between δ_I and δ^*. Hydraulic modelling (Aminian, 2015) also confirmed that the Marsh is not in steady-state during the study period.

The stable water isotope signature of the Marsh varied from west to east with the mid-section most influenced by evaporation, and less influenced by Lake Manitoba or river inputs. Middle section of the Marsh is more prone to evaporation (is more like a reactor/system on its own), while west and east end points are more influenced by Lake Manitoba and groundwater.

An isotopic non-steady state time-series mass balance model was setup for the two-year study period (2013-2014). Due to no significant change in the Marsh volume and negligible isotopic change, a time dependent model was used. Isotope concentrations were paired with inflows from hydraulic (discharges from Delta Channel, the Gap, Portage Creek, and Clandeboye Channel) (Aminian, 2015) and output from the hydrologic model (overland flow and groundwater flow) derived by Schellenberg (2017). The flow in the Marsh and connectivity of the channels was bi-directional, therefore a sign convention was established to define positive inflows and negative outflows.

Time series analyses was performed to examine changes in evapotranspiration (ET) (calculated using Penman-Monteith method) from the Marsh and its relative contribution to the Marsh water balance. It was found that evaporation is likely more dominant (as a component of ET) at the beginning of the season, while later in the season, with increased plant growth, transpiration becomes increasingly more dominant. The water balance did not close for the modelled period of five to six months, again demonstrating that inflow was higher than outflow for this study period.

Depletion due to flooding on July 1st 2014 was captured in the Marsh isotopic signature, with a greater intensity in the East Marsh due to a higher volume of (more isotopically depleted) water from Lake Manitoba entering Delta Marsh through Clandeboye Channel. This demonstrates that isotope records are in fact capable of capturing the relative mixing and changes in source water contributions from the upland watershed and Lake Manitoba, as well as importance of using spatially varying models for the Marsh.

Sensitivity analysis combined with a statistical analysis was conducted in order to verify ET estimated by the Penman-Monteith method (Schellenberg 2017), along with the spatial variability of ET estimates across the Marsh. Final results indicated that ET in 2013 was likely 1.25 times higher than calculated using the Penman-Monteith method; while in 2014 it was likely 1.18 times higher. We found this factor to be temporally dependent, (factor on average larger at the begin of the season, smaller at the end), likely due to changing contribution of transpiration.

The interaction between Lake Manitoba and Delta Marsh was analyzed by isotopic separation of water components (old versus new water). Seasonal hydrologic component analysis assuming old and new water contributions from groundwater versus precipitation and/or Lake Manitoba sources using stable water isotopes was highly variable between 2013 and 2014. In 2013, the surface water component was more dominant at the beginning of the season, due to the contribution of snow melt. Our season started at the beginning May and therefore snow was not captured as a process but wetlands have hydrologic memory (stores water). Later in the season, groundwater contributions increased, while surface water (or new water components) decreased in their relative contribution to maintaining the Marsh water levels. This can have significant implications for the Marsh water temperature and oxygenation, impacting the aquatic habitat of the Marsh. In 2014, due to it being a very wet year and a large flood event in July, component separation analysis failed due to not distinctive isotopic separation between groundwater and Lake Manitoba and the contribution of more than two components. It also means that in cases of high water events (e.g. floods), groundwater is highly influenced (connected to) by Lake Manitoba and that old/ new water separation cannot be applied unless three component analysis is done.

In Chapter 6, IMB methods were used to estimate water loss due to evaporation (x =E/I), residence time (τ) and water yield (WY) for Delta Marsh. For these estimates to be accurate representations of water residence time and losses from the Marsh, a volume-based assessment seeing the Marsh as one body (volume as one unit) was performed. Calculated E/I ratio and τ from the IMB were compared to more traditional hydraulic instrumentation approaches. Evaporation to inflow ratio was 22% and 24% for 2013 and 2014, respectively. WY was

calculated using the isotope method and was found to be ~280 mm/year. Due to Marsh not being in a hydraulic steady state, hydraulic approach of calculating *x* failed, showing that stable water isotopes only are capable of recording *x* and that hydraulic τ should not be applied to the Marsh.

Some limitations of the current study include:

- Non-uniform sampling periods and inconsistent sampling location was a challenge. Better spatial and temporal insight could have been gained with more uniform, consistent sampling.
- More detailed and consistent groundwater sampling throughout the study would be preferable. In 2013, only groundwater well GW01 was sampled; the other wells were added throughout the study period.
- Inclusion of the rest of the Marsh;
- Longer field seasons that include snowmelt and further into the fall would be very beneficial, but were not possible on Delta Marsh due to the duck hunting season;
- Higher resolution Lake Manitoba sampling and concurrent river samples (there were times when there was flow following rainstorms that we did not sample);
- Lidar over the entire Marsh for improved sub-basin and upland area delineation due to flat, low-relief topography;
- Three component mixing model separations to account for groundwater composition being too similar to Lake Manitoba, and snowmelt which was not analyzed;

- More frequent, event-based time series isotopic records for precipitation (to give us time series of evaporated flux);

- More detailed hydraulic measurements to get better estimates of residence time in the Marsh for comparison to IMB methods; and

- Continuous hydrologic modelling of the inflows to the Marsh

7.2 Recommendations

Recommendations for future researches and resource managers specific to this study are:

- Expanding the isotope mass balance model with the necessary fluxes for 2015 and 2016 would be a great addition to the current work and would give us better insight into hydrological behavior of the Marsh between two- and four-year period.
- To look at re-evaporated moisture that influences δ_E (i.e., monitor vapour phase isotopic composition and precipitation, and compare if they are in equilibrium).
- Longer-term monitoring of groundwater GP wells since they were installed end of 2015 and beginning of 2016. Better installation of GP wells and methodology of sampling compared to GW02 – GW05 would give more in-depth look at the impact of groundwater on the Marsh system.

- Observe ET fluxes (using eddy covariance tower), where more detailed monitoring of evaporation would be the most significant improvement for the future understanding of

the Marsh water balance since evaporation is a significant component of the water balance and highly uncertain.

- Couple water quality (WQ), total suspended solids (TSS) and isotope analyses, along with physical properties of water can help with source separation analysis (if we knew the TSS of Lake Manitoba and groundwater we would have more information about separation/contribution).

Appendix A: Supplementary Material

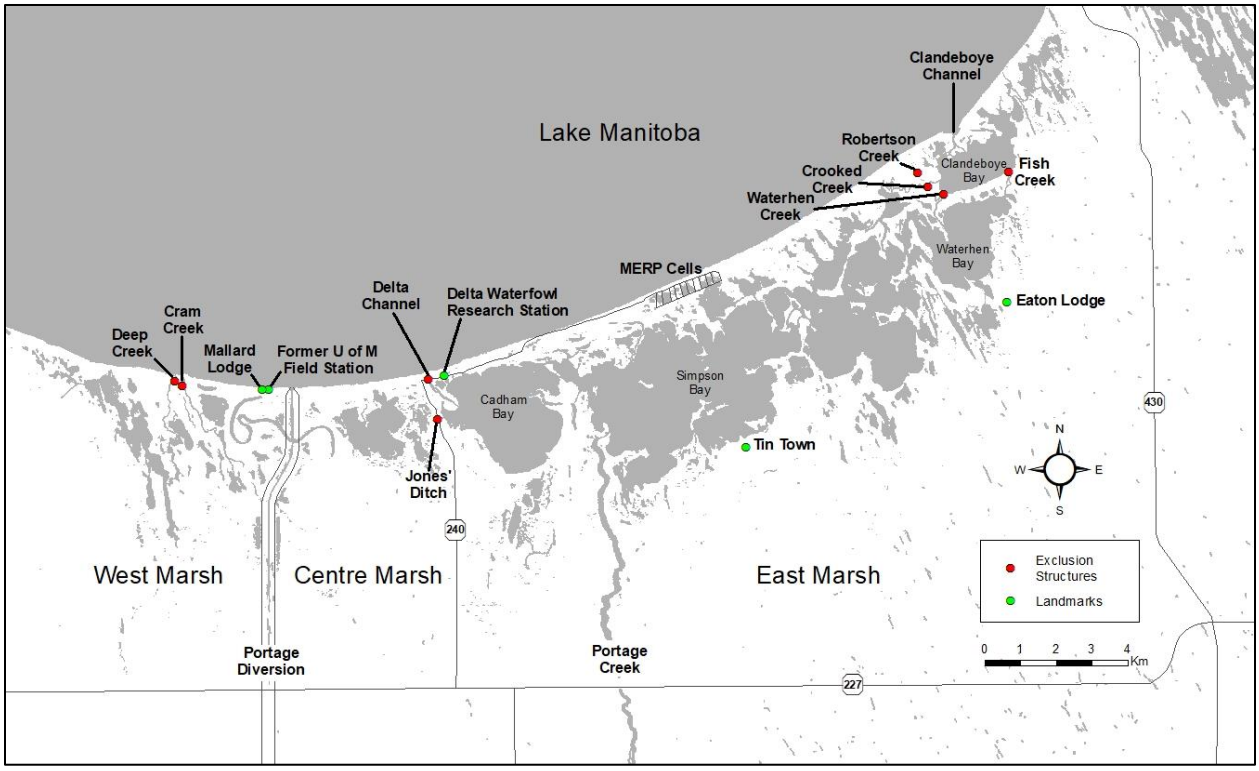

Figure A.1 - Separation of Delta Marsh into West, Central, and East Marsh (Ducks Unlimited Canada, 2020). West Marsh in our study covers Cadham Bay and East Marsh covers area east of Cadham Bay.

Table A.1 - Stable water isotopes sampling locations . "Type" stands for different sampling types: "L"- for Marsh and Lake Manitoba samples, "G"- for groundwater samples, "C" for channels, "R" for rivers, "P" – precipitation, and "E"- evaporation. In bold font are locations that were sampled on a regular basis throughout a four-year period. Non-bolded are location sampled during synoptic survey in 2016.

ID	Short Form ID	Latitude (DD)	Longitude (DD)	Type
01SouthClair	**01SC**	**50.211947**	**-98.156200**	**L**
02SecondLead	02SL	50.218143	-98.167403	L
03Riley	03R	50.222844	-98.153218	L
04SmallBluebill	**04SB**	**50.232025**	**-98.138319**	**L**
05NClandeboye	**05NC**	**50.237792**	**-98.113507**	**L**
06MidClandeboye	**06MC**	**50.236391**	**-98.102104**	**L**
07SouixPass	07SP	50.249463	-98.092153	L
08MidWaterhen	08MW	50.221223	-98.105025	L
09SouthWaterhen	**09SW**	**50.212131**	**-98.116912**	**L**
10SEBluebill	10SEB	50.206581	-98.128632	L
11StMarks	**11SM**	**50.199485**	**-98.099266**	**L**
12MidEBluebill	**12MEB**	**50.198600**	**-98.141600**	**L**

ID	Short Form ID	Latitude (DD)	Longitude (DD)	Type
13JohnsonLk	13JL	50.177490	-98.141275	L
14SWBluebill	14SWB	50.186586	-98.158958	L
15Gadwell	15G	50.215217	-98.150774	**L**
16NWGadwell	**16NWG**	**50.205107**	**-98.158086**	**L**
17EWilson	**17EW**	**50.203717**	**-98.177463**	**L**
18NWilson	18NW	50.207899	-98.178750	C
19HighPtLk	19HPL	50.187970	-98.173923	L
20SBlackfox	**20SB**	**50.189684**	**-98.188617**	**L**
21Lyttle	21L	50.182121	-98.193942	L
22Home	22H	50.173590	-98.207543	L
23TinTown	**23TT**	**50.171257**	**-98.194068**	**L**
24DeltaChannel	**24DC**	**50.181944**	**-98.313294**	**R**
25MidCadham	**25MC**	**50.177137**	**-98.288714**	**L**
26SCadham	26SC	50.168188	-98.272730	L
27Pitblado	27P	50.182653	-98.274682	C
28BellBay	28BB	50.189212	-98.277986	L
29NaegeleIs	**29NI**	**50.183850**	**-98.254100**	**L**
30PortageCrk	**30PC**	**50.161326**	**-98.248795**	**R**
31Division	31D	50.197488	-98.210370	L
3222Bay	**3222B**	**50.202840**	**-98.201520**	**L**
33TwinLakes	33TL	50.207824	-98.191056	L
34Canvasback	34C	50.174721	-98.416820	L
35SBigLk	**35SBL**	**50.150744**	**-98.418792**	**L**
36MidBigLk	36MBL	50.171686	-98.430594	L
37NBigLk	**37NBL**	**50.185116**	**-98.444036**	**L**
38Weedy	**38W**	**50.177288**	**-98.401747**	**L**
39WBlindCh	39WBC	50.180527	-98.391441	C
41Diversion	**41D**	**50.169270**	**-98.371840**	**R**
42EBlindCh	42EBC	50.173545	-98.364081	C
43NWEaglenest	**43NWE**	**50.173448**	**-98.346718**	**L**
44LakeMB	44LMB	50.256128	-98.116660	L
45PortageCrkBay	45PCB	50.161295	-98.238477	L
46MidSimpson	**46MS**	**50.184309**	**-98.204732**	**L**
47LakeMB	47LMB	50.192884	-98.412354	L
76Thompson	76T	50.160835	-98.394099	L
79Crossroads	**79C**	**50.170300**	**-98.398166**	**C**
Portage Diversion	**PDIV**	**50.107870**	**-98.380900**	**R**
Portage Ck @ 227	**PC227**	**50.107916**	**-98.243967**	**R**
227 culvert @ 35W	**RD35W**	**50.108060**	**98.261430**	**R**
DELTA E0	**DeltaE0**	**50.107910**	**-98.229460**	**R**

ID	Short Form ID	Latitude (DD)	Longitude (DD)	Type
DELTA E1	DeltaE1	50.107700	-98.377041	R
DELTA E2	DeltaE2	50.107750	98.358710	R
DELTA E3	DeltaE3	50.107690	-98.339200	R
DELTA E4	Delta E4	50.107650	-98.322200	R
DELTA E5	Delta E5	50.10761	-98.285299	R
DELTA E6	Delta E6	50.108063	-98.261300	R
DELTA E7	Delta E7	50.107620	-98.244330	R
DELTA E8	Delta E8	50.107910	-98.229460	R
DELTA E9	Delta E9	50.137560	-98.145813	R
DELTA W1	DeltaW1	50.107980	-98.433370	R
DELTA W2	DeltaW2	50.176040	-98.313720	R
DELTA W3	DeltaW3	50.107859	-98.390807	R
FishCreekArgo	FCARGO	50.235260	-98.088970	R
CrookedCreekArgo	CCARGO	50.233440	-98.125820	R
WaterhenCreekArgo	WCARGO	50.229810	-98.115830	R
NorthWestCadham	NWC	50.178650	-98.304770	L
BellBayChannel	GAP	50.190080	-98.271190	C
Ground Water 01	GW01	50.152230	-98.313770	G
Ground Water 02	GW02	50.190540	-98.278480	G
Ground Water 03	GW03	50.229799	-98.115784	G
Ground Water 04	GW04	50.199420	-98.086380	G
Ground Water 05	GW05	50.156270	-98.252020	G
Ground Water GP	GP1A	50.199350	-98.087260	G
Ground Water GP	GP1B	50.199350	-98.087260	G
Ground Water GP	GP2	50.199420	-98.086380	G
Ground Water GP	GP3	50.199540	-98.085480	G
Ground Water GP	GP4A	50.170480	-98.193440	G
Ground Water GP	GP4B	50.170480	-98.193440	G
Ground Water GP	GP5	50.169950	-98.193050	G
Ground Water GP	GP6	50.168950	-98.191930	G
Ground Water GP	GP7	50.191470	-98.281830	G
Ground Water GP	GP8	50.191900	-98.282150	G
Precipitation Bucket 1	PRECIP1	50.191230	-98.278590	P
Precipitation Bucket 2	PRECIP2	50.229740	-98.115750	P
Precipitation Bucket 3	PRECIP3	50.199450	-98.086450	P
Precipitation Bucket 4	PRECIP4	50.182850	-98.313120	P
Precipitation Bucket 5	PRECIP5	50.186398	-98.310862	P
Evaporation Bucket 1	EVAP 1	50.191320	-98.278590	E
Evaporation Bucket 2	EVAP 2	50.191378	-98.279191	E

ID	Short Form ID	Latitude (DD)	Longitude (DD)	Type
Evaporation Bucket 3	EVAP 3	50.186398	-98.310862	E
LMB Delta Beach	LLS013	50.216700	-98.383330	L
LMB Delta Station	LLS046	50.186400	-98.334440	L
Lake Manitoba	LMB	50.219700	-98.383330	L
STA	STA	50.287093	-98.069787	L
Delta Beach	DB	50.185052	-98.344318	L
Winter Simpson	WSIM	50.177300	-98.229810	L
Winter Waterhen	WWH	50.216830	-98.106190	L
Winter Blue Bill	WBB	50.194790	-98.157090	L
Winter Lake MB	WMB	50.252400	-98.127380	L
Winter Cadham	WCAD	50.176580	-98.310290	L
Portage Creek	PCS	50.120410	-98.247170	L
BELL MET	BELL	50.191230	-98.278590	
EATON MET	EATON	50.199450	-98.086450	
DELTA MET	DELTA	50.186398	-98.310862	
WEST MET	WEST	50.174414	-98.386925	

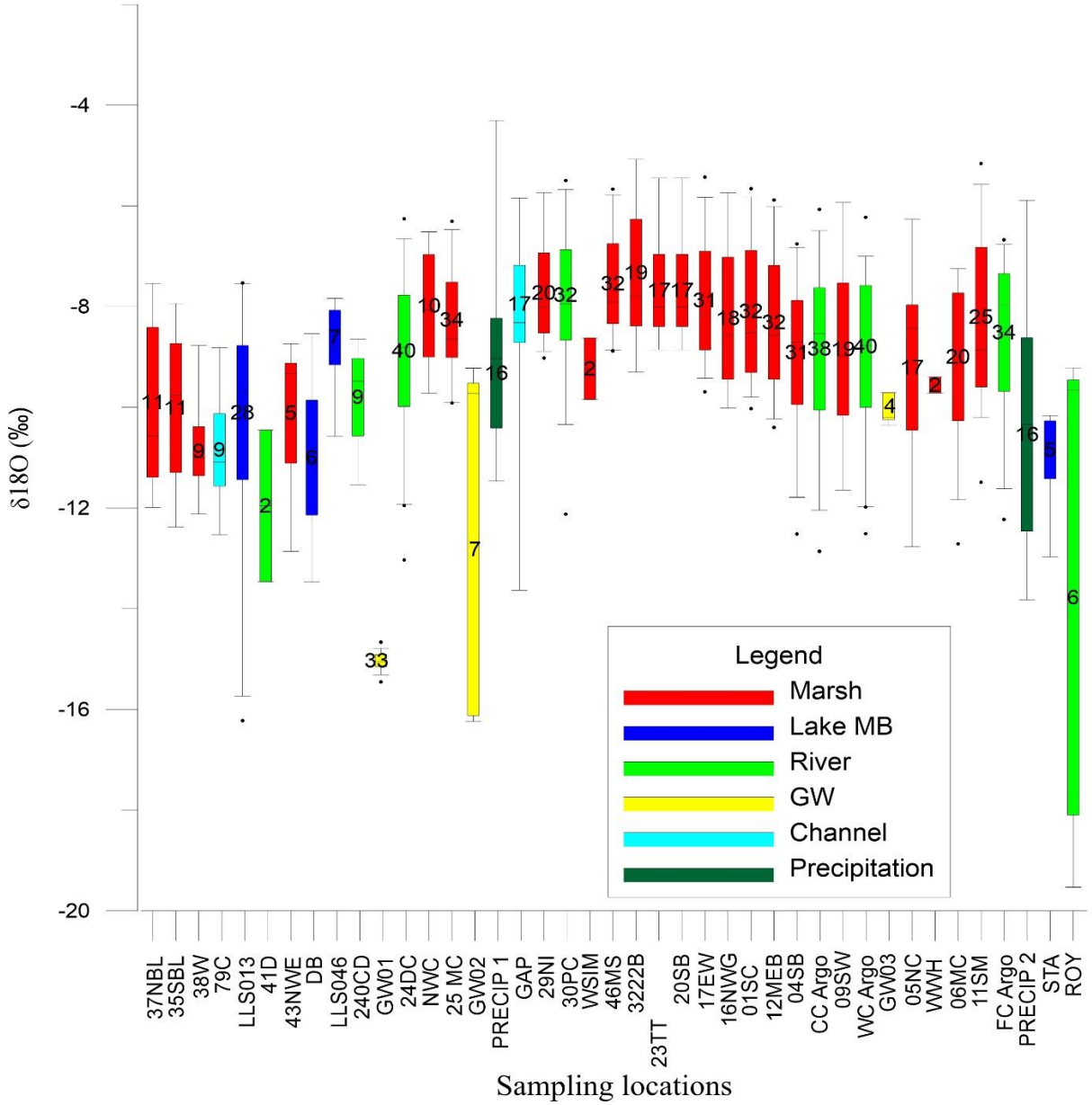

Figure A.2 - Box-whisker plot of variability in $\delta^{18}O$ across Delta Marsh (2013 – 2014). Stations ordered longitudinally from East to West. Numbers in the middle of each bar represent number of samples collected over period of four years. The black dots represent outliers.

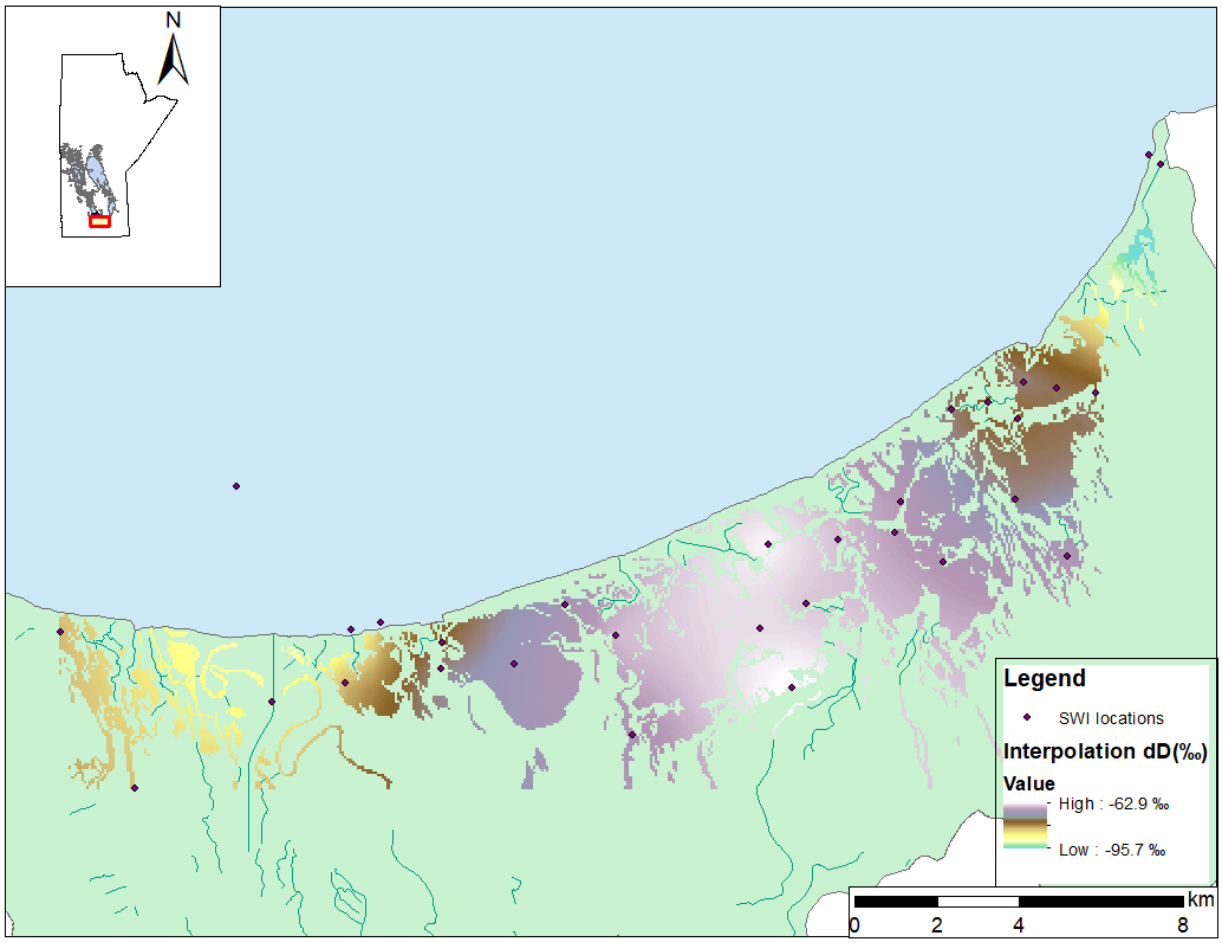

Figure A.3 - Spatial mapping of δD – seasonal average for period 2013 – 2016 . More uniform signature across middle section of Delta Marsh with pronounced depletion toward west and east sections.

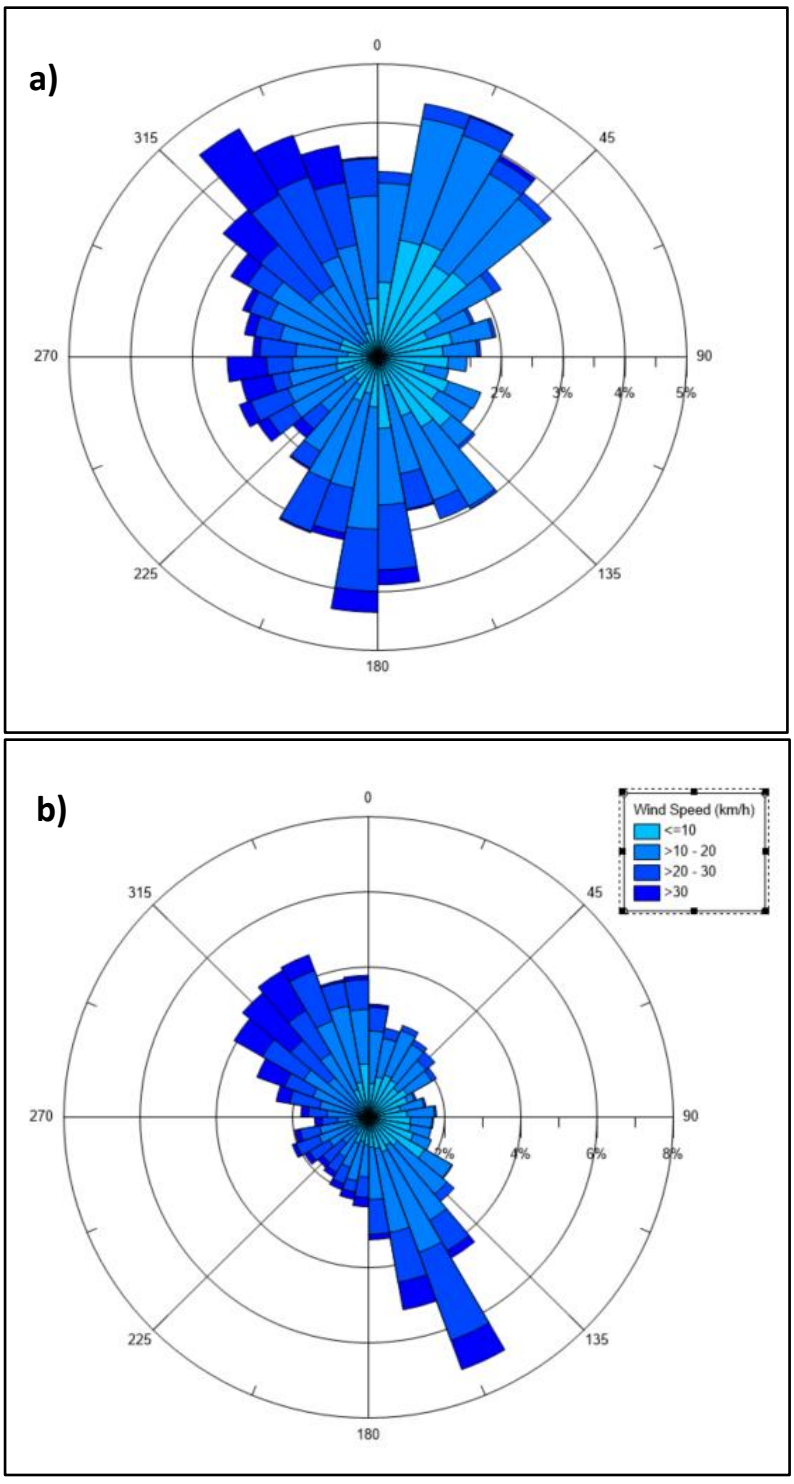

Figure A.4 – Wind rose diagram for Oak Point Station (ID 504K0NM) for a) 2013 and b) 2014. Dominant is north-south direction.

Table A.2 – Mean of all open water samples (Marsh samples)

Location	Date	δD (‰)	$\delta^{18}O$ (‰)	Location	Date	δD (‰)	$\delta^{18}O$ (‰)	Location	Date	δD (‰)	$\delta^{18}O$ (‰)	Location	Date	δD (‰)	$\delta^{18}O$ (‰)	Location	Date	δD (‰)	$\delta^{18}O$ (‰)	Location	Date	δD (‰)	$\delta^{18}O$ (‰)
01SC	6-Jun	-76.791	-8.900	04SB	6-Jun	-75.712	-8.704									09SW	6-Jun	-78.236	-9.055				
01SC	14-Jun	-74.923	-8.448	04SB	14-Jun	-74.587	-8.356									09SW	14-Jun	-76.691	-8.802				
01SC	20-Jun	-73.633	-7.962	04SB	20-Jun	-73.887	-7.981	05NC	19-Jun	-74.631	-8.433	06MC	19-Jun	-74.730	-8.621								
01SC	27-Jun	-70.683	-7.852	04SB	27-Jun	-72.453	-8.250									09SW	27-Jun	-73.033	-8.329				
01SC	3-Jul	-70.037	-7.566	04SB	3-Jul	-71.920	-8.023	05NC	2-Jul	-72.833	-8.022	06MC	2-Jul	-73.104	-8.227					11SM	2-Jul	-72.568	-7.835
01SC	8-Jul	-68.895	-7.410	04SB	8-Jul	-71.062	-8.040	05NC	9-Jul	-74.609	-8.477	06MC	9-Jul	-73.464	-8.292	09SW	8-Jul	-71.286	-7.931	11SM	9-Jul	-70.216	-7.375
01SC	17-Jul	-65.204	-6.988	04SB	17-Jul	-69.609	-7.877	05NC	19-Jul	-72.690	-8.273	06MC	19-Jul	-71.611	-7.850					11SM	17-Jul	-65.628	-6.923
																				11SM	23-Jul	-64.978	-6.823
01SC	24-Jul	-65.756	-6.857	04SB	24-Jul	-71.122	-7.898									09SW	24-Jul	-68.711	-7.425	11SM	24-Jul	-65.624	-6.517
01SC	30-Jul	-66.400	-7.109	04SB	30-Jul	-69.591	-7.948	05NC	1-Aug	-71.960	-8.183	06MC	2-Aug	-71.809	-8.019					11SM	1-Aug	-64.755	-6.720
01SC	7-Aug	-66.331	-6.884	04SB	7-Aug	-69.596	-7.595									09SW	7-Aug	-68.971	-7.532	11SM	7-Aug	-64.520	-6.531
01SC	13-Aug	-66.050	-6.723	04SB	13-Aug	-70.115	-7.783																
01SC	22-Aug	-63.361	-6.378	04SB	22-Aug	-68.337	-7.228	05NC	20-Aug	-71.308	-7.966	06MC	20-Aug	-68.974	-7.731	09SW	22-Aug	-68.197	-7.473	11SM	22-Aug	-61.678	-5.997
01SC	27-Aug	-62.733	-6.357	04SB	27-Aug	-65.438	-6.753																
01SC	4-Sep	-60.144	-6.042	04SB	4-Sep	-66.341	-7.265									09SW	4-Sep	-63.531	-6.663	11SM	4-Sep	-58.911	-5.573
01SC	12-Sep	-59.072	-5.823	04SB	12-Sep	-69.090	-7.664	05NC	11-Sep	-70.954	-7.965	06MC	11-Sep	-69.221	-7.700								
01SC	18-Sep	-58.791	-5.662	04SB	18-Sep	-65.768	-6.826	05NC	18-Sep	-61.869	-6.260	06MC	18-Sep	-66.762	-7.411	09SW	18-Sep	-59.606	-5.932	11SM	18-Sep	-56.787	-5.158
								05NC	9-Oct	-64.743	-6.859	06MC	9-Oct	-67.104	-7.251								
								05NC	30-Oct	-68.008	-7.433	06MC	30-Oct	-70.075	-7.630								

Location	Date	δD (‰)	$\delta^{18}O$ (‰)	Location	Date	δD (‰)	$\delta^{18}O$ (‰)	Location	Date	δD (‰)	$\delta^{18}O$ (‰)	Location	Date	δD (‰)	$\delta^{18}O$ (‰)	Location	Date	δD (‰)	$\delta^{18}O$ (‰)
								17EW	21-May	-78.382	-9.304								
12MEB	6-Jun	-78.233	-8.891	16NWG	6-Jun	-77.310	-8.849	17EW	6-Jun	-76.309	-8.530	20SB	6-Jun	-76.177	-8.641	23TT	6-Jun	-74.219	-8.462
12MEB	13-Jun	-75.496	-8.717	16NWG	13-Jun	-75.913	-8.692	17EW	14-Jun	-76.065	-8.615	20SB	13-Jun	-74.805	-8.352	23TT	14-Jun	-73.203	-8.249
12MEB	20-Jun	-73.778	-8.207					17EW	20-Jun	-73.277	-8.317								
12MEB	28-Jun	-71.677	-8.096	16NWG	27-Jun	-71.994	-7.882	17EW	26-Jun	-71.247	-7.925	20SB	26-Jun	-71.400	-7.925	23TT	26-Jun	-71.648	-7.847
12MEB	3-Jul	-71.602	-7.826					17EW	3-Jul	-70.535	-7.738								
12MEB	8-Jul	-69.875	-7.668	16NWG	8-Jul	-69.940	-7.595	17EW	8-Jul	-69.394	-7.494	20SB	8-Jul	-69.535	-7.401	23TT	8-Jul	-69.308	-7.259
12MEB	17-Jul	-66.906	-7.291					17EW	17-Jul	-66.687	-7.112								
12MEB	24-Jul	-65.605	-7.172	16NWG	24-Jul	-65.395	-6.966	17EW	24-Jul	-65.472	-6.897	20SB	24-Jul	-65.374	-6.825	23TT	24-Jul	-64.418	-6.962
12MEB	30-Jul	-66.722	-7.181					17EW	30-Jul	-62.758	-6.978	20SB							
12MEB	7-Aug	-66.244	-7.247	16NWG	7-Aug	-66.218	-7.019	17EW	7-Aug	-64.930	-6.703	20SB	8-Aug	-64.303	-6.580	23TT	8-Aug	-64.567	-6.603
12MEB	13-Aug	-65.954	-6.963					17EW	13-Aug	-64.999	-6.616								
12MEB	22-Aug	-64.928	-6.598	16NWG	22-Aug	-64.255	-6.594	17EW	22-Aug	-62.944	-6.276	20SB	22-Aug	-62.422	-6.235	23TT	22-Aug	-62.533	-6.241
12MEB	27-Aug	-62.870	-6.654					17EW	27-Aug	-61.977	-6.160	20SB							
12MEB	4-Sep	-60.569	-6.181	16NWG	4-Sep	-60.467	-6.079	17EW	4-Sep	-60.095	-5.873	20SB	4-Sep	-59.587	-6.085	23TT	4-Sep	-59.275	-5.847
12MEB	12-Sep	-61.051	-6.012					17EW	12-Sep	-59.679	-5.828								
12MEB	18-Sep	-59.031	-5.882	16NWG	18-Sep	-58.566	-5.741	17EW	18-Sep	-58.988	-5.429	20SB	18-Sep	-58.229	-5.676	23TT	18-Sep	-58.198	-5.449

Location	Date	δD (‰)	$\delta^{18}O$ (‰)	Location	Date	δD (‰)	$\delta^{18}O$ (‰)	Location	Date	δD (‰)	$\delta^{18}O$ (‰)	Location	Date	δD (‰)	$\delta^{18}O$ (‰)	Location	Date	δD (‰)	$\delta^{18}O$ (‰)
25MC	21-May	-85.548	-9.903	29NI	21-May	-79.503	-8.889	3222B	21-May	-81.421	-9.301	46MS	21-May	-78.208	-8.868	NWC	21-May	-81.353	-9.407
25MC	7-Jun	-78.191	-8.989	29NI	7-Jun	-75.897	-8.542	3222B	6-Jun	-75.738	-8.476	46MS	6-Jun	-75.445	-8.486	NWC	7-Jun	-79.165	-9.001
25MC	13-Jun	-78.347	-8.895	29NI	13-Jun	-75.895	-8.523	3222B	13-Jun	-73.777	-8.386	46MS	13-Jun	-74.944	-8.446	NWC	13-Jun	-77.721	-8.847
25MC	20-Jun	-79.307	-8.998									46MS	20-Jun	-72.604	-7.989				
25MC	26-Jun	-75.469	-8.464	29NI	26-Jun	-71.547	-7.959	3222B	26-Jun	-69.599	-7.440	46MS	26-Jun	-71.951	-7.811	NWC	26-Jun	-75.931	-8.569
25MC	3-Jul	-73.655	-7.956									46MS	3-Jul	-70.634	-7.401				
25MC	9-Jul	-72.043	-8.090	29NI	9-Jul	-68.894	-7.300	3222B	9-Jul	-67.629	-6.953	46MS	8-Jul	-68.674	-7.288				
25MC	17-Jul	-70.463	-7.582									46MS	17-Jul	-66.773	-7.018				
																NWC	24-Jul	-70.225	-7.562
25MC	24-Jul	-68.843	-7.399	29NI	25-Jul	-66.136	-6.935	3222B	24-Jul	-63.299	-6.261	46MS	24-Jul	-65.407	-6.750				
25MC	30-Jul	-69.417	-7.514									46MS	30-Jul	-64.723	-6.822				
25MC	8-Aug	-68.420	-7.172	29NI	8-Aug	-64.381	-6.819	3222B	8-Aug	-63.478	-6.267	46MS	8-Aug	-64.897	-6.460	NWC	8-Aug	-70.085	-7.443
25MC	13-Aug	-68.097	-7.146									46MS	13-Aug	-64.733	-6.738				
25MC	22-Aug	-66.805	-6.797	29NI	22-Aug	-62.558	-6.116	3222B	22-Aug	-60.348	-5.729	46MS	22-Aug	-62.718	-6.138	NWC	22-Aug	-67.234	-6.968
25MC	27-Aug	-65.877	-6.851									46MS	27-Aug	-61.895	-6.204				
25MC	4-Sep	-64.046	-6.812	29NI	4-Sep	-59.907	-5.957	3222B	4-Sep	-58.325	-5.673	46MS	4-Sep	-59.680	-5.952	NWC	4-Sep	-63.744	-6.598
25MC	12-Sep	-63.717	-6.472									46MS	12-Sep	-59.373	-5.780				
25MC	18-Sep	-63.691	-6.305	29NI	18-Sep	-59.072	-5.737	3222B	18-Sep	-55.933	-5.076	46MS	18-Sep	-58.342	-5.666	NWC	18-Sep	-63.115	-6.516

Date	δLmean δD (‰)	δLmean δ18O (‰)
21-May-13	-81.956	-9.274
6-Jun-13	-76.725	-8.733
14-Jun-13	-75.567	-8.564
20-Jun-13	-74.481	-8.313
27-Jun-13	-72.202	-8.027
3-Jul-13	-71.877	-7.844
8-Jul-13	-70.322	-7.638
17-Jul-13	-68.397	-7.435
24-Jul-13	-66.424	-7.017
30-Jul-13	-67.571	-7.386
7-Aug-13	-66.210	-6.878
13-Aug-13	-66.658	-6.995
22-Aug-13	-64.913	-6.633
27-Aug-13	-63.465	-6.496
4-Sep-13	-61.044	-6.154
12-Sep-13	-64.020	-6.656
18-Sep-13	-60.172	-5.881
9-Oct-13	-65.923	-7.055
30-Oct-13	-69.042	-7.531

Location	Date	δD (‰)	$\delta^{18}O$ (‰)	Location	Date	δD (‰)	$\delta^{18}O$ (‰)	Location	Date	δD (‰)	$\delta^{18}O$ (‰)	Location	Date	δD (‰)	$\delta^{18}O$ (‰)	Location	Date	δD (‰)	$\delta^{18}O$ (‰)	Date	δLmean	
																					δD (‰)	$\delta^{18}O$ (‰)
01SC	27-May	-83.429	-9.617	04SB	27-May	-101.870	-12.516					06MC	28-May	-102.969	-12.713	09SW	27-May	-95.725	-11.490			
	4-Jun							05NC	4-Jun	-104.795	-12.769	06MC	4-Jun	-100.465	-11.746					27-May-14	-86.500	-10.083
01SC	10-Jun	-83.571	-9.307	04SB	10-Jun	-99.591	-11.787									09SW	10-Jun	-98.078	-11.616			
01SC	17-Jun	-84.050	-9.745	04SB	17-Jun	-94.624	-11.209	05NC	18-Jun	-98.187	-11.769	06MC	18-Jun	-98.475	-11.838					4-Jun-14	-102.630	-12.258
01SC	24-Jun	-82.229	-9.518	04SB	24-Jun	-89.479	-10.470									09SW	24-Jun	-95.703	-11.646			
01SC	3-Jul	-83.185	-9.707	04SB	3-Jul	-88.396	-10.737	05NC	4-Jul	-92.635	-11.200	06MC	4-Jul	-92.806	-11.122					10-Jun-14	-83.766	-9.443
01SC	14-Jul	-85.065	-10.028	04SB	14-Jul	-85.954	-10.244									09SW	14-Jul	-86.577	-10.278			
01SC	22-Jul	-84.329	-9.800	04SB	22-Jul	-85.330	-10.191	05NC	21-Jul	-91.584	-11.263	06MC	21-Jul	-88.302	-10.266	09SW	22-Jul	-85.917	-10.162	17-Jun-14	-86.822	-10.027
01SC	29-Jul	-82.972	-9.681	04SB	29-Jul	-85.089	-9.948	05NC	1-Aug	-84.026	-9.541	06MC	1-Aug	-84.467	-9.606							
01SC	5-Aug	-81.847	-9.525	04SB	5-Aug	-83.396	-9.703									09SW	5-Aug	-83.093	-9.749	24-Jun-14	-81.065	-9.215
01SC	12-Aug	-80.085	-9.234	04SB	12-Aug	-84.722	-9.915	05NC	11-Aug	-92.050	-10.453	06MC	11-Aug	-86.061	-9.841							
01SC	19-Aug	-77.839	-8.849	04SB	19-Aug	-83.093	-9.771	05NC	21-Aug	-84.412	-9.940	06MC	21-Aug	-85.518	-9.991	09SW	19-Aug	-83.952	-9.866	3-Jul-14	-84.447	-10.000
01SC	3-Sep	-76.217	-8.540	04SB	3-Sep											09SW	3-Sep	-78.429	-8.980			
01SC	10-Sep	-77.299	-8.863	04SB	10-Sep	-82.283	-9.490													14-Jul-14	-81.797	-9.444
01SC	17-Sep	-75.684	-8.614	04SB	17-Sep	-79.434	-9.204									09SW	17-Sep	-81.856	-9.447			
01SC	22-Sep	-74.822	-8.499	04SB	22-Sep	-78.103	-9.114													22-Jul-14	-82.666	-9.637
												06MC	2-Oct	-84.439	-10.050							
01SC	15-Oct	-78.474	-9.054	04SB	15-Oct	-80.323	-9.347									09SW	15-Oct	-77.304	-8.868	29-Jul-14	-82.826	-9.456
Location	Date	δD (‰)	$\delta^{18}O$ (‰)	Location	Date	δD (‰)	$\delta^{18}O$ (‰)	Location	Date	δD (‰)	$\delta^{18}O$ (‰)	Location	Date	δD (‰)	$\delta^{18}O$ (‰)	Location	Date	δD (‰)	$\delta^{18}O$ (‰)			
11SM	27-May	-98.109	-11.487	12MEB	27-May	-86.878	-10.158	16NWG	27-May	-84.544	-9.738	17EW	27-May	-80.912	-9.283	20SB	27-May	-78.482	-8.896	5-Aug-14	-79.181	-9.006
11SM	10-Jun	-90.278	-10.012	12MEB	10-Jun	-89.406	-10.230	16NWG	10-Jun	-80.963	-9.159	17EW	10-Jun	-79.332	-8.871	20SB	10-Jun	-78.970	-8.788	12-Aug-14	-82.032	-9.212
11SM	16-Jun	-87.021	-9.392	12MEB	17-Jun	-84.251	-9.807					17EW	17-Jun	-78.334	-8.859							
11SM	24-Jun	-84.511	-9.504	12MEB	24-Jun	-82.857	-9.503	16NWG	24-Jun	-84.855	-9.850	17EW	24-Jun	-79.464	-8.877	20SB	24-Jun	-78.001	-8.789	19-Aug-14	-77.696	-8.888
11SM	2-Jul	-83.449	-9.763	12MEB	3-Jul	-86.153	-10.402					17EW	3-Jul	-80.314	-9.353							
11SM	14-Jul	-86.476	-10.207	12MEB	3-Jul	-85.366	-9.895	16NWG	14-Jul	-86.241	-10.013	17EW	14-Jul	-83.914	-9.693	20SB	14-Jul	-82.411	-9.575	3-Sep-14	-74.315	-8.339
11SM	22-Jul	-85.439	-9.977	12MEB	22-Jul	-83.855	-9.854	16NWG	22-Jul	-83.840	-9.781	17EW	22-Jul			20SB	22-Jul	-80.375	-9.326			
11SM	30-Jul	-84.272	-9.470	12MEB	29-Jul	-83.420	-9.666					17EW	29-Jul	-81.823	-9.425					10-Sep-14	-76.928	-8.688
11SM	5-Aug	-83.106	-9.594	12MEB	5-Aug	-82.184	-9.445	16NWG	5-Aug	-81.421	-9.446	17EW	5-Aug	-78.663	-8.860	20SB	5-Aug	-78.774	-9.111			
11SM	13-Aug	-80.754	-8.594	12MEB	12-Aug	-81.153	-9.040					17EW	12-Aug	-77.344	-8.467					17-Sep-14	-76.011	-8.645
11SM	19-Aug	-79.231	-9.201	12MEB	19-Aug	-79.184	-9.093	16NWG	19-Aug	-78.684	-9.134	17EW	19-Aug	-75.408	-8.537	20SB	19-Aug	-73.447	-8.366			
11SM	3-Sep	-77.843	-8.866	12MEB	3-Sep	-77.511	-8.813	16NWG	3-Sep	-74.115	-8.456	17EW	3-Sep	-73.308	-8.172	20SB	3-Sep	-73.528	-8.013	22-Sep-14	-74.364	-8.426
				12MEB	10-Sep	-77.048	-8.676					17EW	10-Sep	-76.141	-8.500							
11SM	17-Sep	-76.784	-8.836	12MEB	17-Sep	-75.659	-8.440	16NWG	17-Sep			17EW	17-Sep			20SB	17-Sep	-72.781	-8.147	2-Oct-14	-79.353	-9.304
				12MEB	22-Sep	-74.176	-8.449					17EW	22-Sep	-71.917	-7.987							
																				15-Oct-14	-75.049	-8.494
11SM	15-Oct	-78.984	-8.995	12MEB	15-Oct	-76.840	-9.113	16NWG	15-Oct	-74.146	-8.291	17EW	15-Oct	-73.104	-8.104	20SB	15-Oct	-73.095	-8.171			
Location	Date	δD (‰)	$\delta^{18}O$ (‰)	Location	Date	δD (‰)	$\delta^{18}O$ (‰)	Location	Date	δD (‰)	$\delta^{18}O$ (‰)	Location	Date	δD (‰)	$\delta^{18}O$ (‰)	Location	Date	δD (‰)	$\delta^{18}O$ (‰)			
23TT	27-May	-77.548	-8.857	25MC	27-May	-85.547	-9.917	29NI	27-May	-79.016	-9.022	3222B	27-May	-78.555	-8.653	46MS	27-May	-77.414	-8.809			
23TT	11-Jun	-75.210	-8.171	25MC	10-Jun	-82.787	-9.467	29NI	10-Jun	-78.812	-8.791	3222B	10-Jun	-75.313	-8.119	46MS	10-Jun	-76.649	-8.446			
				25MC	17-Jun	-81.243	-9.286									46MS	17-Jun	-75.215	-8.340			
23TT	24-Jun	-73.949	-8.409	25MC	24-Jun	-78.569	-8.975	29NI	24-Jun	-74.841	-8.035	3222B	24-Jun	-74.282	-7.967	46MS	24-Jun	-75.109	-8.252			
				25MC	3-Jul	-78.325	-9.247									46MS	3-Jul	-74.763	-8.466			
23TT	22-Jul	-75.711	-8.396	25MC	14-Jul	-79.075	-9.014	29NI	14-Jul	-74.362	-8.213	3222B	14-Jul	-73.837	-8.332	46MS	14-Jul	-78.371	-8.880			
				25MC	22-Jul	-78.688	-8.907	29NI	22-Jul	-75.272	-8.586	3222B	22-Jul	-74.311	-8.387	46MS	22-Jul	-77.413	-8.786			
				25MC	29-Jul											46MS	29-Jul	-76.538	-8.313			
23TT	5-Aug	-75.413	-8.486	25MC	5-Aug	-78.682	-8.701	29NI	5-Aug	-73.959	-8.077	3222B	5-Aug	-74.122	-8.103	46MS	5-Aug	-74.693	-8.278			
				25MC	12-Aug											46MS	12-Aug	-74.089	-8.152			
23TT	19-Aug	-72.029	-8.006	25MC	19-Aug	-76.333	-8.947	29NI	19-Aug	-73.022	-7.993	3222B	19-Aug	-70.915	-7.726	46MS	19-Aug	-72.368	-7.901			
23TT	3-Sep	-71.056	-7.959	25MC	3-Sep	-76.227	-8.681	29NI	3-Sep	-71.971	-7.818	3222B	3-Sep	-70.015	-7.785	46MS	3-Sep	-71.565	-7.984			
				25MC	10-Sep											46MS	10-Sep	-71.871	-7.913			
23TT				25MC	17-Sep	-75.411	-8.609	29NI	17-Sep	-70.481	-7.859	3222B	17-Sep			46MS	17-Sep					
				25MC	22-Sep	-75.738	-8.607									46MS	22-Sep	-71.429	-7.904			
				25MC	2-Oct	-74.268	-8.557															
23TT	15-Oct	-71.644	-8.385	25MC	15-Oct	-75.601	-8.618	29NI	15-Oct	-72.164	-8.051	3222B	15-Oct	-71.872	-7.686	46MS	15-Oct	-72.086	-7.738			

Location	Date	δD (‰)	$\delta^{18}O$ (‰)	Location	Date	δD (‰)	$\delta^{18}O$ (‰)	Location	Date	δD (‰)	$\delta^{18}O$ (‰)	Location	Date	δD (‰)	$\delta^{18}O$ (‰)	Location	Date	δD (‰)	$\delta^{18}O$ (‰)
01SC	5-May	-72.645	-8.002	04SB	5-May	-79.718	-9.113	05NC	5-May	-79.084	-9.143	06MC	5-May	-83.11387	-9.711392	09SW	5-May	-78.411	-8.790
01SC	14-May	-71.111	-7.771	04SB	14-May	-79.758	-9.204												
01SC	20-May	-72.840	-8.386	04SB	20-May	-79.318	-9.249									09SW	20-May	-80.157	-9.422
01SC	26-May	-70.259	-7.971	04SB	26-May	-74.209	-8.587												
01SC	10-Jun	-67.881	-7.391	04SB	10-Jun	-72.912	-8.072									09SW	10-Jun	-72.642	-7.913
01SC	16-Jun	-66.758	-7.060	04SB	16-Jun	-72.529	-8.057												
01SC	24-Jun	-64.989	-6.697	04SB	24-Jun	-68.624	-7.244	05NC	25-Jun	-72.657	-7.791	06MC	25-Jun	-71.917	-7.838	09SW	24-Jun	-70.657	-7.643
01SC	2-Jul	-63.427	-6.319	04SB	2-Jul	-67.121	-6.830												
01SC	8-Jul	-63.444	-6.156	04SB	8-Jul	-68.190	-7.110	05NC	8-Jul	-68.987	-7.377	06MC	8-Jul	-70.491	-7.699	09SW	8-Jul	-66.426	-6.711
01SC	16-Jul	-61.296	-6.029	04SB	16-Jul	-61.850	-5.924						16-Jul	-67.598	-7.240				
01SC	21-Jul	-59.999	-5.812	04SB	22-Jul	-66.641	-6.976									09SW	22-Jul	-65.878	-6.828
01SC	30-Jul	-57.349	-5.668	04SB	30-Jul	-59.737	-5.772	05NC	30-Jul	-72.956	-8.234	06MC	30-Jul	-67.779	-7.172				
01SC	5-Aug	-59.268	-5.582	04SB	6-Aug	-68.600	-7.401									09SW	6-Aug	-65.411	-6.787
01SC	13-Aug	-57.630	-5.491	04SB	13-Aug	-60.357	-6.213	05NC	13-Aug	-61.933	-6.397	06MC	13-Aug	-63.493	-6.871				
01SC	19-Aug	-55.211	-5.346	04SB	19-Aug	-59.365	-5.934	05NC	19-Aug	-70.679	-7.872	06MC	19-Aug	-65.272	-6.976	09SW	19-Aug	-60.330	-6.183
01SC	25-Aug	-59.729	-5.959	04SB	25-Aug	-70.766	-7.794	05NC	25-Aug	-69.445	-7.624	06MC	25-Aug	-69.450	-7.381				
01SC	2-Sep	-57.840	-5.442	04SB	2-Sep	-61.910	-6.325	05NC	2-Sep	-59.918	-6.254	06MC				09SW	2-Sep	-58.037	-5.689
01SC	8-Sep	-55.671	-5.410	04SB	8-Sep	-64.936	-7.140	05NC	8-Sep	-63.541	-6.812	06MC	8-Sep	-65.073	-7.102				
01SC	15-Sep	-55.474	-5.299	04SB	15-Sep	-64.099	-6.697	05NC	15-Sep	-65.354	-7.120	06MC	15-Sep	-62.979	-6.768	09SW	15-Sep	-59.893	-6.091
01SC	14-Oct	-54.717	-5.345	04SB	14-Oct	-68.266	-7.458	05NC	14-Oct	-66.449	-7.281	06MC	14-Oct	-67.044	-7.295	09SW	14-Oct	-64.815	-6.831
Location	Date	δD (‰)	$\delta^{18}O$ (‰)	Location	Date	δD (‰)	$\delta^{18}O$ (‰)	Location	Date	δD (‰)	$\delta^{18}O$ (‰)	Location	Date	δD (‰)	$\delta^{18}O$ (‰)	Location	Date	δD (‰)	$\delta^{18}O$ (‰)
11SM	5-May	-74.207	-8.229	12MEB	5-May	-73.159	-8.220	16NWG	5-May	-72.878	-7.886	17EW	5-May	-71.705	-7.902	20SB	6-May	-70.400	-7.780
				12MEB	14-May	-69.864	-7.700					17EW	14-May	-68.989	-7.606				
11SM	20-May	-69.201	-7.690	12MEB	20-May	-72.108	-8.083	16NWG	20-May	-70.209	-7.828	17EW	20-May	-69.476	-7.759	20SB	20-May	-68.758	-7.807
11SM	26-May	-67.415	-7.267	12MEB	26-May	-69.762	-7.948					17EW	26-May	-67.916	-7.561				
11SM	9-Jun	-65.251	-7.017	12MEB	9-Jun	-68.030	-7.384	16NWG	10-Jun	-67.077	-7.173	17EW	10-Jun	-66.238	-7.108	20SB	10-Jun	-66.028	-7.030
11SM	16-Jun	-62.728	-6.474	12MEB	16-Jun	-66.004	-7.004					17EW	16-Jun	-63.925	-6.854	20SB	18-Jun	-64.367	-6.879
11SM	23-Jun	-62.927	-6.267	12MEB	23-Jun	-64.626	-6.722	16NWG	23-Jun	-63.967	-6.812	17EW	23-Jun	-63.198	-6.552	20SB	23-Jun	-63.300	-6.447
11SM	2-Jul	-60.955	-5.968	12MEB	2-Jul	-63.299	-6.287					17EW	2-Jul	-61.520	-6.283				
11SM	7-Jul	-60.905	-5.977	12MEB	7-Jul	-63.398	-6.596	16NWG	8-Jul	-63.003	-6.398	17EW	8-Jul	-62.580	-6.326	20SB	7-Jul	-62.496	-6.317
11SM	16-Jul	-58.477	-5.318	12MEB	16-Jul	-60.904	-6.173					17EW	16-Jul	-60.158	-5.998				
11SM	21-Jul	-57.477	-5.177	12MEB	21-Jul	-60.212	-5.929	16NWG	21-Jul	-60.663	-5.957	17EW	21-Jul	-60.152	-5.774	20SB	21-Jul	-59.860	-5.937
11SM	30-Jul	-56.776	-4.917	12MEB	30-Jul	-59.101	-5.679					17EW	30-Jul	-58.198	-5.531				
11SM	5-Aug	-54.905	-4.648	12MEB	5-Aug	-60.176	-5.745	16NWG	5-Aug	-60.094	-5.813	17EW	5-Aug	-57.352	-5.184	20SB	5-Aug	-57.828	-5.385
11SM	13-Aug	-53.617	-4.620	12MEB	13-Aug	-57.259	-5.460					17EW	13-Aug	-56.086	-5.334				
11SM	18-Aug	-50.350	-4.550	12MEB	18-Aug	-54.465	-5.233	16NWG	19-Aug	-54.252	-5.061	17EW	19-Aug	-55.022	-5.240	20SB	18-Aug	-54.270	-5.258
11SM	25-Aug	-54.095	-4.779	12MEB	25-Aug	-67.822	-7.326					17EW	25-Aug	-59.765	-6.103				
11SM	2-Sep	-52.198	-4.673	12MEB	2-Sep	-55.882	-5.304	16NWG	2-Sep	-56.044	-5.452	17EW	2-Sep	-54.641	-5.210	20SB	2-Sep	-55.184	-5.024
11SM	8-Sep	-50.739	-4.493	12MEB	8-Sep	-54.827	-5.223					17EW	8-Sep	-54.412	-5.228				
11SM	15-Sep	-50.946	-4.370	12MEB	15-Sep	-54.661	-5.268	16NWG	15-Sep	-55.011	-5.072	17EW	15-Sep	-54.438	-4.990	20SB	15-Sep	-53.825	-5.048
11SM	14-Oct	-51.401	-4.876	12MEB	14-Oct	-58.552	-5.946	16NWG	14-Oct	-53.929	-5.336	17EW	14-Oct	-53.581	-5.295	20SB	14-Oct	-54.025	-5.123
Location	Date	δD (‰)	$\delta^{18}O$ (‰)	Location	Date	δD (‰)	$\delta^{18}O$ (‰)	Location	Date	δD (‰)	$\delta^{18}O$ (‰)	Location	Date	δD (‰)	$\delta^{18}O$ (‰)	Location	Date	δD (‰)	$\delta^{18}O$ (‰)
23TT	6-May	-71.030	-7.704	25MC	6-May	-76.670	-8.612	29NI	5-May	-71.386	-7.735	3222B	6-May	-68.921	-7.267	46MS	6-May	-71.111	-7.801
				25MC	14-May	-74.382	-8.437									46MS	14-May	-68.327	-7.571
23TT	21-May	-68.386	-7.664	25MC	21-May	-72.752	-8.325	29NI	21-May	-69.017	-7.805	3222B	20-May	-68.791	-7.619	46MS	21-May	-68.342	-7.615
				25MC	26-May	-72.652	-8.343									46MS	26-May	-67.886	-7.691
23TT	10-Jun	-65.695	-6.930	25MC	9-Jun	-70.579	-7.694	29NI	9-Jun	-69.330	-7.274	3222B	9-Jun	-63.473	-6.823	46MS	10-Jun	-65.715	-6.975
23TT	18-Jun	-63.876	-6.498	25MC	16-Jun	-68.701	-7.580					3222B	18-Jun	-62.063	-6.548	46MS	16-Jun	-64.511	-6.901
23TT	23-Jun	-63.063	-6.655	25MC	23-Jun	-68.496	-7.371	29NI	23-Jun	-63.710	-6.628	3222B	23-Jun	-60.817	-5.953	46MS	23-Jun	-63.504	-6.652
				25MC	2-Jul	-67.046	-7.001									46MS	2-Jul	-62.162	-6.360
23TT	7-Jul	-62.458	-6.348	25MC	7-Jul	-67.362	-7.194	29NI	7-Jul	-64.249	-6.656	3222B	7-Jul	-60.835	-5.797	46MS	7-Jul	-62.315	-6.282
				25MC	16-Jul	-65.217	-6.866									46MS	16-Jul	-60.258	-5.959
23TT	21-Jul	-58.946	-5.919	25MC	21-Jul	-64.882	-6.736	29NI	21-Jul	-60.592	-5.881	3222B	21-Jul	-57.080	-5.400	46MS	21-Jul	-59.287	-5.915
23TT				25MC	30-Jul	-64.107	-6.462	29NI								46MS	30-Jul	-58.583	-5.649
23TT	5-Aug	-57.416	-5.392	25MC	5-Aug	-62.305	-6.008	29NI	5-Aug	-58.240	-5.658	3222B	5-Aug	-56.392	-5.031	46MS	5-Aug	-57.875	-5.301
				25MC	13-Aug	-58.209	-6.185									46MS	13-Aug	-57.256	-5.218
23TT	18-Aug	-54.044	-5.128	25MC	18-Aug	-58.890	-5.895	29NI	18-Aug	-54.893	-5.271	3222B	18-Aug	-52.498	-4.909	46MS	18-Aug	-55.882	-5.556
				25MC	25-Aug	-60.714	-6.204									46MS	25-Aug	-56.516	-5.480
23TT	2-Sep	-54.443	-5.251	25MC	2-Sep	-60.299	-6.023	29NI	2-Sep	-56.360	-5.347	3222B	2-Sep	-53.481	-4.981	46MS	2-Sep	-54.756	-5.172
				25MC	8-Sep	-60.345	-6.201									46MS	8-Sep	-53.823	-5.133
23TT	15-Sep	-53.173	-5.041	25MC	15-Sep	-61.873	-6.236	29NI	15-Sep	-53.922	-5.068	3222B	15-Sep	-52.561	-4.844	46MS	15-Sep	-53.640	-5.038
23TT	14-Oct	-53.462	-5.118	25MC	14-Oct	-57.881	-5.713	29NI	14-Oct	-54.235	-5.249					46MS	14-Oct	-55.289	-5.285

	δLmean	
Date	δD (‰)	$\delta^{18}O$ (‰)
6-May-15	-74.595	-8.315
14-May-15	-72.072	-8.048
21-May-15	-71.489	-8.096
26-May-15	-70.014	-7.910
10-Jun-15	-67.758	-7.291
2-Jul-15	-63.647	-6.435
7-Jul-15	-64.758	-6.645
16-Jul-15	-61.970	-6.188
21-Jul-15	-60.898	-6.019
30-Jul-15	-62.754	-6.332
5-Aug-15	-59.682	-5.687
13-Aug-15	-58.777	-5.818
18-Aug-15	-57.881	-5.768
25-Aug-15	-63.775	-6.628
2-Sep-15	-56.727	-5.493
8-Sep-15	-58.691	-5.955
15-Sep-15	-57.325	-5.629
14-Oct-15	-58.673	-5.962

Location	Date	δD (‰)	$\delta^{18}O$ (‰)	Location	Date	δD (‰)	$\delta^{18}O$ (‰)	Location	Date	δD (‰)	$\delta^{18}O$ (‰)	Location	Date	δD (‰)	$\delta^{18}O$ (‰)	Location	Date	δD (‰)	$\delta^{18}O$ (‰)
01SC	11-May	-68.529	-7.717	04SB	11-May	-70.905	-7.670	05NC	11-May	-70.975	-7.888	06MC	11-May	-71.826	-7.898	09SW	11-May	-71.804	-7.921
01SC	17-May	-70.799	-7.912	04SB	17-May	-75.640	-8.534	05NC	17-May	-74.148	-8.287	06MC	17-May	-73.870	-8.457				
01SC	25-May	-66.040	-7.121	04SB	25-May	-68.810	-7.525	05NC	25-May	-75.747	-8.750	06MC	25-May	-71.649	-8.019	09SW	25-May	-69.800	-7.737
01SC	2-Jun	-68.987	-7.669	04SB	2-Jun	-72.953	-8.210	05NC	2-Jun	-70.789	-7.721	06MC	2-Jun	-71.524	-8.015	09SW	2-Jun	-71.741	-8.125
01SC	8-Jun	-65.744	-7.157	04SB	8-Jun	-72.140	-8.014	05NC	8-Jun	-71.883	-8.004	06MC	8-Jun	-70.629	-7.831				
01SC	15-Jun	-63.800	-6.627	04SB	15-Jun	-67.291	-7.178	05NC	15-Jun	-72.565	-8.130	06MC	15-Jun	-68.566	-7.589	09SW	15-Jun	-65.855	-7.020
01SC	21-Jun	-60.974	-6.430	04SB	21-Jun	-63.286	-6.950	05NC	21-Jun	-70.123	-7.987	06MC	21-Jun	-66.424	-7.256	09SW	21-Jun	-65.089	-7.244
01SC	28-Jun	-58.477	-6.059	04SB	28-Jun	-67.765	-7.518	05NC	28-Jun	-64.804	-7.151	06MC	28-Jun	-64.741	-6.988	09SW	28-Jun	-62.000	-6.502
01SC	5-Jul	-57.182	-5.763	04SB	5-Jul	-63.692	-6.844	05NC	5-Jul	-70.969	-8.049	06MC	5-Jul	-64.620	-6.877				
01SC	13-Jul	-57.130	-5.577	04SB	13-Jul	-65.062	-7.010	05NC	14-Jul	-69.775	-8.046	06MC	14-Jul	-64.343	-6.927	09SW	14-Jul	-63.092	-6.899
01SC	21-Jul	-56.513	-5.540	04SB	21-Jul	-61.984	-6.419	05NC	21-Jul	-63.806	-6.623	06MC	21-Jul	-64.803	-6.952	09SW	21-Jul	-58.681	-5.821
01SC	28-Jul	-55.175	-5.242	04SB	28-Jul	-64.819	-6.867	05NC	28-Jul	-68.086	-7.426	06MC	28-Jul	-66.846	-7.270				
01SC	3-Aug	-52.586	-4.894	04SB	3-Aug	-56.562	-5.514	05NC	3-Aug	-62.393	-6.506	06MC	3-Aug	-61.725	-6.363	09SW	3-Aug	-59.026	-5.942
01SC	10-Aug	-52.451	-4.803	04SB	10-Aug	-64.085	-6.753	05NC	10-Aug	-66.007	-7.068	06MC	10-Aug	-65.417	-7.036	09SW	10-Aug	-60.769	-6.390
01SC	16-Aug	-51.213	-4.840	04SB	16-Aug	-63.246	-6.637	05NC	16-Aug	-65.108	-6.973	06MC	16-Aug	-63.629	-6.813				
01SC	23-Aug	-54.556	-4.884	04SB	23-Aug	-63.967	-6.305	05NC	23-Aug	-62.460	-6.479	06MC	23-Aug	-63.730	-6.697	09SW	23-Aug	-58.988	-5.696
01SC	7-Sep	-50.767	-4.506	04SB	7-Sep	-63.649	-6.666	05NC	7-Sep	-62.489	-6.502	06MC	7-Sep	-65.306	-6.918				
01SC	28-Sep	-57.911	-5.739	04SB	28-Sep	-66.445	-7.284	05NC	28-Sep	-64.910	-7.092	06MC	28-Sep	-67.443	-7.216				
								05NC	5-Oct	-62.005	-6.544	06MC	5-Oct	-63.599	-6.881				
Location	Date	δD (‰)	$\delta^{18}O$ (‰)	Location	Date	δD (‰)	$\delta^{18}O$ (‰)	Location	Date	δD (‰)	$\delta^{18}O$ (‰)	Location	Date	δD (‰)	$\delta^{18}O$ (‰)	Location	Date	δD (‰)	$\delta^{18}O$ (‰)
11SM	11-May	-84.952	-9.931	12MEB	11-May	-69.460	-7.563	16NWG	11-May	-69.603	-7.630	17EW	11-May	-68.151	-7.432	20SB	11-May	-68.379	-7.573
11SM	17-May	-81.451	-9.514	12MEB	17-May	-71.308	-7.901					17EW	17-May	-68.770	-7.612				
11SM	25-May	-76.455	-8.515	12MEB	25-May	-66.721	-7.106	16NWG	25-May	-66.687	-7.141	17EW	25-May	-65.133	-6.932	20SB	25-May	-64.266	-6.851
11SM	2-Jun	-73.452	-8.326	12MEB	2-Jun	-67.099	-7.315	16NWG	2-Jun	-70.778	-7.916	17EW	2-Jun	-65.013	-6.864	20SB	2-Jun	-64.437	-6.919
11SM	8-Jun	-70.666	-7.880	12MEB	8-Jun	-65.488	-7.150					17EW	8-Jun	-64.526	-6.904				
11SM	15-Jun	-68.307	-7.563	12MEB	15-Jun	-63.633	-6.759	16NWG	15-Jun	-63.254	-6.675	17EW	15-Jun	-62.642	-6.597	20SB	15-Jun	-62.546	-6.769
11SM	21-Jun	-63.397	-6.792	12MEB	21-Jun	-60.046	-6.319	16NWG	21-Jun	-58.778	-6.387	17EW	21-Jun	-59.095	-6.255	20SB	21-Jun	-58.117	-6.157
11SM	28-Jun	-60.988	-6.232	12MEB	28-Jun	-58.776	-6.020	16NWG	28-Jun	-58.452	-6.165	17EW	28-Jun	-58.008	-6.091	20SB	28-Jun	-58.631	-6.090
11SM	5-Jul	-59.772	-5.922	12MEB	5-Jul	-57.419	-5.832					17EW	5-Jul	-56.565	-5.770				
11SM	14-Jul	-59.346	-5.697	12MEB	14-Jul	-56.840	-5.703	16NWG	13-Jul	-56.425	-5.847	17EW	13-Jul	-56.145	-5.694	20SB	13-Jul	-56.038	-5.780
				12MEB	21-Jul	-55.975	-5.664	16NWG	21-Jul	-55.235	-5.597	17EW	21-Jul	-54.934	-5.425	20SB	21-Jul	-55.063	-5.426
11SM	28-Jul	-55.202	-5.005	12MEB	28-Jul	-55.279	-5.384					17EW	28-Jul	-54.410	-5.229				
11SM	3-Aug	-50.999	-4.376	12MEB	3-Aug	-51.363	-4.779	16NWG	3-Aug	-52.615	-5.074	17EW	3-Aug	-51.839	-4.853	20SB	3-Aug	-51.357	-4.803
				12MEB	10-Aug	-52.493	-5.034	16NWG	10-Aug	-52.425	-5.033	17EW	10-Aug	-51.658	-4.618	20SB	10-Aug	-50.632	-4.703
11SM	16-Aug	-50.310	-4.294	12MEB	16-Aug	-52.474	-4.939					17EW	16-Aug	-51.371	-4.784				
11SM	23-Aug	-49.633	-4.099	12MEB	23-Aug	-51.363	-4.703	16NWG	23-Aug	-52.846	-4.641	17EW	23-Aug	-49.727	-4.532	20SB	23-Aug	-51.166	-4.288
				12MEB	7-Sep	-51.834	-4.611					17EW	7-Sep	-50.917	-4.711				
11SM	28-Sep	-53.894	-4.845	12MEB	28-Sep	-58.694	-6.073												
				12MEB	5-Oct	-52.553	-5.069												
Location	Date	δD (‰)	$\delta^{18}O$ (‰)	Location	Date	δD (‰)	$\delta^{18}O$ (‰)	Location	Date	δD (‰)	$\delta^{18}O$ (‰)	Location	Date	δD (‰)	$\delta^{18}O$ (‰)	Location	Date	δD (‰)	$\delta^{18}O$ (‰)
23TT	11-May	-67.008	-7.390	25MC	11-May	-72.070	-8.024	29NI	11-May	-71.189	-7.834	3222B	11-May	-65.972	-6.920	46MS	11-May	-67.736	-7.466
				25MC	17-May	-71.865	-8.092									46MS	17-May	-68.147	-7.488
23TT	25-May	-63.358	-6.924	25MC	25-May	-71.563	-7.991	29NI	25-May	-66.297	-7.326	3222B	25-May	-61.806	-6.413	46MS	25-May	-64.067	-6.998
23TT	2-Jun	-63.644	-6.846	25MC	2-Jun	-69.083	-7.769	29NI	2-Jun	-64.461	-6.698	3222B	2-Jun	-63.329	-6.820	46MS	2-Jun	-64.386	-6.787
				25MC	8-Jun	-68.323	-7.644									46MS	8-Jun	-62.988	-6.738
23TT	15-Jun	-61.853	-6.524	25MC	15-Jun	-66.011	-7.239	29NI	15-Jun	-62.742	-6.683	3222B	15-Jun	-59.729	-6.252	46MS	15-Jun	-62.099	-6.651
23TT	21-Jun	-57.889	-6.267	25MC	21-Jun	-63.417	-6.875	29NI	21-Jun	-59.135	-6.245	3222B	21-Jun	-55.986	-5.694	46MS	21-Jun	-59.000	-6.124
23TT	28-Jun	-57.565	-5.960	25MC	28-Jun	-62.044	-6.639	29NI	28-Jun	-57.683	-5.894	3222B	28-Jun	-55.900	-5.694	46MS	28-Jun	-57.528	-5.962
				25MC	5-Jul	-61.538	-6.728									46MS	5-Jul	-56.699	-5.925
23TT	13-Jul	-55.582	-5.652	25MC	13-Jul	-61.761	-6.514	29NI	13-Jul	-60.472	-6.131	3222B	13-Jul	-54.903	-5.332	46MS	13-Jul	-56.546	-5.708
23TT	21-Jul	-54.017	-5.646	25MC	21-Jul	-60.959	-6.280	29NI	21-Jul	-55.849	-5.590	3222B	21-Jul	-52.826	-5.188	46MS	21-Jul	-54.495	-5.583
23TT	28-Jul	-54.243	-5.087	25MC	28-Jul	-60.030	-5.982									46MS	28-Jul	-54.458	-5.201
23TT	3-Aug	-51.671	-4.833	25MC	3-Aug	-57.151	-5.681	29NI	3-Aug	-50.939	-4.617	3222B	3-Aug	-48.219	-4.373	46MS	3-Aug	-51.526	-4.963
23TT	10-Aug	-50.310	-4.818	25MC	10-Aug	-59.150	-6.004	29NI	10-Aug	-51.451	-4.740	3222B	10-Aug	-50.736	-4.392	46MS	10-Aug	-50.621	-4.801
				25MC	16-Aug	-57.074	-5.791									46MS	16-Aug	-50.921	-4.783
23TT	23-Aug	-50.302	-4.456	25MC	23-Aug	-59.378	-5.884	29NI	23-Aug	-52.361	-4.790	3222B	23-Aug	-48.950	-4.165	46MS	23-Aug	-51.767	-4.570
23TT	7-Sep	-50.154	-4.515	25MC	7-Sep	-58.171	-5.768									46MS	7-Sep	-50.460	-4.493

	δLmean	
Date	δD (‰)	$\delta^{18}O$ (‰)
11-May-16	-70.571	-7.790
17-May-16	-72.889	-8.200
25-May-16	-67.893	-7.423
2-Jun-16	-68.112	-7.467
8-Jun-16	-68.043	-7.480
15-Jun-16	-64.726	-6.950
21-Jun-16	-61.384	-6.599
28-Jun-16	-60.224	-6.331
5-Jul-16	-60.940	-6.412
14-Jul-16	-59.564	-6.168
21-Jul-16	-57.510	-5.840
28-Jul-16	-58.855	-5.869
3-Aug-16	-53.998	-5.171
10-Aug-16	-55.586	-5.442
16-Aug-16	-56.150	-5.539
23-Aug-16	-54.746	-5.079
7-Sep-16	-55.972	-5.410

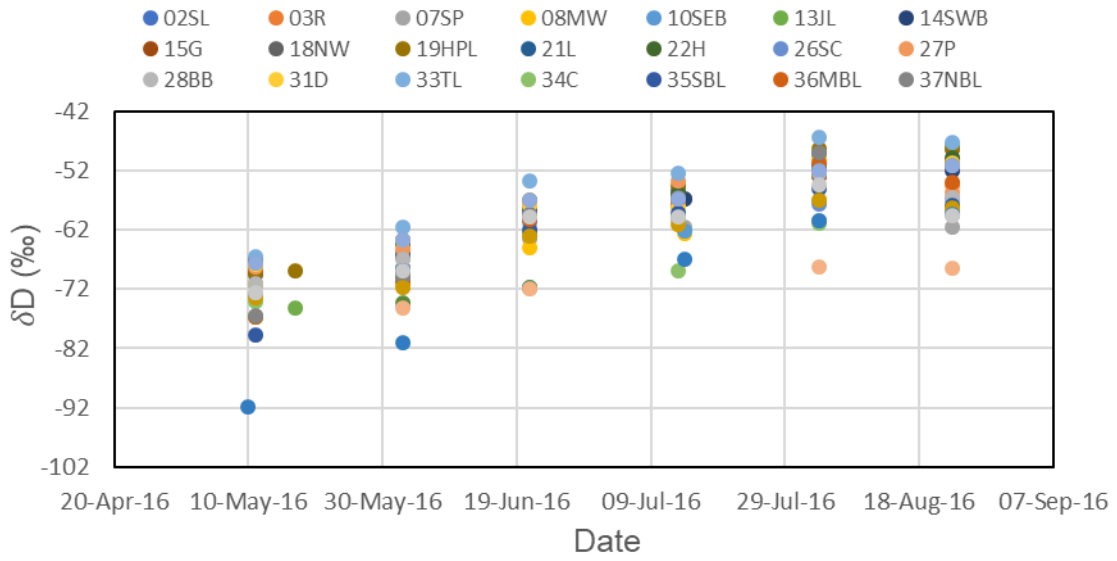

Figure A.5 - Spatial difference in δD (synoptic surveys of Delta Marsh in 2016).

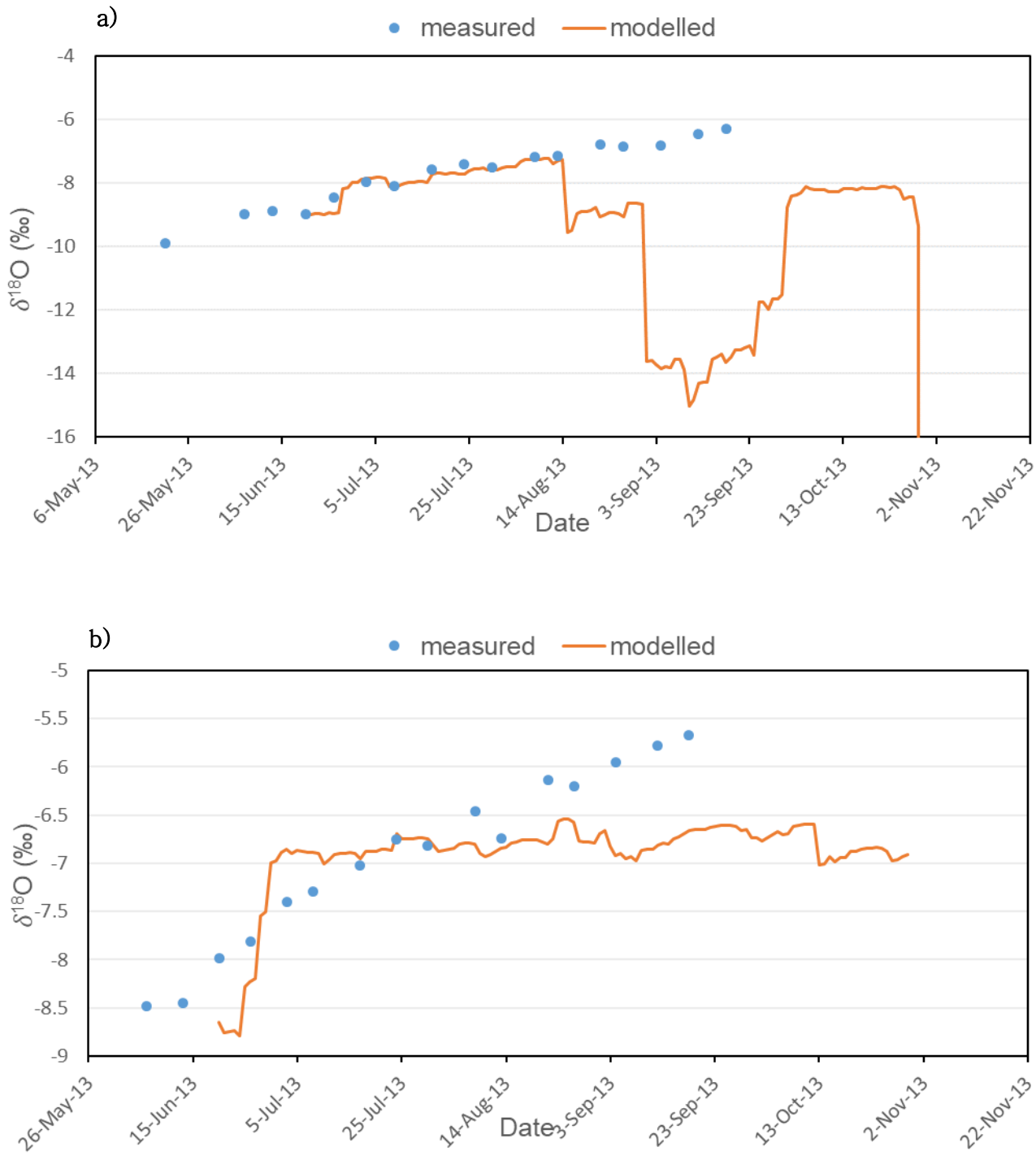

Figure A.6 – Fraction dependent model 2013; comparison of measured and modelled isotopic composition of $\delta^{18}O$ – of a) western and b) eastern CFSTRs. Reference point for the western CFSTR is 25MC and 46MS for the eastern CFSTR.

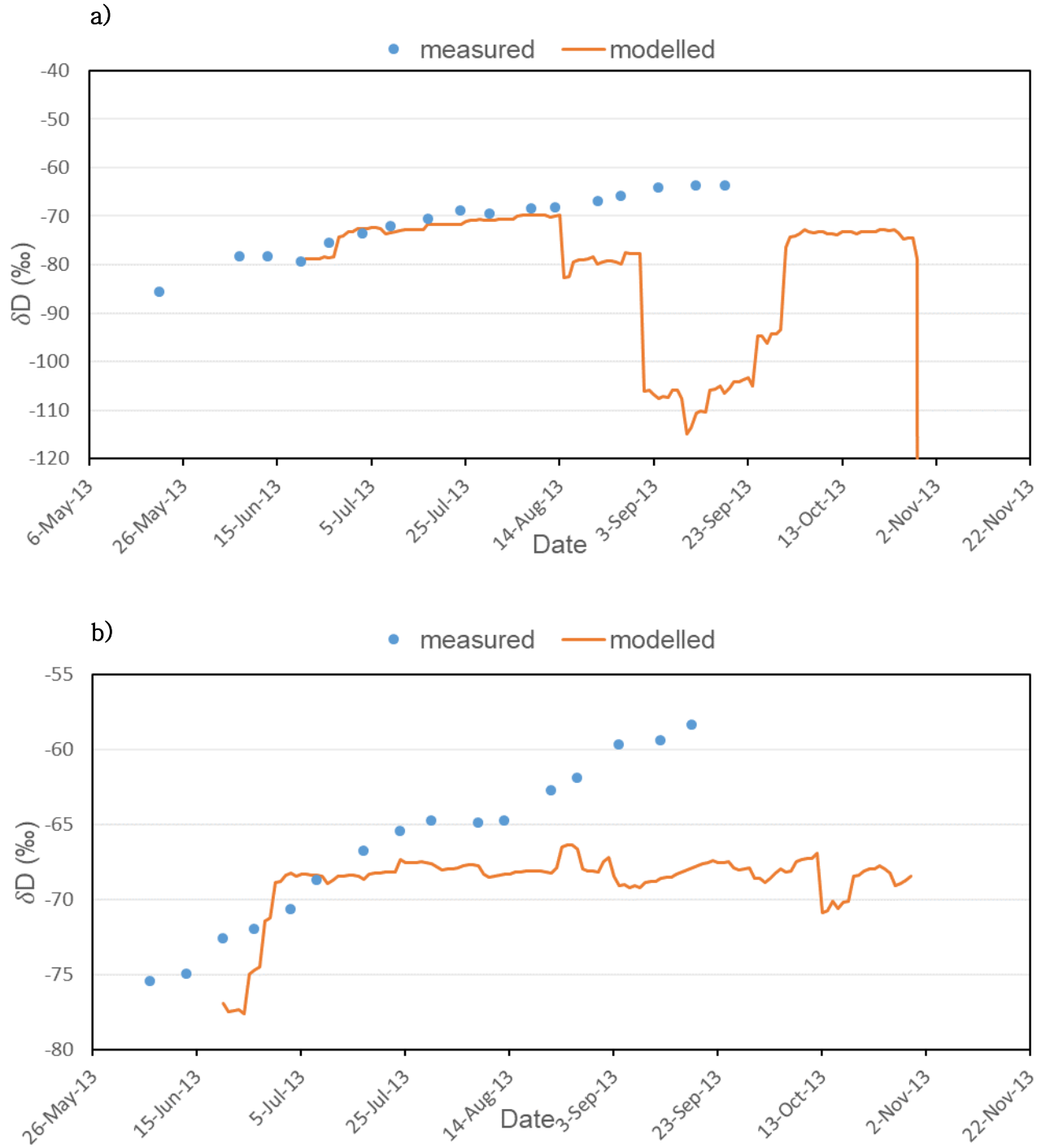

Figure A.7 – Fraction dependent model 2013; comparison of measured and modelled isotopic composition of δD – of a) western and b) eastern CFSTRs. Reference point for the western CFSTR is 25MC and 46MS for the eastern CFSTR.

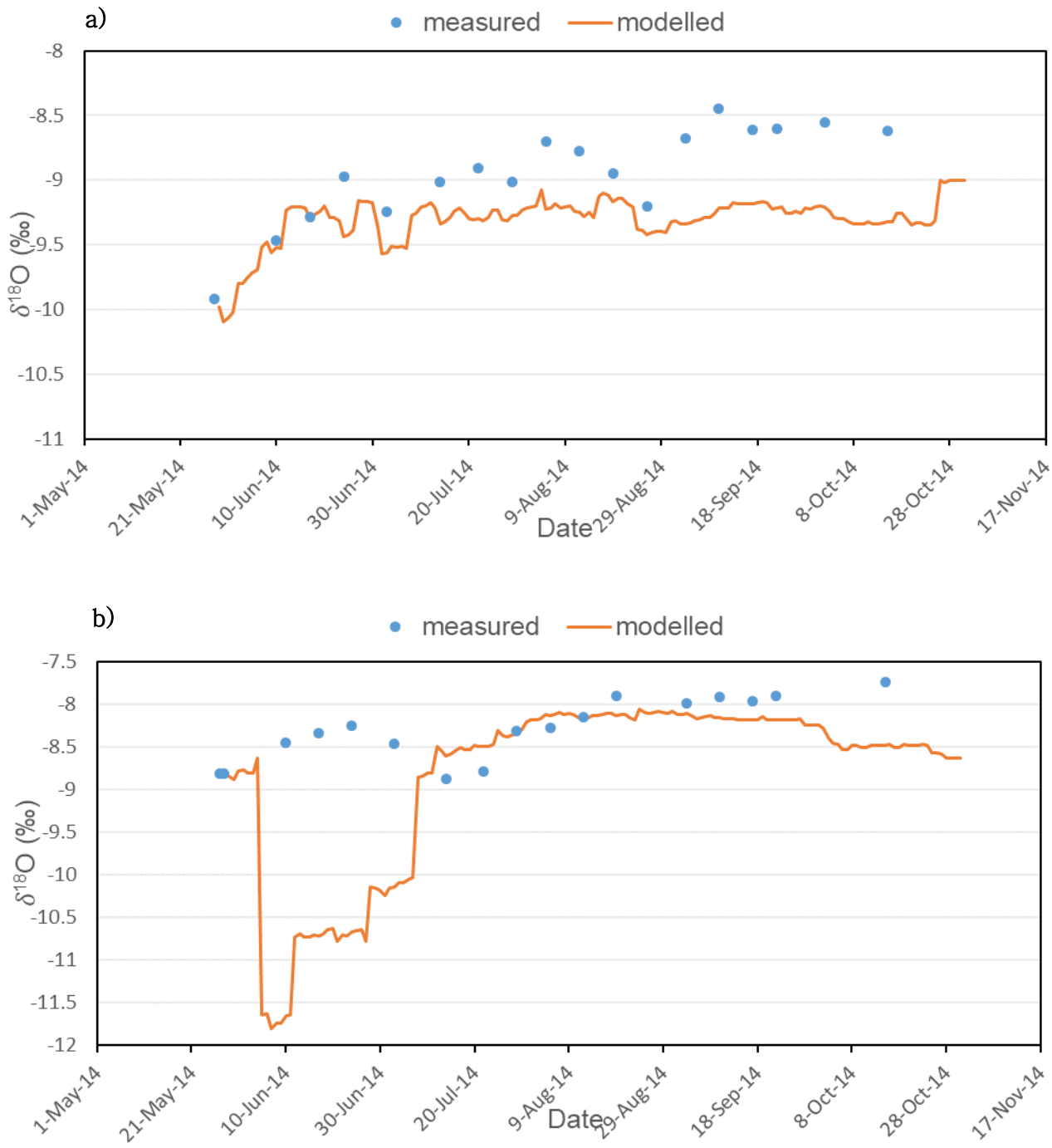

Figure A.8 - Fraction dependent model 2014; comparison of measured and modelled isotopic composition of $\delta^{18}O$ – of a) western and b) eastern CFSTRs. Reference point for the western CFSTR is 25MC and 46MS for the eastern CFSTR.

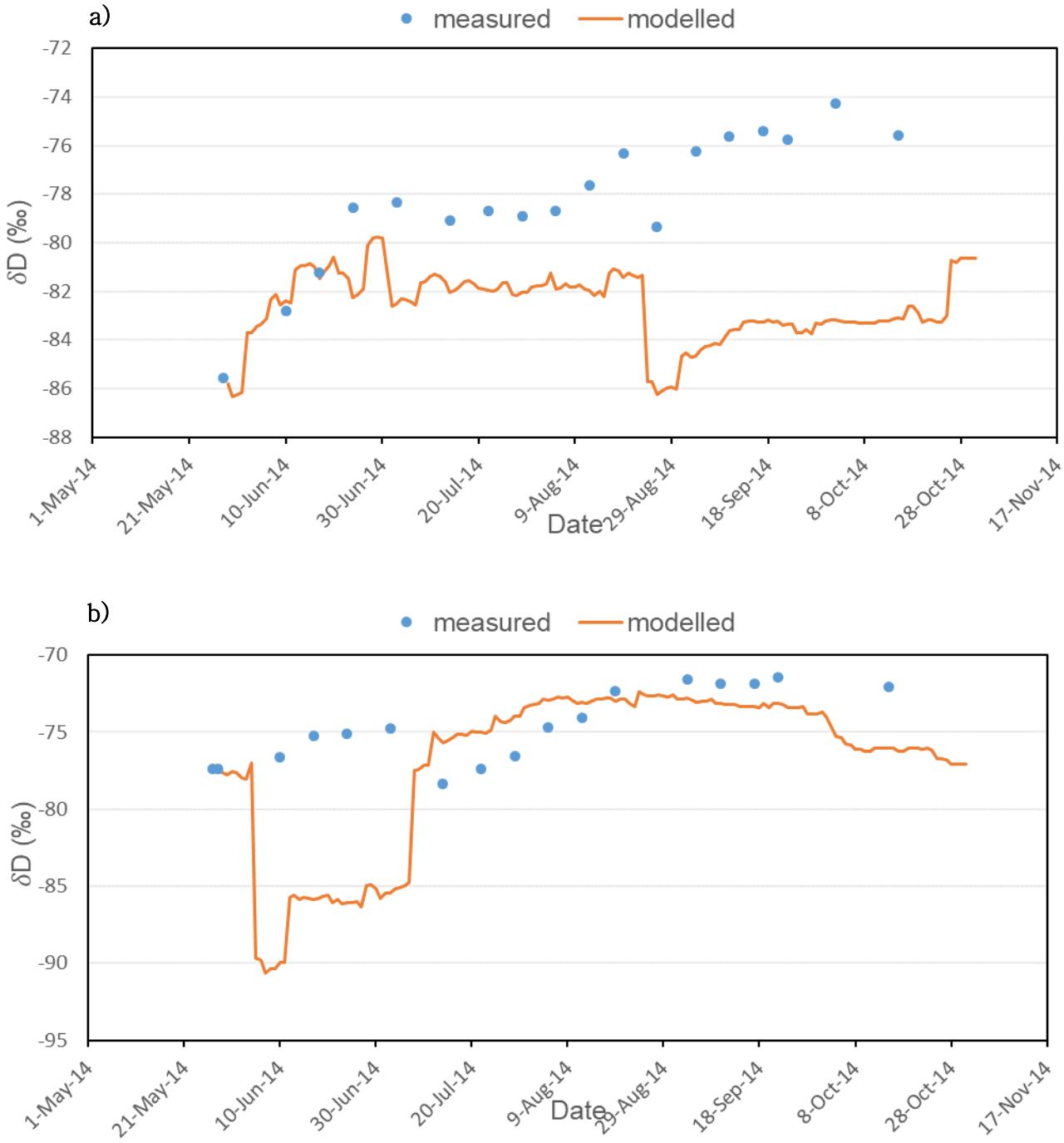

Figure A.9 - Fraction dependent model 2014; comparison of measured and modelled isotopic composition of δD – of a) western and b) eastern CFSTRs. Reference point for the western CFSTR is 25MC and 46MS for the eastern CFSTR.

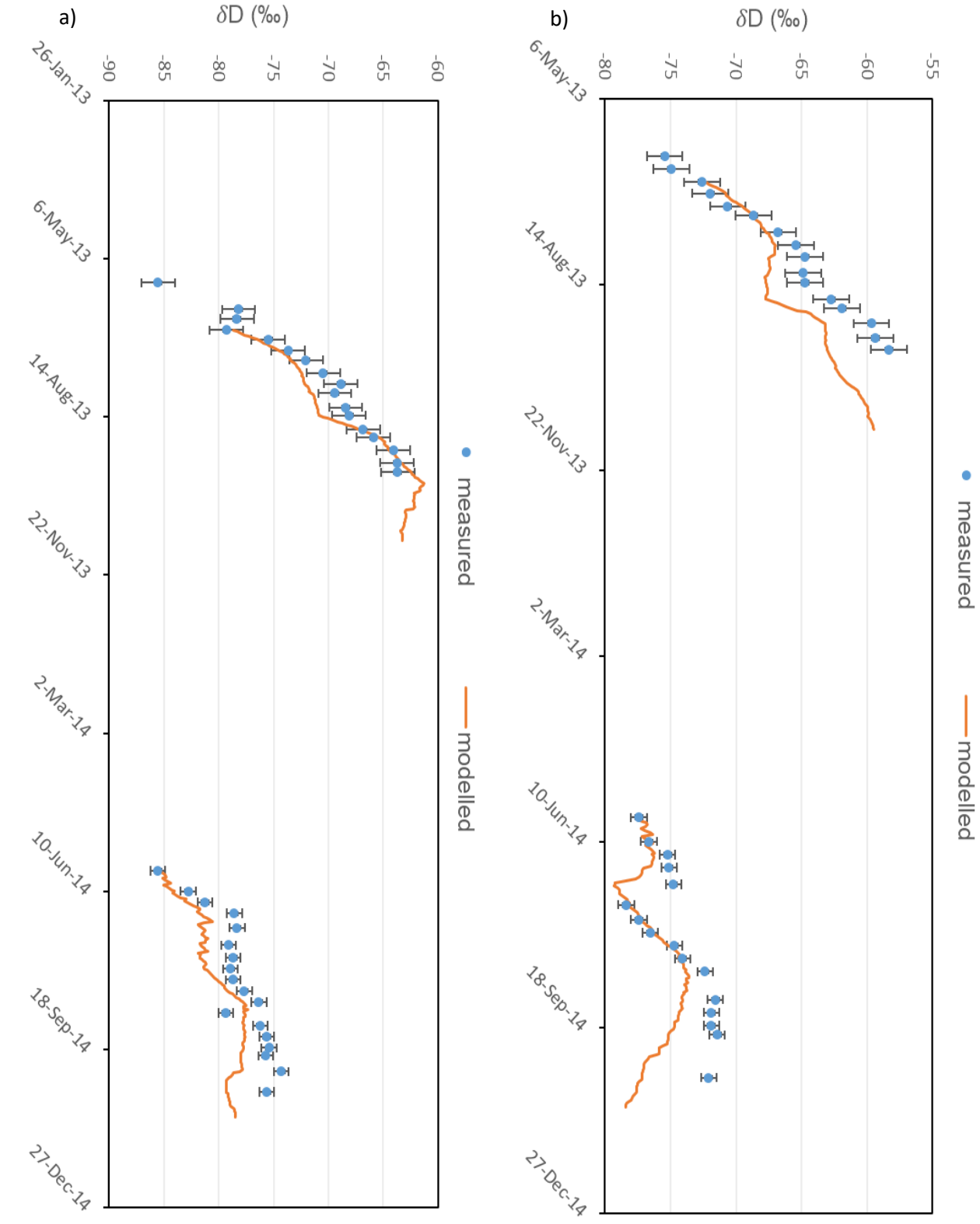
a)
δD (‰)
-90
-85
-80
-75
-70
-65
-60
26-Jan-13
6-May-13
14-Aug-13
22-Nov-13
2-Mar-14
10-Jun-14
18-Sep-14
27-Dec-14
measured
modelled
b)
δD (‰)
-80
-75
-70
-65
-60
-55
6-May-13
14-Aug-13
22-Nov-13
2-Mar-14
10-Jun-14
18-Sep-14
27-Dec-14
measured
modelled

Figure A.10 – Time dependent model for 2013 and 2014; comparison of measured and modelled isotopic composition of δD of for a) west and b) east CFSTR. Measured values are represented in blue circles with error bars representing analytical uncertainty of +/- 1 ‰, while orange line represents model results

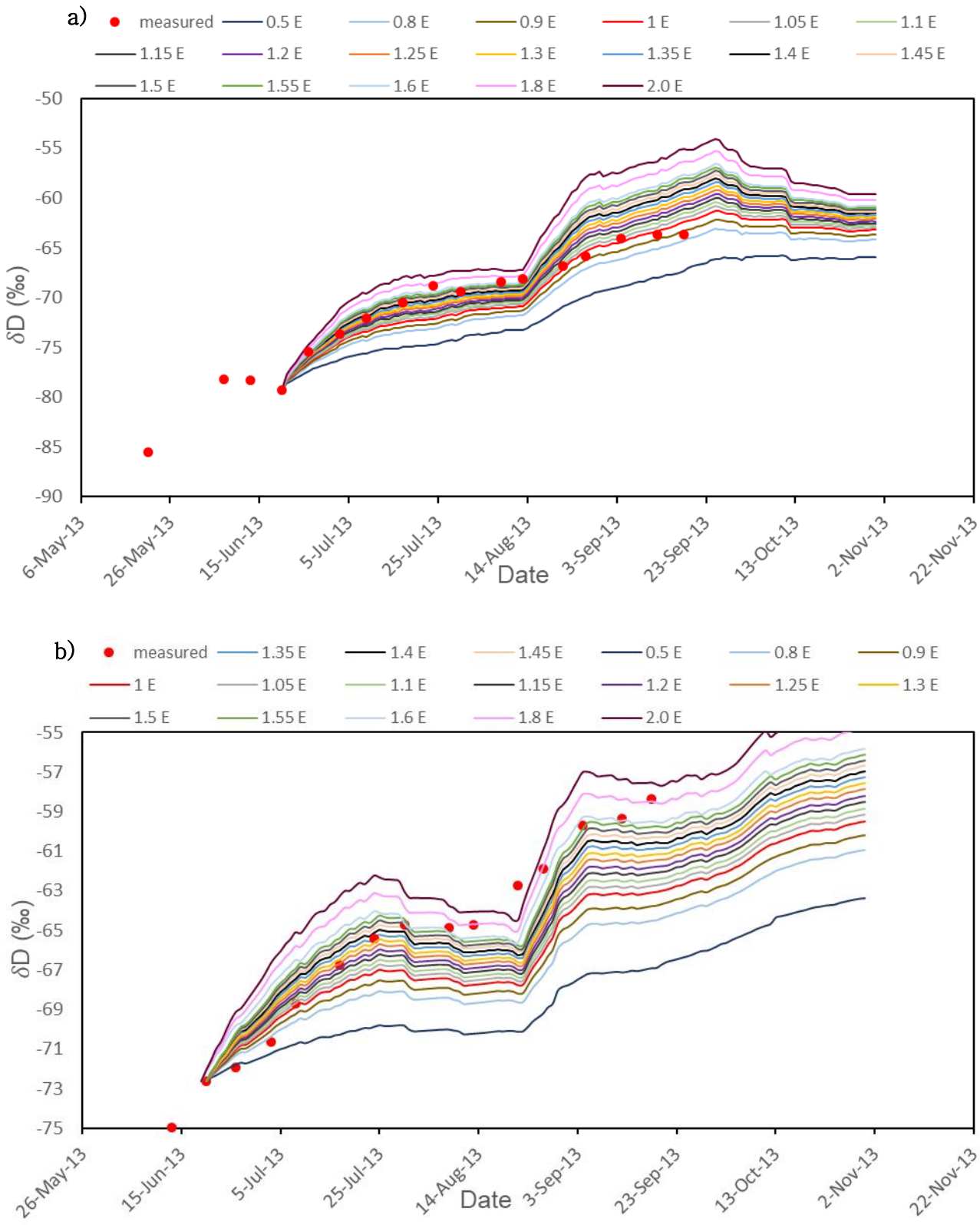

Figure A.11 - ET sensitivity graphs for (a) West and (b) East Marsh in 2013 (δD) . Red dots are measured values, lines represent percentage difference for ET (range 0.5 – 2.0 ET) with different increments.

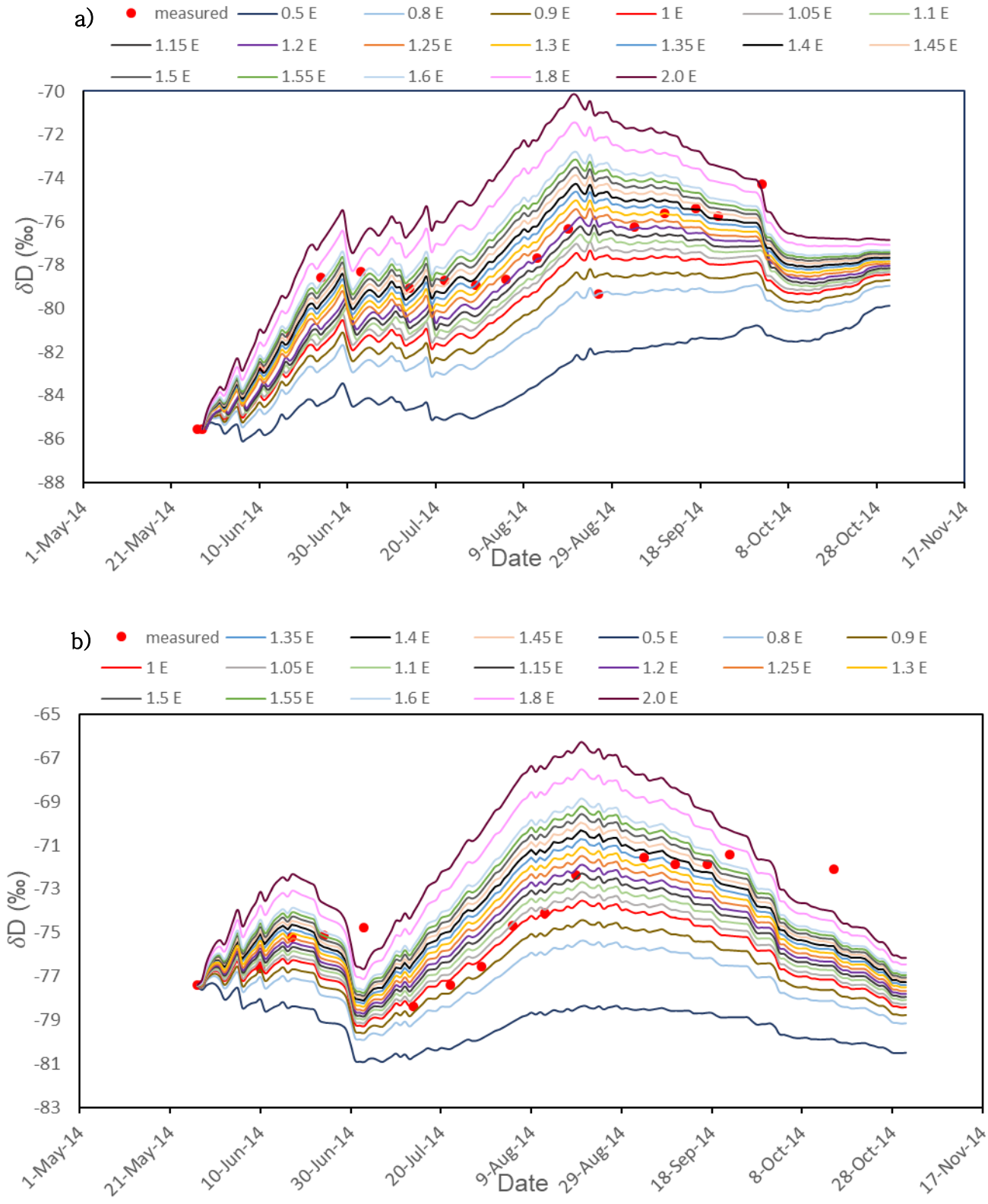

Figure A.12 - ET sensitivity graphs for (a) West and (b) East Marsh in 2014 (δD). Red dots are measured values, lines represent percentage difference for ET (range 0.5 – 2.0 ET) with different increments.

Table A.3 - Water balance for 2013 and 2014. Water balance did not close.

2013 WEST		***2014 WEST***		**2013 *EAST***		***2014 EAST***	
DATE	I -Q - E (mm)	DATE	I -Q - E (mm)	DATE	I - Q - E(mm)	DATE	I -Q - E (mm)
28-May-13	-36.75	28-May-	31.46	28-May-13	-18.83	28-May-14	21.32
29-May-13	87.44	29-May-	-40.99	29-May-13	30.79	29-May-14	-28.83
30-May-13	108.39	30-May-	6.11	30-May-13	9.55	30-May-14	5.16
31-May-13	32.35	31-May-	13.73	31-May-13	52.53	31-May-14	5.92
1-Jun-13	4.40	1-Jun-14	45.39	1-Jun-13	43.79	1-Jun-14	18.86
2-Jun-13	3.66	2-Jun-14	-3.20	2-Jun-13	3.51	2-Jun-14	43.55
3-Jun-13	-33.72	3-Jun-14	-1.98	3-Jun-13	-22.41	3-Jun-14	-25.59
4-Jun-13	-19.04	4-Jun-14	-24.65	4-Jun-13	-10.55	4-Jun-14	-10.90
5-Jun-13	18.64	5-Jun-14	-34.38	5-Jun-13	20.23	5-Jun-14	0.45
6-Jun-13	-32.66	6-Jun-14	85.27	6-Jun-13	-12.31	6-Jun-14	71.50
7-Jun-13	-10.28	7-Jun-14	19.13	7-Jun-13	-30.76	7-Jun-14	-12.59
8-Jun-13	-27.38	8-Jun-14	-17.61	8-Jun-13	-22.30	8-Jun-14	-24.46
9-Jun-13	-29.95	9-Jun-14	-3.81	9-Jun-13	-31.26	9-Jun-14	-12.33
10-Jun-13	-7.63	10-Jun-14	-71.46	10-Jun-13	34.86	10-Jun-14	-29.75
11-Jun-13	79.17	11-Jun-14	71.06	11-Jun-13	34.10	11-Jun-14	42.62
12-Jun-13	38.24	12-Jun-14	5.29	12-Jun-13	35.65	12-Jun-14	2.51
13-Jun-13	-19.74	13-Jun-14	-43.18	13-Jun-13	-28.51	13-Jun-14	-49.23
14-Jun-13	-70.70	14-Jun-14	19.61	14-Jun-13	-25.84	14-Jun-14	12.84
15-Jun-13	-7.42	15-Jun-14	43.41	15-Jun-13	8.00	15-Jun-14	51.21
16-Jun-13	78.91	16-Jun-14	32.21	16-Jun-13	22.03	16-Jun-14	33.74
17-Jun-13	2.79	17-Jun-14	-11.41	17-Jun-13	17.11	17-Jun-14	-9.66
18-Jun-13	-22.36	18-Jun-14	-18.37	18-Jun-13	-22.11	18-Jun-14	-23.98
19-Jun-13	19.14	19-Jun-14	-28.28	19-Jun-13	1.05	19-Jun-14	-10.13
20-Jun-13	-3.65	20-Jun-14	-27.47	20-Jun-13	-1.01	20-Jun-14	-27.80
21-Jun-13	-15.55	21-Jun-14	5.37	21-Jun-13	3.55	21-Jun-14	2.82
22-Jun-13	-18.62	22-Jun-14	8.22	22-Jun-13	-23.25	22-Jun-14	2.71
23-Jun-13	-102.84	23-Jun-14	64.28	23-Jun-13	56.39	23-Jun-14	40.94
24-Jun-13	132.02	24-Jun-14	-12.95	24-Jun-13	-26.71	24-Jun-14	13.29
25-Jun-13	-0.37	25-Jun-14	-28.24	25-Jun-13	2.99	25-Jun-14	-18.80
26-Jun-13	28.65	26-Jun-14	-22.55	26-Jun-13	18.65	26-Jun-14	-24.61
27-Jun-13	93.66	27-Jun-14	1.30	27-Jun-13	83.67	27-Jun-14	-1.66
28-Jun-13	6.44	28-Jun-14	39.48	28-Jun-13	3.64	28-Jun-14	1.10
29-Jun-13	-22.34	29-Jun-14	-222.23	29-Jun-13	-20.07	29-Jun-14	-9.89
30-Jun-13	-8.26	30-Jun-14	232.82	30-Jun-13	-1.71	30-Jun-14	45.33
1-Jul-13	-38.82	1-Jul-14	98.68	1-Jul-13	-27.72	1-Jul-14	95.62
2-Jul-13	-20.85	2-Jul-14	-3.57	2-Jul-13	-16.84	2-Jul-14	7.37
3-Jul-13	-44.88	3-Jul-14	-31.17	3-Jul-13	-28.84	3-Jul-14	-24.26
4-Jul-13	42.10	4-Jul-14	-38.11	4-Jul-13	11.47	4-Jul-14	-36.92
5-Jul-13	24.49	5-Jul-14	23.78	5-Jul-13	23.96	5-Jul-14	19.04
6-Jul-13	-24.52	6-Jul-14	36.94	6-Jul-13	-25.60	6-Jul-14	43.46

7-Jul-13	20.12	7-Jul-14	54.29	7-Jul-13	14.47	7-Jul-14	40.34
8-Jul-13	-1.76	8-Jul-14	9.31	8-Jul-13	-8.01	8-Jul-14	1.31
9-Jul-13	-7.78	9-Jul-14	-52.57	9-Jul-13	65.28	9-Jul-14	-42.54
10-Jul-13	45.11	10-Jul-14	-71.47	10-Jul-13	-16.45	10-Jul-14	-67.50
11-Jul-13	-63.85	11-Jul-14	59.59	11-Jul-13	-57.99	11-Jul-14	51.49
12-Jul-13	-45.71	12-Jul-14	12.60	12-Jul-13	-35.47	12-Jul-14	3.82
13-Jul-13	64.51	13-Jul-14	94.03	13-Jul-13	25.34	13-Jul-14	81.05
14-Jul-13	36.31	14-Jul-14	-15.89	14-Jul-13	36.21	14-Jul-14	-14.61
15-Jul-13	-81.88	15-Jul-14	-50.18	15-Jul-13	-40.41	15-Jul-14	-44.78
16-Jul-13	32.39	16-Jul-14	-54.05	16-Jul-13	27.15	16-Jul-14	-41.48
17-Jul-13	6.96	17-Jul-14	-39.76	17-Jul-13	-15.44	17-Jul-14	-40.37
18-Jul-13	-10.57	18-Jul-14	-132.74	18-Jul-13	-9.49	18-Jul-14	-15.91
19-Jul-13	66.48	19-Jul-14	138.28	19-Jul-13	48.06	19-Jul-14	11.21
20-Jul-13	-35.04	20-Jul-14	-18.15	20-Jul-13	-27.97	20-Jul-14	-8.67
21-Jul-13	-87.81	21-Jul-14	39.21	21-Jul-13	-39.33	21-Jul-14	22.50
22-Jul-13	98.99	22-Jul-14	27.66	22-Jul-13	45.89	22-Jul-14	28.30
23-Jul-13	-52.09	23-Jul-14	-32.64	23-Jul-13	-16.20	23-Jul-14	-27.57
24-Jul-13	31.26	24-Jul-14	-36.94	24-Jul-13	-2.25	24-Jul-14	-30.75
25-Jul-13	7.55	25-Jul-14	-16.85	25-Jul-13	2.85	25-Jul-14	-3.42
26-Jul-13	7.44	26-Jul-14	33.69	26-Jul-13	8.62	26-Jul-14	-1.90
27-Jul-13	-20.07	27-Jul-14	11.20	27-Jul-13	-16.66	27-Jul-14	41.40
28-Jul-13	-17.78	28-Jul-14	38.27	28-Jul-13	-11.44	28-Jul-14	13.32
29-Jul-13	-17.70	29-Jul-14	7.31	29-Jul-13	-30.05	29-Jul-14	2.05
30-Jul-13	9.92	30-Jul-14	-14.53	30-Jul-13	65.62	30-Jul-14	-17.22
31-Jul-13	95.06	31-Jul-14	-15.55	31-Jul-13	51.46	31-Jul-14	-6.51
1-Aug-13	22.03	1-Aug-14	-67.69	1-Aug-13	-3.40	1-Aug-14	-30.19
2-Aug-13	-15.70	2-Aug-14	62.74	2-Aug-13	-8.99	2-Aug-14	21.78
3-Aug-13	-25.74	3-Aug-14	-59.93	3-Aug-13	-18.75	3-Aug-14	-42.12
4-Aug-13	-30.75	4-Aug-14	-11.74	4-Aug-13	-36.09	4-Aug-14	-16.85
5-Aug-13	-2.04	5-Aug-14	-2.75	5-Aug-13	-2.47	5-Aug-14	-9.25
6-Aug-13	11.44	6-Aug-14	-25.53	6-Aug-13	3.12	6-Aug-14	-23.96
7-Aug-13	5.79	7-Aug-14	-89.69	7-Aug-13	10.17	7-Aug-14	-69.48
8-Aug-13	0.92	8-Aug-14	38.40	8-Aug-13	58.07	8-Aug-14	19.63
9-Aug-13	67.79	9-Aug-14	-65.89	9-Aug-13	5.62	9-Aug-14	-17.38
10-Aug-13	-50.37	10-Aug-14	122.36	10-Aug-13	-22.53	10-Aug-14	62.46
11-Aug-13	-27.38	11-Aug-14	-45.70	11-Aug-13	-21.12	11-Aug-14	-22.38
12-Aug-13	2.15	12-Aug-14	58.54	12-Aug-13	-9.92	12-Aug-14	34.31
13-Aug-13	-1.67	13-Aug-14	-32.14	13-Aug-13	-2.52	13-Aug-14	-28.19
14-Aug-13	-55.58	14-Aug-14	-73.06	14-Aug-13	-33.24	14-Aug-14	-58.52
15-Aug-13	1.09	15-Aug-14	33.72	15-Aug-13	-10.86	15-Aug-14	20.92
16-Aug-13	-84.77	16-Aug-14	11.74	16-Aug-13	-31.84	16-Aug-14	16.14
17-Aug-13	-10.55	17-Aug-14	-26.76	17-Aug-13	-36.24	17-Aug-14	-29.16
18-Aug-13	36.91	18-Aug-14	23.89	18-Aug-13	12.64	18-Aug-14	25.83
19-Aug-13	-46.59	19-Aug-14	-11.31	19-Aug-13	-17.94	19-Aug-14	-8.57
20-Aug-13	57.02	20-Aug-14	-45.12	20-Aug-13	23.33	20-Aug-14	-51.92

21-Aug-13	55.79	21-Aug-14	80.74	21-Aug-13	62.85	21-Aug-14	43.39
22-Aug-13	-16.27	22-Aug-14	60.27	22-Aug-13	-23.98	22-Aug-14	48.29
23-Aug-13	-52.60	23-Aug-14	49.64	23-Aug-13	-48.68	23-Aug-14	8.00
24-Aug-13	-51.70	24-Aug-14	-2.30	24-Aug-13	-11.38	24-Aug-14	2.32
25-Aug-13	50.48	25-Aug-14	63.89	25-Aug-13	11.33	25-Aug-14	74.29
26-Aug-13	-25.67	26-Aug-14	-25.85	26-Aug-13	-17.15	26-Aug-14	-43.65
27-Aug-13	13.16	27-Aug-14	-85.23	27-Aug-13	16.20	27-Aug-14	-70.54
28-Aug-13	1.25	28-Aug-14	-77.21	28-Aug-13	-2.48	28-Aug-14	-71.93
29-Aug-13	41.20	29-Aug-14	61.19	29-Aug-13	36.03	29-Aug-14	58.96
30-Aug-13	-76.13	30-Aug-14	-23.24	30-Aug-13	-18.36	30-Aug-14	-23.51
31-Aug-13	109.52	31-Aug-14	-1.46	31-Aug-13	29.25	31-Aug-14	22.03
1-Sep-13	-0.85	1-Sep-14	28.60	1-Sep-13	17.26	1-Sep-14	19.66
2-Sep-13	-89.60	2-Sep-14	-1.92	2-Sep-13	-37.64	2-Sep-14	-13.68
3-Sep-13	58.03	3-Sep-14	10.03	3-Sep-13	7.68	3-Sep-14	-14.00
4-Sep-13	-13.00	4-Sep-14	6.79	4-Sep-13	-6.22	4-Sep-14	45.43
5-Sep-13	-43.71	5-Sep-14	10.86	5-Sep-13	-37.08	5-Sep-14	-9.64
6-Sep-13	17.94	6-Sep-14	-36.40	6-Sep-13	6.13	6-Sep-14	-29.74
7-Sep-13	29.05	7-Sep-14	-43.99	7-Sep-13	18.31	7-Sep-14	-49.96
8-Sep-13	-13.99	8-Sep-14	36.81	8-Sep-13	-1.55	8-Sep-14	28.90
9-Sep-13	1.86	9-Sep-14	27.10	9-Sep-13	-0.90	9-Sep-14	30.19
10-Sep-13	2.08	10-Sep-14	4.21	10-Sep-13	-1.43	10-Sep-14	11.32
11-Sep-13	33.95	11-Sep-14	0.92	11-Sep-13	24.84	11-Sep-14	18.40
12-Sep-13	3.58	12-Sep-14	-55.74	12-Sep-13	5.64	12-Sep-14	-24.80
13-Sep-13	-80.08	13-Sep-14	-25.08	13-Sep-13	-45.09	13-Sep-14	-58.64
14-Sep-13	59.67	14-Sep-14	28.60	14-Sep-13	24.68	14-Sep-14	63.95
15-Sep-13	2.10	15-Sep-14	-49.09	15-Sep-13	5.06	15-Sep-14	-37.09
16-Sep-13	-81.27	16-Sep-14	60.49	16-Sep-13	-37.20	16-Sep-14	-15.05
17-Sep-13	-54.83	17-Sep-14	-31.27	17-Sep-13	-53.10	17-Sep-14	7.02
18-Sep-13	18.32	18-Sep-14	-79.32	18-Sep-13	-14.24	18-Sep-14	-79.62
19-Sep-13	59.09	19-Sep-14	34.53	19-Sep-13	49.28	19-Sep-14	42.61
20-Sep-13	45.27	20-Sep-14	26.89	20-Sep-13	40.53	20-Sep-14	35.23
21-Sep-13	-25.39	21-Sep-14	-2.54	21-Sep-13	-15.97	21-Sep-14	-2.93
22-Sep-13	-26.71	22-Sep-14	-28.12	22-Sep-13	-28.81	22-Sep-14	-42.22
23-Sep-13	-56.21	23-Sep-14	-77.46	23-Sep-13	22.47	23-Sep-14	-54.72
24-Sep-13	36.29	24-Sep-14	12.01	24-Sep-13	-21.67	24-Sep-14	-5.80
25-Sep-13	2.82	25-Sep-14	-48.75	25-Sep-13	-8.44	25-Sep-14	-42.73
26-Sep-13	-118.95	26-Sep-14	-37.11	26-Sep-13	8.11	26-Sep-14	-48.09
27-Sep-13	112.63	27-Sep-14	61.35	27-Sep-13	8.42	27-Sep-14	57.89
28-Sep-13	26.90	28-Sep-14	55.62	28-Sep-13	39.64	28-Sep-14	69.19
29-Sep-13	-36.21	29-Sep-14	-23.66	29-Sep-13	-19.46	29-Sep-14	-18.03
30-Sep-13	-43.35	30-Sep-14	-26.24	30-Sep-13	6.30	30-Sep-14	-25.30
1-Oct-13	-7.43	1-Oct-14	-58.63	1-Oct-13	39.82	1-Oct-14	5.39
2-Oct-13	99.80	2-Oct-14	87.80	2-Oct-13	-14.48	2-Oct-14	41.94
3-Oct-13	39.12	3-Oct-14	186.46	3-Oct-13	24.80	3-Oct-14	146.85
4-Oct-13	16.62	4-Oct-14	14.39	4-Oct-13	18.03	4-Oct-14	7.73

5-Oct-13	0.88	5-Oct-14	-34.81	5-Oct-13	8.06	5-Oct-14	62.17
6-Oct-13	6.53	6-Oct-14	106.48	6-Oct-13	6.83	6-Oct-14	23.68
7-Oct-13	-7.89	7-Oct-14	36.89	7-Oct-13	-15.17	7-Oct-14	25.51
8-Oct-13	-46.10	8-Oct-14	9.94	8-Oct-13	-17.28	8-Oct-14	0.14
9-Oct-13	10.39	9-Oct-14	-69.45	9-Oct-13	-5.36	9-Oct-14	-54.05
10-Oct-13	-3.31	10-Oct-14	-71.55	10-Oct-13	-7.42	10-Oct-14	-65.14
11-Oct-13	0.83	11-Oct-14	-91.74	11-Oct-13	-12.15	11-Oct-14	-89.82
12-Oct-13	44.16	12-Oct-14	-2.20	12-Oct-13	126.58	12-Oct-14	11.50
13-Oct-13	52.43	13-Oct-14	-12.32	13-Oct-13	-1.86	13-Oct-14	-6.91
14-Oct-13	-5.17	14-Oct-14	-36.36	14-Oct-13	-30.81	14-Oct-14	-46.82
15-Oct-13	-44.65	15-Oct-14	-66.68	15-Oct-13	-4.43	15-Oct-14	-55.68
16-Oct-13	30.82	16-Oct-14	76.20	16-Oct-13	5.92	16-Oct-14	42.51
17-Oct-13	10.86	17-Oct-14	21.09	17-Oct-13	11.17	17-Oct-14	59.64
18-Oct-13	9.96	18-Oct-14	-91.32	18-Oct-13	11.09	18-Oct-14	-88.18
19-Oct-13	3.31	19-Oct-14	23.71	19-Oct-13	1.17	19-Oct-14	24.36
20-Oct-13	29.25	20-Oct-14	-4.77	20-Oct-13	40.04	20-Oct-14	-8.57
21-Oct-13	28.16	21-Oct-14	-63.63	21-Oct-13	20.36	21-Oct-14	-75.82
22-Oct-13	-11.89	22-Oct-14	-110.29	22-Oct-13	-6.24	22-Oct-14	-51.32
23-Oct-13	4.05	23-Oct-14	54.37	23-Oct-13	21.03	23-Oct-14	33.51
24-Oct-13	15.42	24-Oct-14	-48.53	24-Oct-13	30.82	24-Oct-14	54.99
25-Oct-13	17.23	25-Oct-14	134.98	25-Oct-13	15.49	25-Oct-14	14.56
26-Oct-13	-3.95	26-Oct-14	5.44	26-Oct-13	-21.01	26-Oct-14	-20.22
27-Oct-13	27.89	27-Oct-14	28.64	27-Oct-13	3.30	27-Oct-14	47.70
28-Oct-13	-67.69	28-Oct-14	83.50	28-Oct-13	-23.02	28-Oct-14	80.97
29-Oct-13	0.77	29-Oct-14	-52.29	29-Oct-13	-18.44	29-Oct-14	-53.42
30-Oct-13	-0.19	30-Oct-14	32.99	30-Oct-13	5.75	30-Oct-14	46.83
31-Oct-13	-74.49	31-Oct-14	-97.89	31-Oct-13	-7.15	31-Oct-14	-89.47
SUM	**30.03**		**-104.92**		**149.04**		**-143.41**

Table A.4 - NSE and RMSE for time dependent model for different increment of E for west and east compartment for 2013 and 2014.

	WEST 2013							***WEST 2014***						
% E	**NSE**		**RMSE**		**f = ((1-NSE)+RMSE)/2**		**mean f(δ(D,^{18}O))**	**NSE**		**RMSE**		**f = ((1-NSE)+RMSE)/2**		**mean f(δ(D,^{18}O))**
	δD	$\delta^{18}O$	δD	$\delta^{18}O$	δD	$\delta^{18}O$		δD	$\delta^{18}O$	δD	$\delta^{18}O$	δD	$\delta^{18}O$	
0.5 E	-0.123	0.053	31.001	3.572	16.062	2.260	9.161	-2.816	-3.128	5.405	0.741	4.611	2.435	3.523
0.8 E	0.609	0.788	30.805	3.522	15.598	1.867	8.733	-0.550	0.031	3.445	0.359	2.498	0.664	1.581
0.9 E	0.736	0.871	30.771	3.516	15.518	1.823	8.670	-0.080	0.436	2.875	0.274	1.978	0.419	1.198
1 E	0.813	0.887	30.751	3.515	15.469	1.814	8.642	0.270	0.571	2.364	0.239	1.547	0.334	0.941
1.05 E	0.834	0.871	30.745	3.516	15.456	1.823	***8.639***	0.403	0.547	2.138	0.246	1.368	0.350	0.859
1.1 E	0.844	0.840	30.742	3.518	15.449	1.839	8.644	0.510	0.466	1.937	0.267	1.214	0.401	0.807
1.15 E	0.844	0.796	30.742	3.521	15.449	1.863	8.656	0.592	0.330	1.767	0.299	1.088	0.485	**0.786**
1.2 E	0.833	0.739	30.745	3.525	15.456	1.893	8.675	0.651	0.144	1.636	0.338	0.993	0.597	0.795
1.25 E	0.813	0.669	30.751	3.530	15.469	1.931	8.700	0.687	-0.090	1.549	0.381	0.931	0.736	0.833
1.3 E	0.784	0.587	30.759	3.536	15.488	1.975	8.731	0.701	-0.370	1.512	0.427	0.906	0.899	0.902
1.35 E	0.746	0.494	30.769	3.542	15.512	2.024	8.768	0.695	-0.693	1.527	0.475	0.916	1.084	1.000
1.4 E	0.699	0.390	30.781	3.549	15.541	2.080	8.810	0.670	-1.057	1.589	0.523	0.960	1.290	1.125
1.45 E	0.645	0.277	30.796	3.557	15.576	2.140	8.858	0.627	-1.459	1.690	0.572	1.032	1.516	1.274
1.5 E	0.583	0.153	30.813	3.565	15.615	2.206	8.911	0.566	-1.897	1.824	0.621	1.129	1.759	1.444
1.55 E	0.513	0.021	30.831	3.574	15.659	2.277	8.968	0.488	-2.370	1.980	0.670	1.246	2.020	1.633
1.6 E	0.437	-0.120	30.852	3.583	15.708	2.352	9.030	0.394	-2.874	2.154	0.718	1.380	2.296	1.838
1.8 E	0.069	-0.761	30.951	3.626	15.941	2.694	9.317	-0.124	-5.178	2.933	0.907	2.028	3.542	2.785
2.0 E	-0.388	-1.506	31.072	3.675	16.230	3.091	9.660	-0.838	-7.863	3.751	1.086	2.795	4.974	3.884
	EAST 2013							***EAST 2014***						
% E	**NSE**		**RMSE**		**f = ((1-NSE)+RMSE)/2**		**mean f(δ(D,^{18}O))**	**NSE**		**RMSE**		**f = ((1-NSE)+RMSE)/2**		**mean f(δ(D,^{18}O))**
	δD	$\delta^{18}O$	δD	$\delta^{18}O$	δD	$\delta^{18}O$		δD	$\delta^{18}O$	δD	$\delta^{18}O$	δD	$\delta^{18}O$	
0.5 E	-0.498	-0.459	5.410	0.851	3.454	1.155	2.305	-4.070	-5.780	5.160	0.820	5.115	3.800	4.458
0.8 E	0.254	0.491	3.818	0.503	2.282	0.506	1.394	-1.050	-1.180	3.280	0.460	2.665	1.320	1.993
0.9 E	0.428	0.673	3.342	0.403	1.957	0.365	1.161	-0.460	-0.380	2.770	0.370	2.115	0.875	1.495
1 E	0.570	0.799	2.899	0.315	1.665	0.258	0.961	-0.050	0.110	2.340	0.290	1.695	0.590	1.143
1.05 E	0.629	0.843	2.692	0.279	1.532	0.218	0.875	0.100	0.260	2.170	0.270	1.535	0.505	1.020
1.1 E	0.681	0.875	2.495	0.249	1.407	0.187	0.797	0.210	0.350	2.030	0.250	1.410	0.450	0.930
1.15 E	0.727	0.895	2.310	0.228	1.292	0.167	0.729	0.290	0.370	1.930	0.250	1.320	0.440	0.880
1.2 E	0.766	0.905	2.139	0.217	1.187	0.156	0.671	0.330	0.350	1.870	0.250	1.270	0.450	**0.860**
1.25 E	*0.799*	*0.905*	1.984	0.218	1.093	0.157	0.625	0.350	0.270	1.850	0.270	1.250	0.500	0.875
1.3 E	0.825	0.894	1.848	0.229	1.012	0.168	0.590	0.330	0.140	1.870	0.290	1.270	0.575	0.923
1.35 E	0.846	0.875	1.732	0.249	0.943	0.187	0.565	0.290	-0.030	1.940	0.320	1.325	0.675	1.000
1.4 E	0.862	0.847	1.641	0.275	0.890	0.214	0.552	0.220	-0.240	2.030	0.350	1.405	0.795	1.100
1.45 E	0.873	0.811	1.577	0.306	0.852	0.248	***0.550***	0.120	-0.490	2.150	0.380	1.515	0.935	1.225
1.5 E	0.878	0.767	1.541	0.340	0.832	0.287	0.559	0.004	-0.780	2.287	0.418	1.641	1.099	1.370
1.55 E	0.879	0.716	1.535	0.375	0.828	0.330	0.579	-0.135	-1.102	2.442	0.454	1.788	1.278	1.533
1.6 E	0.876	0.658	1.558	0.412	0.841	0.377	0.609	-0.296	-1.456	2.608	0.491	1.952	1.474	1.713
1.8 E	0.821	0.363	1.871	0.562	1.025	0.600	0.812	-1.119	-3.153	3.336	0.639	2.728	2.396	2.562
2.0 E	0.709	-0.016	2.384	0.710	1.337	0.863	1.100	-2.187	-5.211	4.091	0.781	3.639	3.496	3.568

References

Aeschbach-Hertig, W., 2010. *Physics of aquatic systems; Part II:Isotope Hydrology,* s.l.: s.n.

Aminian, P., 2015. *Hydrodynamic Modelling of Delta Marsh and Simplified Methods of Discharge Estimation for Discontinuous Inland Coastal Wetlands. Master Thesis, Department of Civil Engineering, University of Manitoba,* Winnipeg: Available from https://mspace.lib.umanitoba.ca/handle/1993/31013.

Araguàs-Araguàs, L., Froehlich, K. & Rozanski, K., 2000. Deuterium and oxygen-18 isotope composition of precipitation and atmospheric moisture. *Hydrol.Process,* Volume 14, pp. 1341-1355.

Badiou, P., 2005. *Ecological impacts of an exotic benthivorous wish in wetlands: A comparison between common carp(Cyprinus carpio L.) additions in large experimental wetlands and small mesocosms in Delta Marsh, Manitoba. Doctor of Philosophy Thesis, Department of Botany,* Winnipeg, Manitoba: Available from https://mspace.lib.umanitoba.ca/handle/193/7869.

Badiou, P. & Goldsborough, G., 2014. Ecological impact of an exotic benthivorous fish, the common carp (Cyprinus carpio L.), on water quality, sedimantation, and submerged macrophyte biomass in wetland mesocosms. *Hydrobiologia.,* Volume 755, pp. 107-121.

Badiou, P. H. & Goldsborough, L. G., 2010. Ecological Impact of an Exotic Benthivorous Fish in Large Experimental Wetlands, Delta Marsh, Canada. *Wetlands,* pp. 657-667.

Baertschi, P., 1976. Absolute 18O content of Standard Mean Ocean Water. *Earth Planet. Science Letters,* Volume 31, pp. 341-344.

Bansah, S. & Ali, G., 2017. Evaluating th eeffects of traicer choice and end-member definitions on hydrograph separation results across nested seasonally cold watersheds. *Agu Publications,* Volume 53, pp. 8851-8871.

Baschuk, M., 2011. *Mapping of emergent vegetation in Delta Marsh, Manitoba; A comparison of heads-up digitizing and object-based classification,* s.l.: DUC.

Bemrose , R., Kemp, L., Henry, M. & Soulard , F., 2009. *The Water Yield for Canada As a Thirty-year Average (1971 to 2000): Concepts, Methodology and Initial results.,* Otawa: Statistics Canada.

Bennett, K., Gibson, J. & McEachern, P., 2008. Water yield estimatesfor critical loadings assessment: comparison of gauging methods versus an isotopic approach. *Can. J. Fish. Aquat. Sci,* Issue 65, pp. 83-99.

Birks, S. & Edwards, T., 2009. Atmospheric circulation controls on precipitation isotope-climate relations in western Canada. *Tellus,* Volume 61B, pp. 566-576.

Birks, S., Remenda, V. & Edwards, T., 2000. Clay aquitards as isotopic archives of holocene Paleoclimate in the Northern Great Planes: sensitivity analysis. *Hydrological Processes,* Volume 14, pp. 1523-1536.

Blume, T., Zehe, E. & Bronstert, A., 2008. Investigation of runoff generation in a pristine, poorly gauged catchment in the Chilean Andes II: qualitative and quantitative use of tracers at three spatial scales. *Hydrol. Process,* Volume 22, pp. 3676-3688.

Bortoluzzi, T., 2013. *Spatial and temporal patterns inthe hydrology, water chemistry and algal nutrient status of a coastal freshwater marsh, Delta Marsh, as influenced by the hydrology of adjoining Lake Manitoba, located in south-central Manitoba, Canada. Doctor of Philosophy,* Winnipeg, Manitoba: Available from https://mspace.lib.umanitoba.ca/handle/1993/19686.

Brooks, J., Gibson, J., Birks, S. & Weber, M., 2014. Stable isotope estimates of evaporation: inflow and water residence time for lakes across the United States as a tool for national lake water quality assessments. *Limnology and Oceanography,* Volume 59, pp. 2150-2165.

Buttle, J. & McDonnell, J., 2004. Isotope tracers in catchment hydrology in the humid tropics. In: *Forest, Water and People inthe Humid Tropics.* Cambridge, UK: Cambridge University Press.

Carey, S., Boucher, J. & Duarte, C., 2013. Inferring groundwater contributions and pathways to streamflow during snowmelt over multiple years in a discontinuous permafrot subarctic environment (Yucon, Canada). *Hydrogeol. J.,* Volume 21, pp. 67-77.

Carey, S. & Quinton, W., 2005. Evaluating runoff generation during summer using hydrometric, stable isotope and hydrochemical methods in a discontinuous permafrost alpine catchments. *Hydrol. Process ,* Volume 19, pp. 95-114.

Chapra, S. C., 2008. *Surface water-quality modelling.* Long Grove,IL: Waveland Press, Inc..

Chen, D. & Chen, H., 2013. Using Köppen classification to quantify climate variation and change: An example for 1901-2010. *Environmental Development,* Volume 6, pp. 69-79.

Clark, I. & Fritz, P., 1997. *Environmental Isotopes in Hydrogeology.* New York: Lewis Publishers.

Coles, A., McConkey, B. & McDonnell, J., 2017. Climate change impacts on hillslope runoff on the northern Great Plains,1962-2013. *Journal of Hydrology,* Volume 550, pp. 538-548.

Coles, A. & McDonnell, J., 2018. Fill and spill drives runoff connectivity over frozen ground. *Journal of Hydrology,* pp. 115-128.

Coplen, T., 1996. New guidelines for reporting stable hydrogen, carbon, and oxygen isotope-ratio data. *Geochim.Cosmochim. Acta,* Volume 60, pp. 3359-3360.

Craig, H., 1961. Standard for reporting concentrations of deuterium and oxygen-18 in natural waters. *Science,* Volume 133, p. 1833.

Craig, H. & Gordon, L., 1965. Deuterium and oxygen-18 in the ocean and marine atmosphere. *Stable Isotopes in Oceanographic Studies and Paleotemperatures, Spoleto, Italy.,* pp. 9-130.

Dansgaard, W., 1964. Stable isotopes in precipitation. *Tellus,* Volume 16, pp. 436-468.

De Wit, J., Van der Straaten, M. & Mook, W., 1980. Determination of the absolute hydrogen isotopic ratio of V-SMOW and SLAP. *Geostandards Newsletter,* Volume 4, pp. 33-36.

Delavau, C. et al., 2015. North American precipitation isotope (δ18O) zones revealed in time series modelling across Canada and northern United States. *Water Resource Research,* pp. 1284-1299.

Dingman, S. L., 2015. *Physical hydrology.* Third ed. Long Grove,IL: Waveland Press, Inc..

Douglas, M., Clark, I., Raven, K. & Bottomley, D., 2000. Groundwater mixing dynamics at a Canadian Shield mine. *Journal of Hydrology,* Volume 235, pp. 88-103.

Ducks Unlimited Canada, 2009. *Restoring the Tradition at Delta Marsh. Public information document,* Winnipeg: DUC.

Ducks Unlimited Canada, 2013. *Restoring the tradition at Delta Marsh: Science Guiding Restoration. Techincal report.,* Winnipeg: DUC.

Edwards, T., Wolfe, B., Gibson, J. & Hammarlund, D., 2004. Use of water isotope traicers in High-latitude hydrology and paleohydrology.. In: *Long -term environmental change in arctic and Antarctic lakes: Developments in Paleoenvironmental research.* Dordrecht, The Netherlands: Kluwer Academic Publishers.

Emery, B. & Wrubleski, D., 2015. *Summary of 2014 Scientific Activities at Delta Marsh, Manitoba, Canada,* s.l.: DUC.

Falcone, M., 2007. *Assessing hydrological processes controlling the water balance of lakes in the Peace-Athabasca Delta, Alberta, Canada using water isotope tracers. MSc Thesis in Earth Sciences at University of Waterloo,* Waterloo: Available from: http://hdl.handle.net/10012/3081.

Gat, J., 1981. *Lakes (Technical Report No. Series 210),* Vienna, AU: International Atomic Energy Agency.

Gat, J., 1996. Oxygen and hydrogen isotopes in the hydrologic cycle. *Earth Planet Sci.,* Volume 24, pp. 225-262.

Gat, J. & Levy, Y., 1978. Isotope hydrology of inland Sabkhas in the Bardwil area, Sinai. *Limnology and Oceanography,* Volume 23, pp. 841-850.

Genereux, D., 1998. Quantifyong uncertainty in tracer-based hydrograph separation. *Water Resources Research,* Volume 34, pp. 915-919.

Giauque, W. & Johnston, H., 1929a. An isotope of oxygen, mass 18. *j. Am. Chem. Soc,* Volume 51, p. 1436.

Giauque, W. & Johnston, H., 1929b. An isotope of oxygen, mass 17, in the Earth's Atmosphere. *Am. Chem. Soc,* Volume 51, pp. 3528-3534.

Gibson, J., 1996. *Non-steady isotopic methods for estimating lake evaporation: Development and validation in arctic Canada. PhD. Thesis, Department of Earth Science, University of Waterloo,* ON: University of Waterloo.

Gibson, J., 2002. Short-term evaporation and water budget comparisons in shallow Artic lakes using non-steady isotope mass balance. *Journal of Hydrology,* 264(1-4), pp. 242-261.

Gibson, J., Birks, S. & Edwards, T., 2008. Global prediction of δA and δ2H-δ18O evaporation slopes for lakes and soil water accounting for seasonality. *Global Biochemical Cycles,* Volume 22, pp. 1-12.

Gibson, J. et al., 2010a. Site-specific estimates of water yield applied in regional acid sensitivity surveys across western Canada. *J.Limnol.,* Volume 69, pp. 67-76.

Gibson, J., Birks, S., Jeffries, D. & Yi, Y., 2017. Regional trends in evaporation loss and water yield based on stable isotope mass balance of lakes: The Ontario Precambrian Shield surveys. *Journal of Hydrology,* Volume 544, pp. 500-510.

Gibson, J. et al., 2010b. Inter-annual variations in water yield to lakes in northeastern Alberta: implications for estimating critical loads of acidity. *J.Limnol.,* Volume 69, pp. 126-134.

Gibson, J., Birks, S. & Moncur, M., 2019. Mapping water yield distribution across the South Athabasca Oil Sands (SAOS) area: Baseline surveys applying isotope mass balance of lakes. *Journal of Hydrology,* Issue 21, pp. 1-13.

Gibson, J., Birks, S. & Yi, Y., 2015a. Stable isotope mass balance of lakes: a contemporary perspective. *Quaternary Science Reviews,* pp. 1-13.

Gibson, J. et al., 2016. Stable isotope mass balance of fifty lakes in central Alberta: Assessing the role of water balance parameters in determining trophic status and lake level. *Journal of Hydrology: Regional studies,* Volume 6, pp. 13-25.

Gibson, J., Birks, S., Yi, Y. & Vitt, D., 2015b. Runoff to boreal lakes linked to land cover, watershed morphology and permafrost thaw: a 9-year isotope mass balance assessment. *Hydrological Processes,* Volume 29, pp. 3848-3861.

Gibson, J., Edwards, T., Bursey, G. & Prowse, T., 1993. Estimating evaporation using stable isotopes: quantitative results and sensitivity analysis for two catchments in northern Canada. *Nordic Hydrology,* Volume 24, pp. 79-94.

Gibson, J., Edwards, T. & Prowse, T., 1999. Pan-derived isotopic composition of water vapour and and its variability in northern Canada. *J.Hydrol.,* Issue 217, pp. 55-74.

Gibson, J. et al., 2005. Progress in isotope tracer hydrology in Canada. *Hydrological Processes,* Volume 19, pp. 303-327.

Gibson, J. & Edward, T., 2002. Regional water balance trends and evaporation-transpiration partitioning from a stable isotope survey of lakes in northern Canada. *Global Biochemical Cycles,* Volume 16, p. 1026.

Gibson, J., Prepas, E. & McEachern, P., 2002. Quantitative comparison of lake throughflow, residency, and catchment runoff using stable isotopes: modelling and results from a regional survey of Boreal lakes. *Journal of hydrology,* Volume 262, pp. 128-144.

Gibson, J. & Reid, R., 2014. Water balance along a chain of tundra lakes: A 20-year isotopic perspective. *Journal of Hydrology,* Volume 519, pp. 2148-2164.

Gionfiantini, R., 1986. Environmental Isotopes in lake studies. InP.Fritz, & J. - Fontes (Eds.). In: *Handbook of environmental isotope geochemistry, the terrestrial environment.* NY: Elsevier, pp. 113-168.

Goldsborough, S. & Suggett, G., 2015. *Delta A Prairie and its People.* Winnipeg: Delta Marsh History Group.

Good, S., Soderberg, k., Wang, L. & Caylor, K., 2012. Uncertanties in the assessement of the isotopic ratios in surface fluxes: a direct comparison of techniques using laser-based water vapour isotopic analyzers. *J.Geophys.Res.*

Haig, H., 2018. *Analysis of lakewater isotopes in Northern Great Plains: insight from long-term monitoring and spatial survey.PhD Thesis,* Saskatchewan: University of Regina.

Haig, H. et al., 2020. Comparison of isotopic mass balance and instrumental techniques as estimates of basin hydrology in seven connected lakes over 12 years. *Journal of hydrology X,* Volume 6, pp. 1-14.

Hertam, S.C., 2010. *The Effects of Common Carp (Cyprinus carpio L.) on Water Quality, Algae and Submerged Vegetation in Delta Marsh, Manitoba. Master Thesis, Department of Biological Sciences, University of Manitoba,* Winnipeg, Manitoba: Available from https://mspace.lib.umanitoba.ca/handle/193/4207.

Hope, C., 2020. *Historical Loading and Current Sorption Capacity of Phosphorus in the sediments of Delta Marsh.Master Thesis. Department of Biological Sciences, University of Manitoba,* Winnipeg: Available from: http://hdl.handle.net/1993/34627.

Horita, J., Rozanski, K. & Cohen, S., 2008. Isotope effects in evaporation of water: a status report of the Craig-Gordon model. *Isotopes Environ Health Stud,* pp. 23-49.

Horita, J. & Wesolowski, D., 1994. Liquid-vapour fractination of oxygenand hydrogen isotopes of water from freezing to the critical temperature. *Geochim. Cosmochim. Acta ,* pp. 3425-3437.

Hrachowitz, M. et al., 2011. On the value of combined event runoff and tracer analysis to improve understanding of catchment functioning in data-scarce semi-arid area. *Hydrol. Earth Syst. Sci.,* Volume 15, pp. 2007-2024.

Huddart, P., Longstaffe, F. & Crowe, A., 1999. δD and δ18O evidence for inputs to groundwater at a wetland coastal boundary in the southern Graeat lakes of Canada. *Journal of Hydrology,* Volume 214, pp. 18-31.

IAEA, 2000a. *Environmental Isotopes in the Hydrological Cycle; Principles and Applications Vol.1.* Vienna,AU: IAEA.

IAEA, 2000b. *Environmental Isotopes in the Hydrological Cycle; Principles and Applications Vol.2.* Vienna,AU: IAEA.

IAEA, 2000c. *Environmental Isotopes in the Hydrological Cycle; Principles and Applications Vol 3.* Vienna, AU: IAEA.

IAEA, 2018. *Isotope enabled models for improved estimates of water balance in catchments (2018-2021), CRP F31005. RCM 1 Report,* Vienna, AU: IAEA.

Iwagami, S. et al., 2010. Role of bedrock groundwater in the rainfall-runoff process in a small headwater catchment underlain by volcanic rock. *Hydrol. Process,* Volume 24, pp. 2771-2783.

James, A. & Roulet, N., 2009. Antecendent moisture conditions and catchment morphology as controls on spatial patterns of hydrograph separation in small forest cathcments. *Journal of Hydrology,* Volume 377, pp. 351-366.

Jasechko, S. et al., 2013. Terrestrial water fluxes dominated by transportation. *Nature,* Volume 496, pp. 347-350.

Jenkins, A., Ferrier, R., Harriman, R. & Oqunkoya, Y., 1994. A case study in catchment hydrochemistry - conflicting interpretations from hydrological and chemical observations. *J.Hydrol.,* Volume 8, pp. 335-349.

Kendall, C. & Coplen, T., 2001. Distribution of oxygen - 18 and deuterium in river waters across United States. *Hydrol. Process.,* 15(7), pp. 1363-1393.

Klaus, J. & McDonnell, J., 2013. Hydrograph separation using stable isotopes: Review and evaluation. *Journal of Hydrology,* Volume 505, pp. 47-64.

Last, W. M. & Teller, J. T., 2002. Paleolimnology of Lake Manitoba: The Lithostratigraphic Evidence. *Georaphie,* pp. 135-154.

McCuen, R. H., Knight, Z. & Cutter, A. G., 2006. Evaluation of the Nash-Sutcliffe efficiency index. *J.Hydrol.Eng.*

McDonnell, J., Stewart, M. & Owens, I., 1991. Effects of catchment-scale subsurface mixing on stream isotopic response. *Water Resour. Res.,* Volume 27, pp. 3065-3073.

McGlynn, B. & McDonnell, J., 2003. Quantifying relative contributions of riparian and hillslope zones to catchment runoff. *Water Resour. Res.,* Volume 39.

McGuire, K. & McDonnell, J., 2010. Hydrological connectivity of hillslopes and streams:characteristic time scales and nonlinearities. *Water Resour. Res.,* Volume 46.

McHale, M., McDonnell, J., Mitchell, M. & Cirmo, C., 2002. A field-based study of soil water and groundwater nitrate release in an Adirondrack forested watershed. *Water Resour. Res,* Volume 38, p. 1031.

Metcalfe, R. & Buttle, J., 2001. Soil partitioning and surface store controls on spring runoff from a boreal forest peatland basin in north-central Manitoba, CAnada. *Hydrol. Process.,* Volume 15, pp. 2305-2324.

Moser, H. & Stichler, W., 1980. Environmental isotopes in ice and snow.. In: *P.Fritz & J.C. Fontes (Eds.): Handbook of environmental isotope geochemistry.* New York: Elsevier, pp. 141-178.

Muñoz-Villers, L. & McDonnell, J., 2012. Runoff generation in a steep, tropical, montane cloud forest catchment on a permeable volvanic substrate. *Water Resour. Res.,* Volume 48.

Murkin, H. et al., 2000. *Prairie wetland ecology the contribution of the Marsh Ecology Research Program (Chapter 1).* s.l.:Ames Iowa State University Press.

Nash, J. & Sutcliffe, J., 1970. River flow forecastingthrough conceptual models part I - a discussion of principles. *Journal of Hydrology.*

Nelson, S., 2000. A simple,practical methodology for routine VSMOW/SLAP normalization of water samples analyzed by continuous flow methods. *Rapid Commun Mass Spectrom,* Volume 15, pp. 1044-1046.

Ogunkoya, O. & Jenkins, A., 1993. Analysis os storm hydrograph and flow pathways using a three-component hydrograph separation model. *J.Hydrol.,* Volume 142, pp. 71-88.

Orlowski, N., 2010. *Construction and specification of a cryogenic vacuum extraction device for application in stable water isotope analysis. MSc. Thesis,* Gießen: Justus-Liebig-Universität.

Phillips, S., 1976. *The relationship between evapotranspiration by phragmites communities trin. and water table fluctuations in Delta Marsh, Manitoba.Doctor of Philosophy Thesis University of Manitoba, Department of Botany,* Winnipeg,Manitoba: s.n.

Pomeroy, J. et al., 2007. The cold regions hydrological model: a platform for basing process representation and model structure on physical evidence. *Hydrological Processes,* Volume 21, pp. 2650-2667.

Remenda, V. & Birks, S., 1999. *Groundwater in Palliser Triangle; an overview of its vurnerability and potential to archive climate information,* s.l.: s.n.

Rozanski, K., Araguas-Araguas, L. & Gonfiantini, R., 1993. Isotopic patterns in modern global precipitation. In: P. Swart, J. McKenzie, K. Lohmann & S. Savin, eds. *Climate Change in Continetntal Isotopic Records.* Washington, DC: American Geophysical Union.

Rozanski, K., Froelich, K. & Mook, W., 2001. *Sutface water,* (Technical document No. 39 Vol. III). UNESCO,Paris: International Atomic Energy Agency.

Rozanski, K., Froelich, K., Mook, W. & Stichler, W., 2008. *Surface water.* Vienna, AU: IAEA.

SAHRA, 2005. *SAHRA: Sustainability of semi-arid hydrology and riparian areas.* [Online] Available at: http://www.sahra.arizona.edu/programs/isotopes/oxygen.html [Accessed January 2020].

Schellenberg, G., 2017. *Hydrology of the Delta Marsh Watershed: Water Balance Characterization and Analysis of Land Use Changes. Master Thesis. Department of Civil Engineering, University of Manitoba.,* Winnipeg: Available from https://mspace.lib.umanitoba.handle/1993/32779.

Schotterer, U., Oldfield, F. & Frohlick, K., 1996. *lobal network for isotopes in precipitation,* Bern, Switzerland: IAEA; PAGES; WHO; IAHS.

Sharpley, A., Kleinman, P., Flaten, D. & Buda, A., 2011. Critical source area management of agricultural phosphorus: experiences, challenges, and opportunities. *Water Science an technology,* 64(4), p. 945–952.

Sherry, M. & Soranno, P., 2006. Lake landscape position: relationship to hydrologic connectivity and lanscape features. *Limnol. Oceanorg.,* Volume 5, pp. 801-814.

Sie, P. & Frape, S., 2002. Evaluations of groundwaters from the Stripa Mine using stable chlorine isotopes. *Chemical Geology,* Volume 182, pp. 565-582.

Sklash, M. & Farvolden, R., 1979. the role of groundwater in storm runoff. *Developments in Water science,* Volume 12, pp. 45-65.

Smith, A., Delavau, C. & Stadnyk, T., 2015. Identification of geographical influences and flow regime characteristics using regional water isotope surveys in the lower Nelson River, Canada. *Can. Water Res. Journal,* Volume 40, pp. 23-35.

Soddy, F., 1913. The radiolelement and the periodic law. *Chem.News,* Volume 107, p. 97.

St.Amour, N. et al., 2005. Isotopic time-series partitioning of streamflow components in wetland-dominated catchments, lower Liard River basin, Northwest Territories, canada. *Hydrol. Process.,* Volume 19, pp. 3357-3381.

Stadnyk-Falcone, T., 2008. *Mesoscale hydrological model validation and verification using stable water isotopes: the iso WATFLOOD model. PhD Thesis,* Waterloo: University of Watreloo.

Stadnyk, T. & Holmes, T., 2020. On the value of isotope-enabled hydrologic model calibration. *Hydrol. Sciences J.,* 65(9), pp. 1525-1538.

Stanley, M., 2017. *Spatial variation of water quality and algal production, and the relationship between land use and nutrient loading in Delta Marsh. Master Thesis. Department of Biological Sciences, University of Manitoba ,* Winnipeg: Available from http://hdl.handle.net/1993/32502.

Stichler, W., Rauert, W. & Martinec, J., 1981. Environmental isotope studies of an alpine snowpack. *Nordic Hydrology,* Volume 12, pp. 297-308.

Sveinson, J., 2003. *Restoring tallgrass prairie in southern Manitoba, Canada Ph.D Thesis,* Winnipeg: University of Manitoba .

Urey, H., Brickwedde, F. & Murphy, G., 1932. A hydrogen isotope of mass 2. *Phys.rev,* Volume 39, p. 1645.

Van Der Valk, A., 2005. Water-level fluctuations in North American prairie wetlands. *Hydrobiologia,* Volume 539, pp. 171-188.

Vreca, P., Bronic, I., Horvatincic, N. & Baresic, J., 2006. Isotopic characteristics of precipitation in Slovenia and Croatia: Comparison of continental and maritime stations. *Journal of Hydrology,* 330(3-4), pp. 457-469.

Welhan, J. & Fritz, P., 1977. Evaporation pan isotopic behaviour as an index of isotopic evaporation conditions. *Geochim.Cosmochim. Acta,* Volume 41, pp. 682-686.

Wenninger, J., Uhlenbrook, S., Tilch, N. & Leinbundgut, C., 2004. Experimental evidence of fast groundwater responces ina hillslope/floodplain area in the Black Forest Mountains, Ge. *Hydrological Processes,* Volume 18, pp. 3305-3322.

Yamanaka, T. & Shimizu, R., 2007. Spatial distribution of deuterim in atmospheric water vapour: diagnosing sources and the mixing of atmospheric moisture. *Geochim.Cosmoshim.Acta,* Issue 71, pp. 3162-3169.

Yi, Y., 2008. *Developing and refining the use of water isotope tracers in hydrology and paleohydrology; PhD Thesis in Earth Sciences at University of Watreloo,* Waterloo: Available from: http://hdl.handle.net/10012/3903.

Yi, Y. et al., 2008. A coupled isotope tracer method to characterize input water to lakes. *Journal of Hydrology,* Volume 350, pp. 1-13.